University of Leicester

Department of Engineering

Supervisors: Doctor David Weston, Professor Sarah Hainsworth

Tribological Studies of Artificial Sports Pitches

A thesis submitted for the degree of Master of Philosophy at the University of Leicester

Timothy Devenport

092284090

February 2016

Abstract

The aim of this project was to investigate the wear of artificial sports pitch materials and characterise the wear mechanisms. The project was in collaboration with Notts Sports Ltd. who wished to compare the performance of existing pitches with potential new, improved artificial sports turfs.

The various materials (from different manufacturers, and of differing pile yarn weight and worn in situ and new) were imaged by optical microscopy and scanning electron microscopy to assess the tribological behaviour of the artificial sports turfs. X-ray computed tomography (X-ray CT) and Magnetic Resonance Imaging (MRI) was used to assess the structure of the artificial sports turfs. Pin on disk wear testing, tensile and fatigue testing was conducted on the artificial sports turfs to assess the wear life/mechanisms and how the structure performs under loading.

Optical and scanning electron microscopy reveal the wear mechanisms can be identified by the damage incurred as either adhesive, or abrasive or both. Additionally a directionality in the mechanical properties of the materials was observed. Visual and structural investigation by X-ray CT revealed a directionality to the materials. X-ray CT also showed inconsistencies in the structure negatively affect the performance of the artificial sports turfs, which was seen to be the case with some tensile and fatigue experiments. MRI was explored but found not useful in assessing the structure of the artificial sports turfs.

Wear testing showed different behaviour for differing artificial sports turfs, whilst the tensile and fatigue testing showed the orientation of the samples affects these properties, in that the horizontal orientation was stronger than vertical orientation.

Tensile testing revealed the artificial sports turfs behave similarly to randomly orientated short fibre composites.

Rawsons artificial sports turfs have more even fibre distribution in the horizontal and vertical directions in comparison to the Leigh Spinners artificial sports turfs, which has led to more uniform mechanical and tribological properties.

Acknowledgements

I would like to thank my supervisors Dr David Weston and Professor Sarah Hainsworth for their support and guidance during this project. I would also like to thank Mr Graham Clarke, Mr Vinay Patel and Mr Paul Williams for their help with experimental equipment, and Dr Alex Goddard, Dr Andrew D Ballantyne and Mr Stefan Davis for their assistance when I was using some of the equipment in their lab. Additionally I wish to thank the workshop staff, Mr Barry Chester and Mr Keith Stanley in particular, for constructing the specialised clamps required for the tensile testing and fatigue testing parts of this project. Further thanks to Dr Michael Kelly and his colleague Justyna Janus for their knowledge of and facilitating the Micro X-ray CT and NMRI imagery. I would also like to thank Andrew Norman for his assistance in writing some code that was used for the pre-processing of the data generated during the fatigue testing. A final thank you to Teresa Smith in the IRSA department and Steve Foxon from Notts Sport Ltd. for facilitating the project by providing the funding and artificial sports pitches materials used in this research, and some guidance throughout the research.

Contents

1 - Introduction 1
1.1 Manufacturing Method and Installation of Surfaces 2
1.2 Products Tested 4
1.3 Introduction Summary 6
2 - Literature review 7
2.1 Medical/Biomechanical Literature 8
2.2 Carpet Literature 12
2.3 Engineering Literature 22
2.3.1 Composite Materials 22
2.3.2 Tensile Testing 24
2.3.2.1 Tensile Behaviour and Failures of Polymers 26
2.3.2.2 Tensile Behaviour and Failures of Composites 27
2.3.3 Fatigue Testing 28
2.3.3.1 Fatigue Behaviour and Failures of Polymers 32
2.3.3.2 Fatigue Behaviour and Failures of Composites 33
2.3.4 Wear Testing 34
2.3.4.1 Polymer Tribology 38
2.3.4.2 Tribology of Composite Materials 39
2.3.5 Imaging 41
2.4 Literature Review Summary 44
3 - Experimental Methods and Procedures 45
3.1 Recap of artificial sports turfs tested 45
3.2 Optical Imaging 45
3.3 Environmental Scanning Electron Microscope 46
3.4 Resin ESEM 47
3.5 Filler Materials 48
3.6 Hardness Testing of Filler Materials 48
3.7 X-Ray CT 48
3.8 Micro X-ray CT 48
3.9 Nuclear Magnetic Resonance Imaging 50
3.10 Tensile Testing Procedure 50
3.11 Tensile Testing of Worn In Situ Samples 52
3.12 Tensile Testing of American Samples 53
3.13 Tensile Testing of X-ray CT Scanned Samples 53
3.14 Fatigue Testing Procedure 54

3.15 Fatigue Testing – Small Samples 54
3.16 Fatigue Testing – Large Samples Preliminary 55
3.17 Fatigue Testing – Large Samples 56
3.18 Wear Testing 57
3.19 Experimental Methods and Procedures Summary 61
4 - Characterisation 62
4.1 Optical 62
4.2 ESEM 66
4.2.1 Unmounted Samples 66
4.2.1.1 Unworn 66
4.2.1.2 Worn in situ 69
4.2.1.3 Wear testing worn fibres 71
4.2.2 Worn fibre length 72
4.2.3 Mounted in Resin 74
4.2.4 Sand Particles 76
4.2.5 Egg Shell Particles 77
4.3 X-ray CT 78
4.4 Micro X-ray CT 81
4.5 MRI 85
4.6 Characterisation Summary 85
5 - Tensile Testing 86
5.1 Leigh Spinners artificial sports turfs 86
5.2 Rawsons artificial sports turfs 89
5.3 NottsFilm Stiff, No Latex and American Samples 93
5.4 Worn in Situ Artificial sports turf 95
5.5 Fracture Points All artificial sports turfs 98
5.6 Product Comparisons 101
5.6.1 1150/1300 and Leigh Spinners/Rawsons 101
5.6.2 Leigh Spinners and Rawsons/Worn in Situ Artificial sports turf 102
5.6.3 Leigh Spinners and Rawsons/American. 102
5.6.4 Other – NottsFilm Stiff/No Latex 103
5.7 Tensile Testing Summary 103
6 - Wear, Hardness and Fatigue Testing 104
6.1 Wear Testing 104
6.1.1 Leigh Spinners 1150 artificial sports turfs 105
6.1.2 Leigh Spinners 1300 artificial sports turfs 107

6.1.3 Rawsons 1150 artificial sports turfs 109
6.1.4 Rawsons 1300 artificial sports turfs 111
6.1.5 Mass changes and counter faces 112
6.1.6 Product comparison 119
6.1.6.1 1150/1300 119
6.1.6.2 Leigh Spinners/Rawsons 119
6.2 Hardness Testing of Filler Materials 120
6.3 Fatigue Testing – Small Samples 121
6.4 Fatigue Testing – Large Samples Preliminary 124
6.5 Fatigue Testing – Large Samples 124
6.6 Product Comparison 125
6.6.1 Leigh Spinners/Rawsons 125
6.6.2 Leigh Spinners/American. 125
6.7 Wear, Hardness and Fatigue Testing Summary 125
7 - Discussion 126
7.1 Tensile Testing 126
7.2 Fatigue/X-ray CT 127
7.3 Wear/Hardness Testing 128
7.4 Optical Imagery 130
7.5 ESEM Imagery 131
7.5.1 Unworn 131
7.5.2 Worn in situ 131
7.5.3 Wear testing worn fibre 131
7.5.4 Worn Fibre Length 131
7.5.5 Resin ESEM 132
7.5.6 Sand and Egg Particles 132
7.6 X-ray CT 133
7.7 MRI 134
8 - Conclusions, Further Work. 135
8.1 Conclusions 135
8.2 Further Work 137
9 Appendix 1 – Foot loading force calculation for fatigue testing 139
10 Appendix 2 – Wear testing variables calculation 140
11 Appendix 3 – Calibration data for LVDT 140
12 Appendix 4 – Fatigue Raw Data 140
13 Bibliography/References 141

List of Tables

Table 1 - List of FIFA tests from (12) 10
Table 2 – Surfaces for sports areas – synthetic turf and needle punched surfaces primarily designed for outdoor use. 12
Table 3 - Types of damage in fibres, from (19) 17
Table 4 - Artificial sports turfs tested 45
Table 5 - List of grit levels of SiC abrasive papers 47
Table 6 - Results for t-tests of fracture points. 98
Table 7 - Data from Tensile Testing 101
Table 8 - Mass changes of samples 112
Table 9 - Wear testing data 119
Table 10 - Hardness testing data 121
Table 11 - Data from preliminary fatigue experiments 121
Table 12 - Fatigue data 125

List of Figures

Figure 1 - Illustration of manufacturing process, from (2) 3
Figure 2 - Illustration of structure of artificial sports turf 3
Figure 3 - Repeat unit of polypropylene, from (4) 4
Figure 4 - Chemical structure of SBR, from (4) 4
Figure 5 - Monomers of SBR, from (4) 4
Figure 6 - Diagram of forces involved in foot strike, from (7). 8
Figure 7 - Diagram of angles in fibre deflection of an older carpet, from (16) 15
Figure 8 - SEM images of fibre failures, from (19). Letters correspond to type of damage, type H not shown 17
Figure 9 – Tensile fatigue failures of nylon (a-d) and polyester (e-g) from (22) 19
Figure 10 – Axial splitting Polyester fibres from (22) 19
Figure 11 - Biaxial rotation fatigue of polyester fibres from (22) 20
Figure 12 - Surface abrasion of various kinds of fibres from (22) 20
Figure 13 - Diagram of a large particle composite 23
Figure 14 - Diagram of dispersion strengthened composite 23
Figure 15 - Diagram of a reinforced material 24
Figure 16 - Stress strain curve for brittle and ductile metal (left) and calculation of yield strength (right), reproduced from (27) 25
Figure 17 - Diagram of a reversed stress cycle 29
Figure 18 - Diagram of a repeated stress cycle 29
Figure 19 - Diagram of a random stress cycle 29
Figure 20 - Typical S-N curve of a material that exhibits a fatigue limit, reproduced from (27) 31
Figure 21 - Typical S-N curve of a material that does not exhibit a fatigue limit, reproduced from (27) 31
Figure 22 - Diagram of craze formation, reproduced from (29) 33
Figure 23 –Diagram of craze formation preceding a crack, reproduced from (29) 33
Figure 24 - Diagram of abrasive wear reproduced from (32). 36
Figure 25 - Diagram of adhesive wear, reproduced from (32) 36
Figure 26 - Diagram of fatigue wear reproduced from (32). 37
Figure 27 - Diagram showing a wear process in a composite, reproduced from (37) 40
Figure 28 - Schematic of SEM interaction volume, reproduced from (41) 42
Figure 29 - Schematic drawing of flaring 42
Figure 30 - Diagram showing positions of images on a 77 mm diameter disk 46
Figure 31 - Diagram of tensile test dog bone, reproduced from (45) 50
Figure 32 - Diagram illustrating the vertical orientation 51
Figure 33 - Diagram illustrating the horizontal orientation 51
Figure 34 – Macro photo of a tensile dog bone – horizontal orientation. 51
Figure 35 - Clamp used for tensile testing 52
Figure 36 - Wedge grip clamp 54
Figure 37 – Clamp for initial fatigue testing of larger samples 55
Figure 38 - Clamp used for fatigue testing of larger samples 57
Figure 39 - Shoe from which counter faces were cut. Lower right shows shoe with studs removed 59
Figure 40 - Schematic of wear rig 60
Figure 41 - Macro photo of wear rig 60

Figure 42 - Optical Image of the backing on the American artificial sports turf. 62
Figure 43 - Optical Image of the fibres on the American artificial sports turf............................ 62
Figure 44 - Optical Image of the backing on the worn in situ square sample 63
Figure 45 - Optical Image of the fibres on the worn in situ square sample 63
Figure 46 - Optical Image of the backing on the Leigh Spinners 1300 artificial sports turf 64
Figure 47 - Optical Image of the fibres on the Leigh Spinners 1300 artificial sports turf........... 64
Figure 48 - Optical Image of the backing on the Leigh Spinners 1150 artificial sports turf 65
Figure 49 - Optical Image of the fibres on the Leigh Spinners 1150 artificial sports turf........... 65
Figure 50 – Typical ESEM image of the fibres in the American artificial sports turf. 66
Figure 51 - Typical ESEM image of the backing fibres in an unworn sample of the American artificial sports turf. 67
Figure 52 - ESEM image of the pile of a Leigh Spinners 1300 grass green 68
Figure 53 - ESEM image of the backing of a Leigh Spinners 1300 grass green.......................... 68
Figure 54 - ESEM Image of fibres from worn in situ rectangular sample, position 1. 69
Figure 55 - Close up of a broken fibre end from the worn in situ rectangular sample, position 1. 70
Figure 56 - ESEM image of the backing of a sample worn in situ rectangular sample. 70
Figure 57 - ESEM image of a worn sample of a Leigh Spinners artificial sports turf. 71
Figure 58 - Image of individual worn in situ fibre... 72
Figure 59 - Image of individual worn in situ backing fibre 73
Figure 60 - An ESEM Image of fibres and latex in the 1150 Leigh Spinners artificial sports turf 74
Figure 61 - ESEM Image of a region of latex in the American Sample 75
Figure 62 - SEM Image of a sand particle with rounded edges and surfaces 76
Figure 63 - SEM Image of a sand particle with angular edges and surface of grain 76
Figure 64 - ESEM Image of egg shell particles 77
Figure 65 - X-ray CT image of Leigh Spinners 1150 grass green artificial sports turf. 78
Figure 66 - X- ray CT image of a Rawsons 1150 artificial sports turf 78
Figure 67 - X ray CT image overlaid with positions of tensile "dog bone" shapes. 79
Figure 68 - A graph showing the performance of the 11 samples. 80
Figure 69 - Graph showing the relation of the Mass of a sample and its fracture point 80
Figure 70 - No latex 70 kV 81
Figure 71 - American 70 kV... 81
Figure 72 - Rawsons 70 kV 82
Figure 73 - Leigh Spinners 70 kV 82
Figure 74 – X-ray CT Image of an American sample (vertical orientation) after fatigue testing 83
Figure 75 - X-ray CT of the American artificial sports turf after tensile testing......................... 84
Figure 76 - MRI Image of a sample of Leigh spinners. 85
Figure 77 – Force extension graph of the Leigh Spinners 1150 artificial sports turf.................. 87
Figure 78 - Force extension graph for the Leigh Spinners 1150 grass green artificial sports turf 87
Figure 79 – Force extension graph of the Leigh Spinners 1300 artificial sports turf.................. 88
Figure 80 - Force extension graph of the Leigh Spinners 1300 grass green artificial sports turf 88
Figure 81 – Force extension graph for the Rawsons 1150 olive green artificial sports turf....... 90
Figure 82 – Force extension graph for the Rawsons 1150 Lavender artificial sports turf.......... 91
Figure 83 - Force extension graph for the 1300 Rawsons Terracotta samples. 91
Figure 84 – Force extension graph for the 1300 Rawsons olive Green samples. 92
Figure 85 – Force extension graph for the NottsFilm Stiff samples. 94
Figure 86 – Force extension graph of the "No latex" samples. 94

Figure 87 – Force extension graph of the American samples. 95
Figure 88 – Graph of the tensile testing of the samples of artificial sports turf worn in situ, square sample....... 96
Figure 89 - Tensile results of the samples cut from position 1....... 96
Figure 90 – Tensile results of the samples cut from position 2 97
Figure 91 – Fracture points of the worn in situ artificial sports turf 97
Figure 92 - Fracture points of the artificial sports turfs....... 99
Figure 93 – Wear test result from preliminary experiment 104
Figure 94 - Wear test result for Leigh Spinners 1150 with 2.55 N load on counter face 105
Figure 95 - Wear test result for Leigh Spinners 1150 with 7.65 N load on counter face 106
Figure 96 - Wear test result for Leigh Spinners 1150 with 2.55 N load on counter face with sand filler 106
Figure 97 - Wear test result for Leigh Spinners 1150 with 7.65 N load on counter face with sand filler 106
Figure 98 - Wear test result for Leigh Spinners 1300 with 2.55 N load on counter face 107
Figure 99 - Wear test result for Leigh Spinners 1300 with 7.65 N load on counter face 108
Figure 100 - Wear test result for Leigh Spinners 1300 with 2.55 N load on counter face with sand filler 108
Figure 101 - Wear test result for Leigh Spinners 1300 with 7.65 N load on counter face with sand filler 108
Figure 102 - Wear test result for Rawsons 1150 with 2.55 N load on counter face 109
Figure 103 - Wear test result for Rawsons 1150 with 7.65 N load on counter face 110
Figure 104 - Wear test result for Rawsons 1150 with 2.55 N load on counter face with sand filler....... 110
Figure 105 - Wear test result for Rawsons 1150 with 7.65 N load on counter face with sand filler....... 110
Figure 106 - Wear test result for Rawsons 1300 with 2.55 N load on counter face 111
Figure 107 - Wear test result for Rawsons 1300 with 2.55 N load on counter face with sand filler....... 111
Figure 108 - Optical Image of a sample of Leigh Spinners 1150 before a test. 112
Figure 109 - Optical Image of a sample of Leigh Spinners 1150 after a test. 113
Figure 110 - Undamaged counter face - no sand counter face 114
Figure 111 - No sand counter face (after 1 test) 114
Figure 112 – No sand counter face, 2.55 N load (after 2 tests)....... 115
Figure 113 – No sand counter face 2.55 N load (after 4 tests)....... 115
Figure 114 – Sand counter face (before test) 116
Figure 115 – Sand counter face (after 1 test) 117
Figure 116 – Sand counter face (after 4 tests) 117
Figure 117 - Mass of counter faces....... 118
Figure 118 - Typical fatigue performance of the better samples of the Leigh Spinners 1150 artificial sports turf in preliminary fatigue tests. 122
Figure 119 - Manually cut small sample 122
Figure 120 - Typical fatigue performance of a poor sample (Rawsons 1150 green sample 8) 123
Figure 121 - Fatigue performance of the 1st full size sample. 124
Figure 122 - Calibration data for Pin on wheel wear testing 140

List of Abbreviations

Anteroposterior (AP)

Analysis of variance (ANOVA)

Bodyweight (BW)

Computed tomography (CT)

Critical Fibre Length (L_c)

Environmental scanning electron microscope (ESEM)

Field of View (FOV)

Generated separated electron (GSE)

Linear variable differential transformer (LVDT)

Mediolateral (ML)

Non applicable (N/A)

[Nuclear] Magnetic Resonance Imaging ([N] MRI)

Parts per million (ppm)

Polypropylene (PP)

Position 1 (P1)

Position 2 (P2)

Pressure limiting apertures (PLA)

Radio-frequency (RF)

Small to Medium enterprise (SME)

Styrene Butadiene Rubber (SBR)

Ultimate tensile strength (UTS)

Ultra-high molecular weight polyethylene (UHMWPE)

Vaporised Hydrogen Peroxide (VHP)

Vertical Force (Fz)

1 - Introduction

Notts Sport Ltd. is a UK based SME and a leading specialist in the design, advice and supply of artificial sports turf ranging from cricket, tennis, football and hockey pitches to multi-sports and children's play areas. (1)

Notts Sport Ltd. held a patent for its NottsSward product up until recently which allowed it to supply a unique product into the market for Sport & Play. With the patent expiring, other companies introduced copycat products reducing the capacity for Notts Sport Ltd. to supply customers based on the uniqueness of the product.

The aim of this project was to collaborate with Notts Sport Ltd. to look at ways to improve upon the current design of product to give a unique selling point, such as stability, durability or longevity and recyclability.

This was to be achieved by: 1) Developing techniques for analysing the tribological performance of materials used in artificial sports pitches. 2) Developing techniques for tribological study of artificial sports pitches. 3) Developing techniques for identifying wear mechanisms in different polymers. 4) Researching the different factors contributing to damage of artificial sports pitches.

Whilst the issue of recyclability is outside this project, it is a major concern for Notts Sport Ltd. At the moment when a surface is replaced, the existing turfs can only be re-purposed by removing the fibres and re-forming the backing into objects such as drain pipes, or cut up and used as fuel in power stations. This is because whilst one of the constituent parts of the artificial sports turf is recyclable (the fibres), the backing is a latex rubber, which cannot be melted down and recycled because heating causes the cross linked elastomers to break resulting in an unusable material. Additionally, once installed the artificial sports turf is bedded with sand to help increase the longevity of the turf. The sand particles become embedded in the artificial sports turf over time, making it difficult to remove and this would in turn cause excess wear/damage to the machines during the recycling process. (2)

Notts Sport Ltd. want to look at different options for backing and fibres and therefore need a suitably robust testing regime to ensure any new product improvements are fit for purpose and that the surface is likely to still give its current life expectancy and performance for at least 8 to 10 years in a range of environments. This project will assess and compare the tribological performance of Notts Sport's existing artificial sports turf materials in comparison to new compositions to determine if alternative production materials match the wear performance of the existing product range.

1.1 Manufacturing Method and Installation of Surfaces

Although the exact manufacturing process differs from manufacturer to manufacturer, the general process is as follows.

The yarn/pile of polypropylene (PP) fibres is passed through a series of spiked rollers. The spikes on the rollers pull the yarn through the rollers, and connect the layers of the yarn together into a sort of web. The yarn is then run through a second carte which is perpendicular to the first. This further helps to connect the layers together to form a web of fibres. This web is then run though a needling loom to give the needle punched structure. The web is then run through a second needling loom, which has slightly lower needling rate to prevent the pile from disintegrating.

This is then run through a structuring loom, which is similar to the needling looms but differs in size and shape of the needles, after which the backing is applied. Initially the pile impregnated with Styrene Butadiene Rubber (SBR) latex (approximately 20% of the applied SBR is retained by the web), which is then heated in an oven for approximately 10 minutes, which allows the SBR to cure and form a matrix around the fibres to form the final product, which is then rolled up and stored. Figure 1 provides an illustration of the manufacturing process. (3)

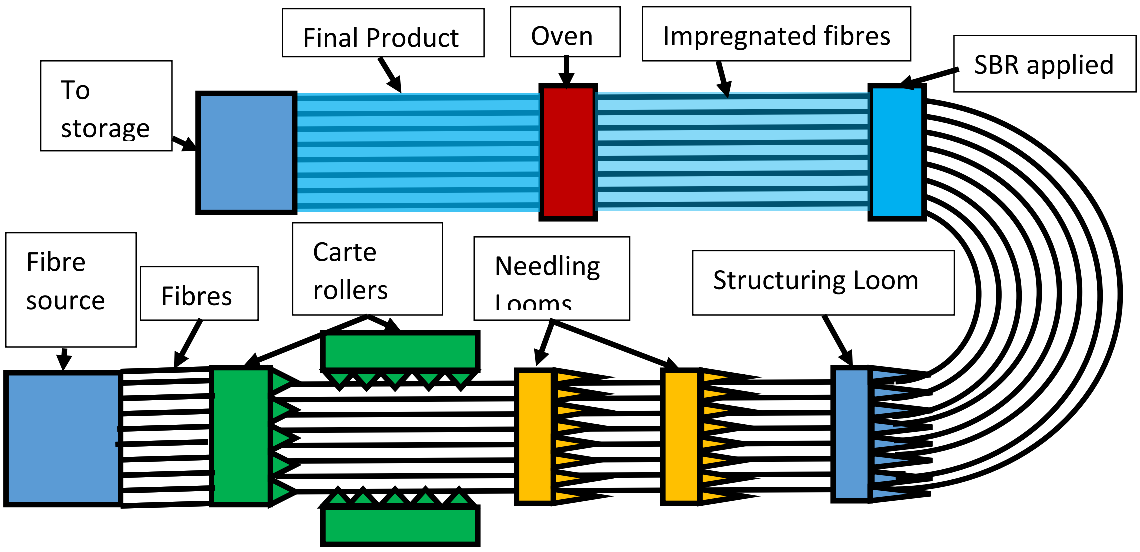

Figure 1 - Illustration of manufacturing process, from (2)

When the products are installed, lengths of the artificial sports turf are rolled out over the area required. The lengths are attached together by an adhesive, akin to sticky tape, to give a single surface with no gaps before being bedded down with sand to prevent the surface from moving. Typically 15 – 18 kg/m^2 is used with the result that approximately 2 mm of fibres are above the sand. The sand is also believed to contribute towards increasing the lifetime of the artificial sports turfs when in use. (2) An illustration of the artificial sports turf structure is shown in Figure 2.

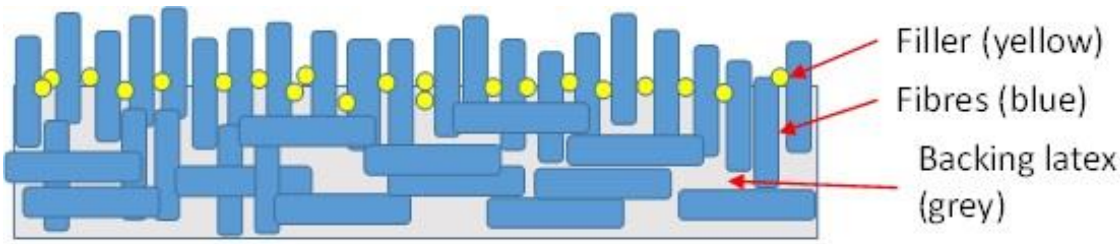

Figure 2 - Illustration of structure of artificial sports turf

Chemically, the fibres are typically PP polymers, which are long chains of carbon and hydrogen (repeat structure shown in Figure 3) linked together by covalent bonds. (4) PP has a good resistance to most forms of chemical attack and has excellent fatigue resistance, and has a range of applications including carpeting. (5)

The backing is SBR latex, a synthetic rubber. Compared to natural rubber, SBR has better processability, heat aging and abrasion resistance, although SBR exhibits poorer elongation, hot tear strength, hysteresis, resilience and tensile strength. Its most popular application is in the manufacture of tyres and tyre products. It is produced by copolymerising butadiene and styrene in a 3:1 ratio by weight. The chemical structure of SBR is shown in Figure 4, and the monomers are shown in Figure 5. (6)

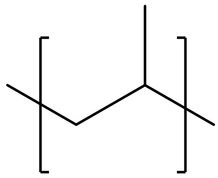

Figure 3 - Repeat unit of polypropylene, from (4)

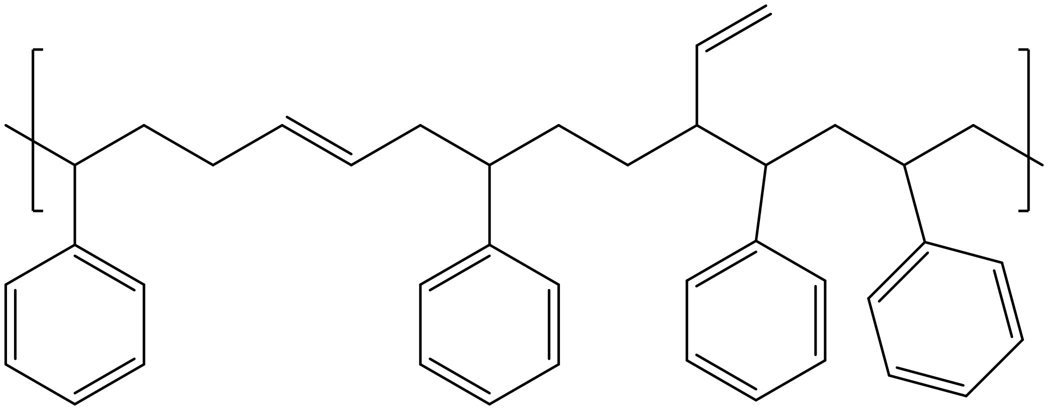

Figure 4 - Chemical structure of SBR, from (4)

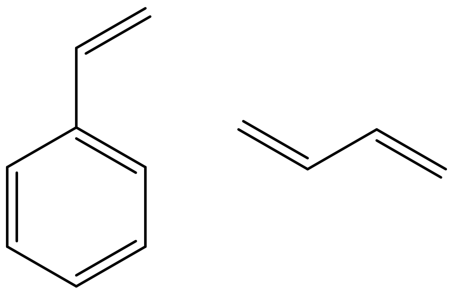

Figure 5 - Monomers of SBR, from (4)

1.2 Products Tested

Initially, six different artificial sports turfs were supplied by Notts Sport Ltd. for investigation as part of the project. There were two different manufacturers, Leigh Spinners who provided 2 artificial sports turfs, and Rawsons who provided a further 4. Half of the products from each manufacturer provided differ in the average pile yarn weight of the artificial sports turf, 1150 grams/m^2 and 1300 grams/m^2, (defined in 2.2).The differing average pile yarn weight is believed to lead to differing density of backing latex in the artificial sports turfs, because of the manufacturing process already discussed.

Additionally, an artificial sports turf made by an American manufacturer was provided. The exact manufacturing process of this product was protected by industrial secrecy, however it is believed a similar process is followed, except the backing is polypropylene which is applied as a powder, and then melted with infrared radiation before being allowed to cool.

An artificial sports turf of an unknown manufacturer, although known to be the 1300 grams/m^2 product type, which had been used for approximately 13 years was provided. This artificial sports turf had been used predominately for football, with some hockey and tennis usage, but the number of hours in use is unknown. It had been protected from the weather by use of an inflatable dome that completely covered the surface, which was kept inflated by warm air. Samples of this product are referred to as “worn in situ” artificial sports turf, to distinguish it them from the samples that underwent wear testing. Two sections of this artificial sports turf were provided, one a square measuring 1 m by 1 m, the other a rectangle of 1 m by 2.56 m.

In addition a sample of different product, NottsFilm Stiff was provided. This product differs from the other products in both constituent materials and manufacture in that it is a thin geotextextile needle-punched from polyester, and then resin bonded with SBR latex.

Finally, a sample of artificial sports turf that had not had the latex backing applied was provided.

In addition to the samples of artificial sports turf which were provided, approximately 5 kg of sand that is currently used as a filler material for the artificial sports turfs (discussed in 1.1) and 0.5 kg of potential new filler, ground up egg shell particles was provided.

The sand particles were specified to be of size 0.25 mm to 1 mm diameter rounded or sub rounded and are kiln dried to remove any shale.

The egg shell particles were also specified to be of size 0.25 mm to 1 mm diameter. The shape was unknown as was whether any drying process was applied.

1.3 Introduction Summary

This chapter has covered the problems investigated in this project, why they are investigated, what artificial sports turfs are available for the project and their chemical composition and how they are manufactured and installed. Moving forward a review of the literature was conducted.

2 - Literature review

Initially the literature was investigated to find what factors affect the quality of the pitch from the athletes' perspective. Additionally the literature was investigated for research on the bio-mechanics of running, to better understand the forces involved in the boot/surface interaction, as the forces experienced by the foot upon impact must be translated into the artificial sports turf, as described by Newton's second law. It has been assumed that the majority of contact events the artificial sports turf investigated in this project are from straight line running. There is a large amount of data available because there has been a lot of work done for medical journals investigating the difference between running on natural grass and artificial sports turf, and relating this to the risk of injuries. It is from this data that the variables used in the testing procedure were calculated. To the author's knowledge, the bulk of these papers do not concern themselves with translating and comparing the parameters they measure with the mechanical properties of the artificial sports turf.

With this in mind, work that investigated the ergonomics of carpets in terms of standing, walking, wear mechanisms and modelling of carpets was reviewed. This literature was used to further understand the construction of the carpets and how the construction affects the mechanical properties of the carpet, and to assess the work already conducted on the wear of carpets.

In addition to this the literature was investigated to find what factors affect the quality of the pitch from an engineering perspective. From this direction it was found that there has been work commissioned by governing bodies of various sports, such as FIFA and England Rugby, for the purposes of determining whether a match played on artificial sports turf will be the same as a match played on natural turf, so factors like ball roll, for example, are investigated. Additionally safety factors such as head impact severity have been considered by these governing bodies.

Further to this, the industry standard "Surfaces for sports areas - synthetic turf and needle punched surfaces primarily designed for outdoor use" were assessed with particular focus on how well the tests emulated the boot/surface interaction and where their short falls are.

Finally, the literature was investigated to identify work that had been conducted on polymer tribology and tribology of composite materials, as well as the tensile and fatigue behaviour of polymer and composite materials. There has been a significant amount of work done in these fields, as other applications of this knowledge are important in other industries, however finding work that was relevant was troublesome. To the authors knowledge, outside the “carpet literature” not much work has been done on the tribology of essentially loose fibres anchored further down their length, nor has there been much work on the tensile and fatigue behaviour of composite materials with a similar structure as the artificial sports turfs.

2.1 Medical/Biomechanical Literature

The forces from a foot strike can be resolved into 3 directions, the vertical force (F_z) the anteroposterior force (AP) and mediolateral force (ML), as shown in Figure 6. (7)

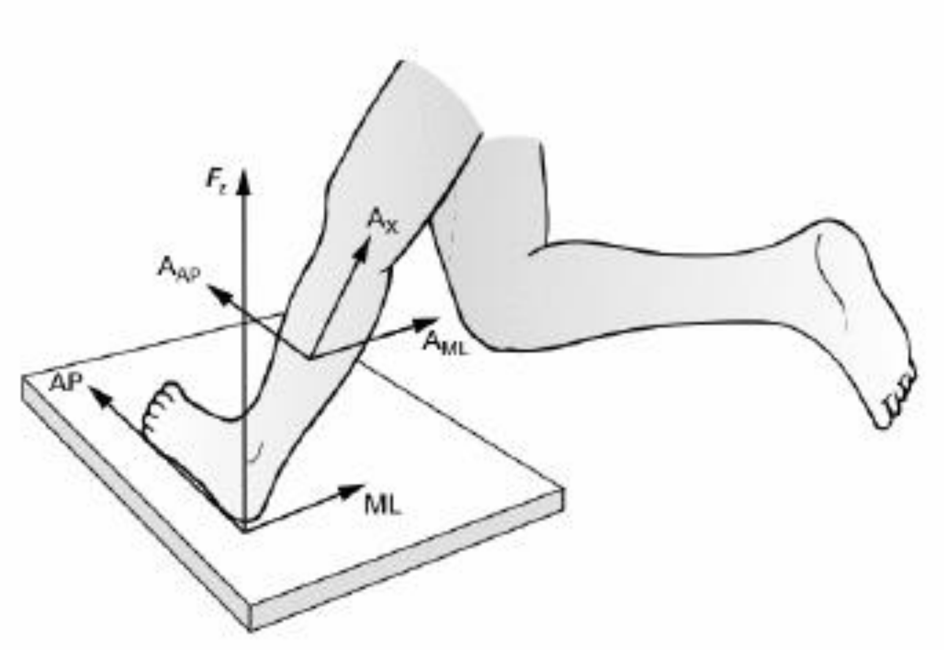

Figure 6 - Diagram of forces involved in foot strike, from (7).

Although there is disagreement in the literature with regards to the absolute magnitude of the 3 forces, as they depend upon both the mass of the athlete and the running velocity. To the authors knowledge no-one has derived a model that accounts for these variables apart from giving the force in BW, which still does not account for different velocities. The literature does agree that F_z is the largest force, typically greater than twice the athlete’s bodyweight (BW) for an athlete with a bodyweight of 100 kg, Fz ≥

1.962 kN. The AP force is typically equal to a tenth to a half the athlete's bodyweight (0.098 kN for 0.1 BW, 0.4905 kN for 0.5 BW), whilst the ML force is typically 0.2 BW (0.1962 kN). These measurements are acquired in a variety of different experimental procedures, from force plates (as in (8) and (9)) to accelerometers (9). Whilst these forces are roughly constant (within an order of magnitude) across the literature for running, when different sporting actions are considered the forces can vary greatly. For example, the F_z for a cricket bowler at release is 6.7 BW ≈ 6.572 kN for an athlete with a body mass of 100 kg (10).

The contact time for an entire event during running is 200 ms to 225 ms, depending on the surface. (11) This is expected to vary between sports and the running velocity but is in agreement with other works.

The reason for this disagreement is that whilst all the studies use good methods, all the studies are limited by the number of variables for the athlete causing slight differences. Some use semi-professional to professional runners, whilst other studies use amateur athletes. It can be argued either is appropriate to this research, as it can be assumed the majority of the use will be from amateur players, however the professionals assumed better technique will give better data. Additionally, there are slight differences in speed, which is known to affect the data, for example Hong et al (11) uses male amateur runners at 3.8 m/s, however Dixon et al uses well trained female runners (9) 3.3 m/s.

The literature indicated the loading phase of the foot throughout a step is a complex process, as there are different styles of running, heel strike (where the heel impacts the floor first before rolling on through the rest of the foot) and midstrike, where the heel and the midsole land together, followed by a rolling on to the toes. In both cases, initially the velocity of the foot decelerates to zero and the reaction force increases to a maximum acting against the direction of propagation, known as the breaking phase. After this, the acceleration phase occurs, where the runner pushes off.

There has been work done by various sporting bodies which is predominately focussed on how well artificial sports surfaces mimic natural grass, with some safety considerations. This can be seen in the list of FIFA tests in Table 1, which clearly shows that the majority of the tests focus on the ball behaviour. The ball behaviour is not considered in this research.

Mimic tests	Safety tests
Determination of football rebound	Determination of Skin/surface friction and skin abrasion
Determination of Angle ball rebound	N/A
Determination of ball roll	N/A
Determination of Shock absorption	N/A
Determination of Standard vertical deformation	N/A
Determination of Energy restitution	N/A
Determination of Linear friction stud slide value and stud deceleration value	N/A

Table 1 - List of FIFA tests from (12)

Other sporting bodies, such as England Rugby, have conducted other tests to examine the safety of players on artificial sports turf, such as head impact tests.

The industry standard BS EN 15330, “Surfaces for sports areas - synthetic turf and needle punched surfaces primarily designed for outdoor use” were investigated for tests that are applicable to this research. There is no standard for fatigue testing, however there are standards for tensile testing and abrasion testing. All of the standards made available by Notts Sports Ltd are discussed in Table 2.

Standard code	Name	Applicable?	Comment
15306_2014	Exposure to simulated wear	Yes	Test apparatus uses studs to generate wear. Artificial sports turfs tested in this research does not permit use of studs, and so test is unfair.
1969	Thickness of sport surface	No	Not relevant to this research.
5079	Fibre strength	Yes	Would have used if wear tests had shown clear evidence of fibres breaking, however this did not occur.
12228_2013	Joint strength	No	Not testing strength of joins.
12230	Determination of tensile properties of synthetic sports surfaces	Yes	Was adhered to for sample preparation and tensile testing. Also adhered to for sample preparation for fatigue testing.
12234_2013	Ball Roll	No	Not relevant to this research.
12235_2013	Determination of vertical ball behaviour	No	Not relevant to this research.
12616_2013	Determination of water infiltration	No	Not relevant to this research.
13036_7	Straightedge	No	Not relevant to this research.
13672	Determination of resistance to abrasion of non-filled synthetic turf	Yes	Whilst allows for measuring mass loss of unfilled sample, does not allow for testing the effect the filler material has on the wear rate, which was to be investigated in this research.

13744	Water ageing	Yes	Details method for accelerated ageing of artificial sports turfs via immersion in water bath.
13865	Angle tennis rebound	No	Not considering ball behaviour on carpets.
14808	Determination of shock absorption	No	Not relevant to this research.
14809	Determination of Vertical deformation	No	Not relevant to this research.
14836	Exposure to artificial weathering	Yes	Details method for ageing artificial sports turfs via exposure to UV radiation.
15301-1	Determination of Rotational resistance	No	Not relevant to this research.
5470-1	Taber abrader	Yes	Details how to use Taber abrader apparatus for 13672.
5470-2	Martindale abrader	Yes	Details how to use Martindale abrader apparatus for 13672.

Table 2 – Surfaces for sports areas – synthetic turf and needle punched surfaces primarily designed for outdoor use.

2.2 Carpet Literature

There has been considerable work conducted on carpets investigating essentially three areas, the wear on carpets, and the comfort/ergonomics of carpets and automatic detection of wear on carpet.

There is some important carpet terminology that needs covering before looking at the literature that has been covered. A yarn is a continuous strand composed of fibres or filaments that form carpets and other fabrics. When referring to the directions of the yarns in a carpet, warp and weft directions are used. The warp direction is the lengthwise direction in the carpet; the weft direction is transverse to the warp direction. The visible surface of the carpet is called the pile, and the mass of the pile per unit area is termed the average pile yarn weight. (13) As there is no warp and weft directions in the artificial sports turfs tested (which are a needled punched web, not woven), the terms vertical and horizontal are used. In this context, vertical refers to the direction that follows the fibres and SBR latex. Horizontal is perpendicular to the vertical, as discussed in 3.10.

Onder and Berkalp (14) conducted a review/study on the properties of carpets and investigated the mechanical properties of woven carpets finding that structural factors influence tribological factors. Wear can be characterised in a number of different ways, such as terms of texture and colour differences, pile flattening, and reduction in tuft clarity, shading, soiling, and loss of colour. They also state that the ability to resist these changes varies between carpets due to a number of manufacturing variables, fibre composition, and yarn processing route, carpet structure, tuft morphology, and pile dimensions.

Onder and Berkalp also state the resilience of carpet depends on the compression and recovery behaviour of the pile. “A pile returns to its original state if the energies preventing the recovery are smaller than the elastic energy released during yarn bending. Dynamic-compression properties of carpets are characterized by several unique features: the stress/strain compression curve is nonlinear, there is hysteresis during a compression-release cycle, and the compression modulus and energy dissipation per cycle are affected by the magnitude of the pressure displacement involved.”

As a part of the review Onder and Berkalp conducted they identify two other features related to carpet mechanical properties - inelastic mechanisms and fatigue mechanisms. Inter-fibre and inter-yarn frictional sliding during yarn bending and viscoelastic properties of pile yarns are two important inelastic mechanisms influencing the flattening of carpets.

A carpet’s fatigue mechanism is one of pile loss from the carpet’s surface due to abrasive wear. If the fatigue regions are not partial and distributed along the pile length, the pile weight left after walking on the carpet depends on the number of repetition cycles, the pile density, the linear density of the fibres, and the percent of damaged fibres.

From the experiments Onder and Berkalp conducted on 12 face to face woven carpets, with wool and acrylic piles it was found that, there was no significant change in surface structure and colour in shorter duration tests for all carpet types. During longer duration tests, only a slight or moderate change in structure was found. The denser carpets kept their pattern clarity. Colour changes in the carpets were influenced by fibre dullness or brightness, colour shade (light or dark), and pattern type. For these reasons, these results showed no relationship between wear induced changes in surface structure and colour. The polypropylene carpet specimens showed substantial tuft flattening in the longer duration tests.

Also from the experiments conducted, wool carpets showed evidence of lack of abrasion as partial revealing of backing on each carpet specimen. In carpets made of synthetic fibre yarns, this phenomenon took place simultaneously all over the surface; in particular, fibres of polypropylene piles initially flattened and then melted with rubbing as would a thermoplastic, and retreated to reveal the backing. Abrasion resistance results were better for denser carpets, and increased pile height normally increased abrasion resistance.

To summarise, the work Onder and Berkalp conducted found that weft density was the determining factor in abrasion resistance with pile height a smaller contributing factor, whilst resistance to tuft withdrawal is dependent on both pile height and weft density. (14)

Zhou and Warner investigated the sizes of pores in latex backed carpets made from a polypropylene backing, cross linked styrene butadiene rubber adhesive with a nylon pile, which is similar to those in the current work. This was conducted as they wished to develop an economical method for drying carpets. This paper attempted to measure the size of pores in the backing material using liquid extrusion and optical microscopy methods, and with these methods found pores with an effective capillary diameter of up to 200 μm, whilst the majority (80%) of the pores were larger than 252 μm. This is very precise, and one wonders how accurate these measurements are, as no errors are given. They also found the height of the pile, which varies between the different artificial sports turfs used in this project, has little effect on the pore size and distribution. A relationship between the pile yarn count, stitch density and tufting pattern that affects the distribution of these pores was found. (15)

There has been some modelling done to understand how carpets deform. Dayiary et al theoretically analysed the compression behaviour of cut pile carpet. They state that the mechanism of pile deformation under load is different for new and used carpets, in that in newer carpets the deflection of the pile is along the entire length, whilst in older carpets the deflection occurs mainly at the bottom of the pile leading to a flat top section, before discussing the model they develop. (16)

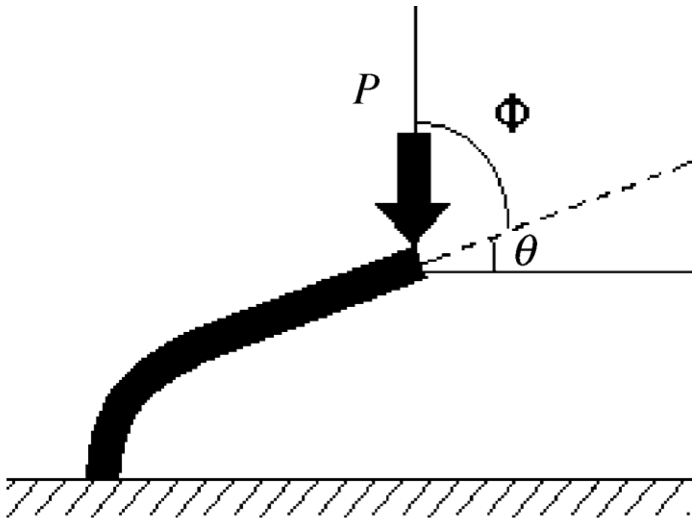

Figure 7 - Diagram of angles in fibre deflection of an older carpet, from (16)

Wu, Pan and Williams investigated how the compliance modulus (the inverse of the stiffness) of different carpets affects standing in terms of perceived comfort and postural sway. They found, using a force plate covered with samples of carpet that more compliant (less stiff) carpets were reported to be more comfortable to barefoot subjects. (17)

Hearle has conducted an SEM study on the wear of wool carpets, in which he identifies several ways in which fibres can fail, both in tufts and as individual fibres. 7 tufts of wool fibres, taken from carpet which was 30 years old are examined in this work. All of the tufts exhibited the same general features. It is identified that some fibres become fatigued and break which causes the upper portion of the fibre to become "lost" in the pile. It was also found that the development of fibre breaks is strongly distributed below the dominant wear line, but is absent deeper in the pile. (18)

In this work Hearle identifies that “the major form of fatigue leading to breakage is multiple splitting, which is most likely due to shear stresses.” Although he does state that similar damage may be caused by twisting or bending/twisting combined, reported in an earlier piece of work by Hearle. With regards to the fibres splitting, Hearle Identifies that it may occur across the whole cross section of the fibre, or only on either the inside/outside of the bend in the fibre.

In type and location of fatigue breaks in wool fibres carpets part 1, eight mechanisms of fibre damage are identified with pictures from samples of wool carpet which were subjected to both straight walk and walk trials. Main form of damage as identified as axial compression fatigue and not fibre splitting (19).

The eight types of damage are given in Table 3

Damage type	Name	Description
A	Incipient distortion	Slight bending of fibres with some flattening and squashing of the fibre
B	Bulbous, kink bands and cracks	Bulbous features with kink bands and cracks.
C	Gash, half fibre width	Localised rupture in the side of the fibre, often half the width, generally with very little fibrillation.
D	Fibrillation across whole fibre	High degree of fibrillation, often right across fibre, sometimes only on edge.
E	Kink band to crack	Starts as deep kink band, axial split may appear. Only occurs on one edge, almost no fibrillation.
F	Clear kink bands to cracks	Very clear kink bands, even seen in unworn fibres, kink bands may develop in to cracks.

G	Various ends	Axial splitting, ranging from one or two splits to extensive fibrillation, which may be spread over a range of lengths. Some broken ends maybe final stage of type D.
H	Variant of 2, bulbous only.	Bulbous features without kink bands and cracks

Table 3 - Types of damage in fibres, from (19)

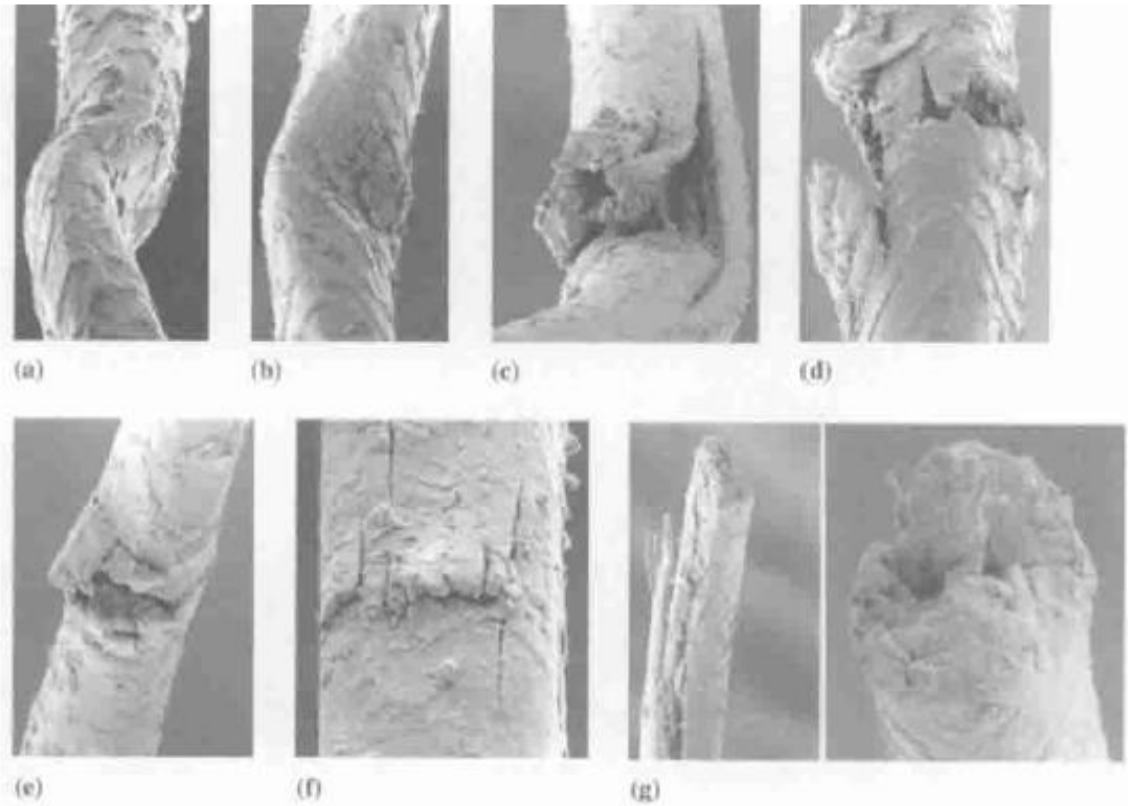

Figure 8 - SEM images of fibre failures, from (19). Letters correspond to type of damage, type H not shown.

These damage mechanisms are not indicative of worsening damage or indeed different mechanical properties. Of course, these are all wool fibres, and therefore unlikely to be seen in the failures of fibres in this project.

In the follow up paper, part 2, statistical analysis is used to develop a model which relates the probability density function on to the number of breaks. The probability density function increases from base to tip according to a simple power law (not included for brevity) (20).

Fiber Fracture is a compilation of works from several authors then relevant works are discussed here. (21)

The chapter “Forms of Fibre Fracture” by Hearle identifies and classifies what differing failures of fibres look like, as can be seen from Figure 9, Figure 10, Figure 11 and Figure 12. Fatigue of the fibres gave tensile breaks at the peak cyclic load, however when the maximum cyclic load is 50% of the break load, the sequence of images a - d in Figure 9 are produced. (22)

Of course, the fibres being tested will deflect under the applied load. The shear stress caused by the deflection results in axial splitting, shown in Figure 10, where each fibre has been bent over a pin, under a strain of 10% and a load of 10% of the fibre break load. For these fibres Hearle discusses that surface wear dominates during deflection. The combination of twisting and bending can lead to failure by multiple splitting, due to the presence of compressive, tensile and shear stresses in the fibre, shown in Figure 11. (22)

Hearle has studied yarn on yarn surface abrasion by cyclic displacement of a twisted loop or abrading a hanging fibre against a rotating pin. It is identified that severe wear reduces the fibre cross section until the fibre fails under tensile loading, and that for nylon and polyester local shear stresses caused by the surface friction cause wear by surface peeling. (22)

“Fracture of common textile fibres” by Hearle, also a chapter in (21), discusses the fracture of polymeric fibres among other materials. It is identified that fracture of melt spun synthetic fibres, which PP is identified as, occurs at the yield strength of the material. It is also explicitly stated that an unorientated fibre will fail at the same load as an orientated fibre, but at a higher extension, because the polymer chains are able to deform, but at some point the structure can no longer deform and as a result the polymer chains break, and rupture occurs. Whilst the work is very informative, it does not mention PP which is of course the material under investigation, and so it has been assumed that PP fails in a similar manner. (23)

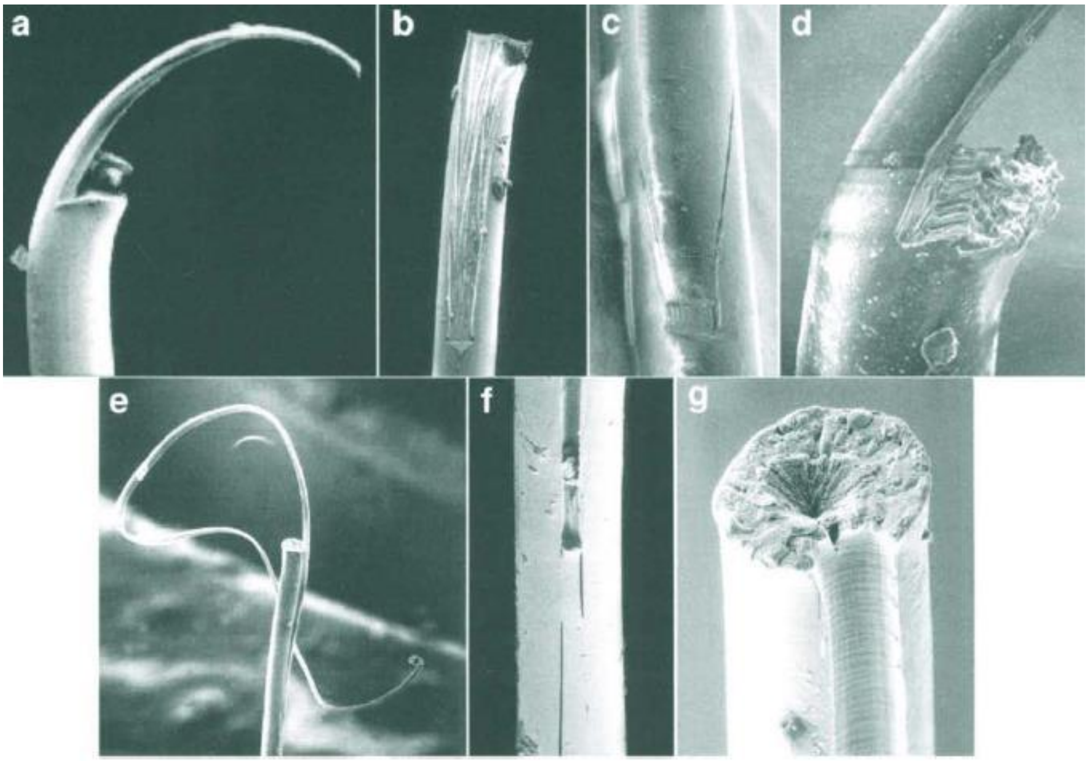

Figure 9 – Tensile fatigue failures of nylon (a-d) and polyester (e-g) from (22)

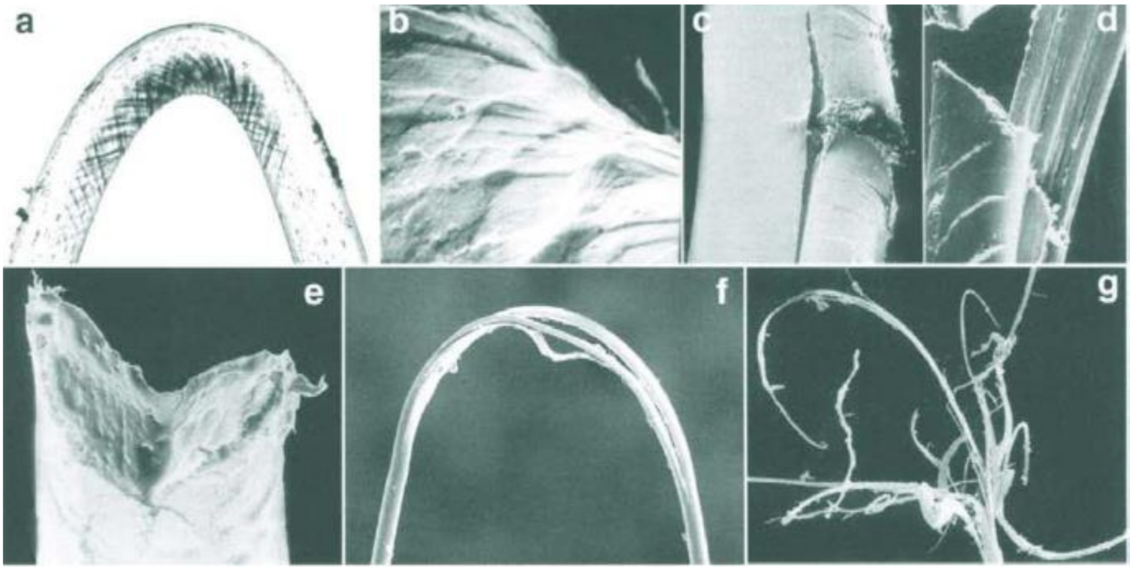

Figure 10 – Axial splitting Polyester fibres from (22)

Figure 11 - Biaxial rotation fatigue of polyester fibres from (22)

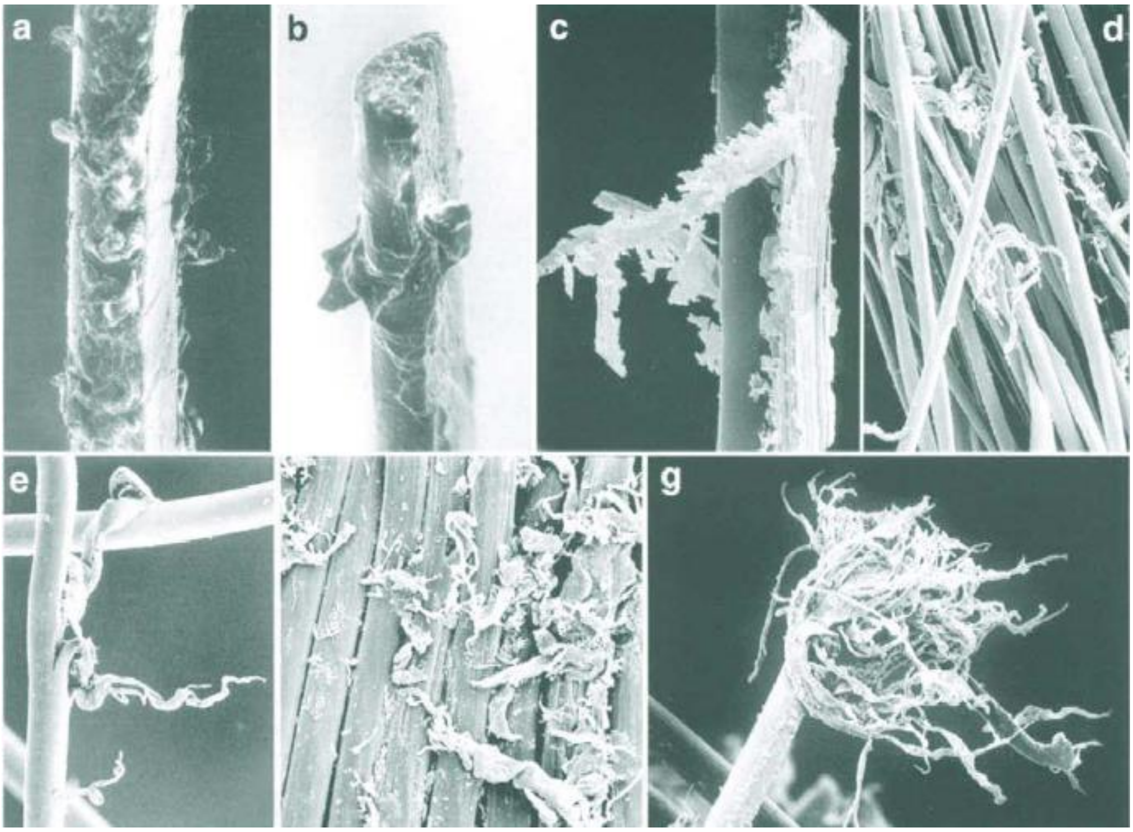

Figure 12 - Surface abrasion of various kinds of fibres from (22)

Lui, Tandon and Wood built on the work by Carnaby developing a model to predict the lifetime of wool carpets. Knowing Carnaby proposed the durability of wool carpet is determined by its initial conditions, life distribution of fibres, and fatigue site distribution along fibres, whilst assuming the contact distance between fatigue sites is constant. This assumption was made because it was believed the main form of fatigue failure was inter fibre contact, however this was no longer believed to be true. Thus the authors develop the model given by Carnaby, by allowing for arbitrary initial conditions, life distribution and fatigue site distribution along a fibre, allowing for the now believed major causes of fatigue failure in wool carpets, axial compression and surface shear forces. Additionally in this paper they identify that the properties of carpets evolves with time and that the state of each event depends on the entire history of the carpet. (24)

2.3 Engineering Literature

As with the carpet literature where work has been done to investigate how carpets affect walking, there is some literature that has investigated the relationship between the composition of the sports surface from a more mechanical/engineering perspective and how this relates to biomechanical aspects, such as Zanetti et al (25). In this particular study energy storage, energy losses and traction coefficient were investigated and it was found that the various artificial sports turfs tested were less stiff and provided more traction than natural turf. This type of work looked at how the artificial sports turfs compared to natural grass, and did not consider the variation of mechanical properties over their lifetime or how these might be improved.

Given the structure and composition of the artificial sports turfs it is important to understand the nature of composite and polymeric materials in relation to their tensile, fatigue and tribological behaviour. Finally, it is important to understand the factors that are important when imaging the samples.

2.3.1 Composite Materials

Given the nature of the artificial sports turf and its construction it was assumed the artificial sports turfs will behave broadly similarly to a composite material, with the SBR latex acting as the matrix for the PP fibres and the filler material taking a non-structural role.

A composite material is any material that contains any two or more components with distinct properties and boundaries combined (26). One of the materials comprises the matrix (essentially the bulk) of the composite. The other material is of the form of the reinforcing component that increases the properties of the matrix in some way, for example the stiffness.

As well as the properties of the matrix and the reinforcing component, the properties of the interface between the two is an important factor in the properties of the composite as whole, as the interface has a significant influence on the crack propagation in the composite.

There are two types of composite material. The first type, of which there are two subtypes, are called filled materials. The main feature of this type is a matrix which is filled with particles of another material to improve the properties of the material. The first subtype, large – particle composites, is filled with particles large enough such that the particle – matrix interactions are not atomic, shown in Figure 13. Typically these particles are larger than 500 µm. For this type of filled material under load the matrix transfers some of the applied stress to the particles, and failure occurs when the bonding between the particles and the matrix is insufficient to restrain movement of the matrix. The second subtype, dispersion-strengthened composites, are filled with much smaller particles, typically 0.01 to 0.1 µm such that the strengthening mechanisms occur on the atomic level shown in Figure 14. As this type of composite is not the type of material the artificial sports turfs are, they are not considered in the project. For this second type of filled material under load the matrix provides most of the mechanical properties whilst the filler prevents dislocation movements within the matrix. As such, failure occurs when a crack is initiated in the matrix that is not stopped by the filler as it propagates through the matrix. (4)

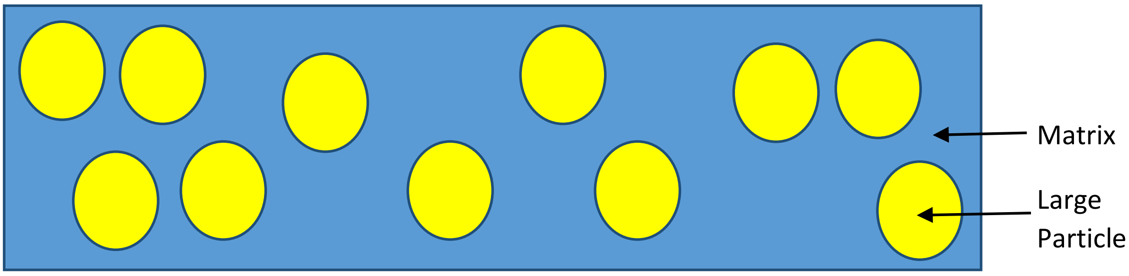

Figure 13 - Diagram of a large particle composite

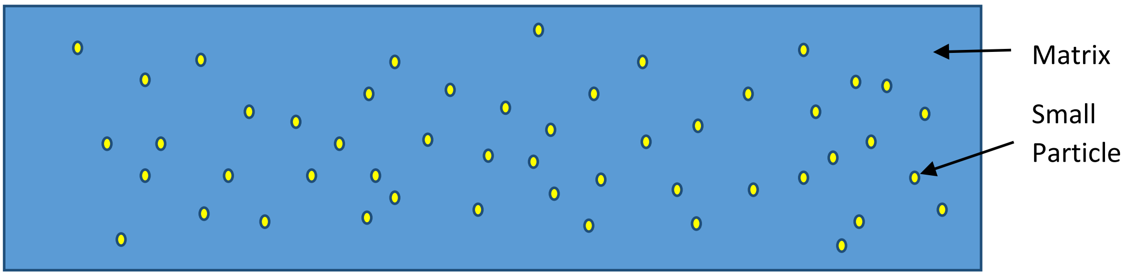

Figure 14 - Diagram of dispersion strengthened composite

The second type of composite materials are called reinforced materials, sometimes called advanced composites. These composites consist of a matrix whose properties are improved by the presence of long thin fibres which possess high stiffness and strength as shown in Figure 15. Normally the volume fraction of the matrix is less than 50%, and the fibre length (L) is at least 15 times greater than the critical fibre length (L_c), the length at which the fibres produce effective strengthening or stiffening. The properties of this type of composite are usually determined by the properties of the fibres themselves. (26) This second type is not to be confused with composite laminates, a form composite that are made up from layers of fibres.

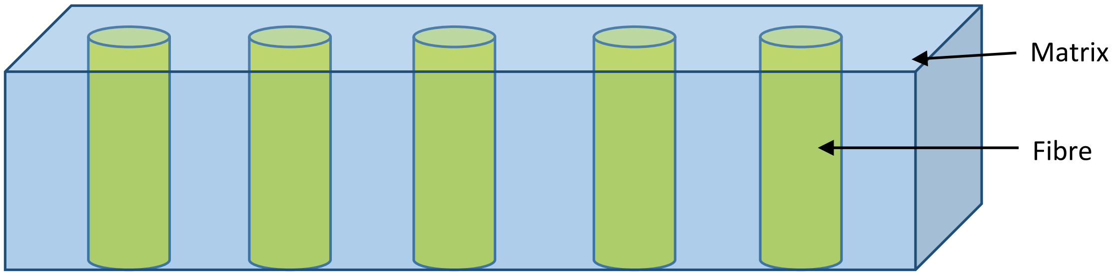

Figure 15 - Diagram of a reinforced material

There are composites that only have short fibres in the matrix, where L <15L_c. Under load, the matrix deforms around the fibre to the extent that there is virtually no stress transference to the fibres, and the fibres offer virtually no reinforcement.

Additionally, there are composites that employ short and randomly oriented fibre reinforcements. Normally when the fibre orientation is random, short and discontinuous fibres are used. Applications experiencing totally multidirectional applied stresses (such as running/turning in different directions) normally use this type of composite, as the mechanical characteristics are isotropic, albeit lower than aligned composites. (4)

Polymer matrix composites consist of a polymer resin as the matrix, with the fibres as the reinforcement medium. This type of composite is used in the widest range of applications due to the ease of fabrication, room temperature properties and low cost. Examples of this type of composite are; aramid fibre reinforced polymer composites (AFRP), carbon fibre reinforced polymer composites (CFRP) and glass fibre reinforced polymer composites (GFRP). (4)

2.3.2 Tensile Testing

Tensile testing is widely used to establish the mechanical properties of engineering materials. Typically when a tensile test is conducted, the load initially causes the specimen to deform elastically until the yield point is reached, after which the specimen deforms in both an elastic and plastic manner.

The mechanical properties that can be obtained include the ultimate tensile strength (UTS), the strength of the material when fracture occurs, the proportional limit, when the sample no longer obeys Hooke's Law (Equation 1) and the yield strength or proof strength of the material.

$$F = -kx$$

Equation 1 - Hooke's Law

In Equation 1 F is the applied force, k the spring constant of the material, and x the displacement.

The yield strength is the strength at which the material being tested stops being wholly elastic and plastic deformation occurs, and thus the sample becomes a plastic material. This is to be avoided because a structure that has plastically deformed may not be capable of functioning as intended.

The UTS is calculated by finding the maximum value on the stress strain curve. An example stress strain curve for both a brittle and ductile material is shown in Figure 16. The proportional limit is where the of the elastic region gradient deviates from a straight line. The yield strength is the intersection of the stress strain cure with a straight line, with the same gradient as the elastic region of the stress strain curve, however at some strain offset, typically 0.002. This is also known as the 0.2% proof stress, also shown in in Figure 16. (4)

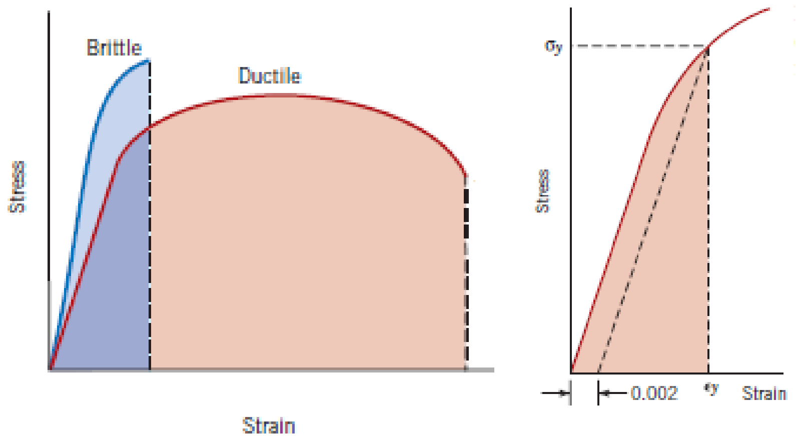

Figure 16 - Stress strain curve for brittle and ductile metal (left) and calculation of yield strength (right), reproduced from (27)

Tensile testing also gives an indication of the ductility and stiffness of the material. Ductility can be found by measuring the length of the test piece accurately along the gauge length before and after the test and or the smallest diameter of the test piece after the fracture has occurred. The results are reported as elongation and reduction in area respectively. The stiffness is the gradient of the elastic region.

Factors that should be considered in the tensile test are specimen shape, specimen dimension, and grip and face selection, specimen alignment and more.

A test specimen can take various dimensions but certain characteristics are common. The central portion, the gauge length must be straight and aligned with the direction of the applied load. If the gauge length is not straight, estimation of the cross sectional area becomes difficult, as the failure will occur at an area not representative of the specimen as a whole. Additionally, any defect in the gauge length from the cutting of the sample must be avoided, as any cut or notch could contribute to a failure occurring where one would not occur normally. Finally, the gauge length must smoothly merge with the heads of the sample, to prevent any stress concentrations. For these reasons, it is necessary to ensure the sample preparation is conducted carefully.

If the sample is not correctly aligned with the direction of the applied load, a bending moment could be generated, and side slip could occur, which invalidates the test.

Face and grip selection is important. If improper grips are used, specimens may slip or break inside the clamped area, (known as jaw break) which invalidates the test. The faces should cover the entire area to be gripped. Serrated faces should not be used when testing ductile materials, as the serrations may cause damage that could contribute to jaw break.

2.3.2.1 Tensile Behaviour and Failures of Polymers

On the basis of stress strain behaviour, polymers can fail in three different methods, brittle, plastic and highly elastic. Brittle failures are characterised by a fracture during elastic deformation. The plastic method is similar to the way metallic materials fail, with an initial elastic deformation followed by a transition to plastic deformation. Highly elastic failures only have elastic deformation and do not transition into plastic deformation. (4) The polymers that fail in this manner are called elastomers, and typically have low elastic moduli. Styrene butadiene is an elastomer. (5)

Polymers are neither as strong nor as stiff as metals. For example PP has a UTS of 27 MPa to 40 MPa and an elastic modulus approximately 0.5 to 1.9 GPa, (5) whereas 1020 steel has a UTS of 380 MPa and an elastic modulus of 207 GPa (27), although the properties depend on the processing. Additionally unlike metals, the behaviours of polymers are sensitive to changes in environmental conditions and strain rate.

A number of polymers, including PP and PE exhibit viscoelastic behaviour, in that at certain temperatures they behave as both an elastic material and a viscous material.

Both brittle and ductile fracture modes are possible for polymers. Some materials transition from failing in a ductile mode to a brittle failure mode depending on temperatures. Some polymers exhibit crazing during failure (discussed in 2.3.3.1) which can increase the ductility and toughness of the material. (4)

2.3.2.2 Tensile Behaviour and Failures of Composites

As stated above, failure for large particle filled materials occur when the bonding between the particles and the matrix is insufficient to restrain movement of the matrix in the presence of a load.

Additionally, failure occurs for dispersion-strengthened composites when a crack is initiated in the matrix that is not stopped by the filler as it propagates through the matrix.

When the fibres are very stiff and the matrix is relatively soft, reinforced materials normally fail when an applied load is great enough to either break the cohesion between the fibres/matrix, pulling the fibres out of the matrix, or when the applied load causes the fibres to break within the matrix. (4) In both situations the failure causes the matrix to take the load, which it cannot handle, and also fails. This gives great toughness because the failure occurs over the fibre – matrix interface, which increases the surface area of the fracture surface.

This is the case for the artificial sports turfs provided given the elastic modulus of Styrene Butadiene is 0.002 GPa to 0.01 GPa (27), and the elastic modulus of PP is 1.14 to 1.55 GPa (4).

2.3.3 Fatigue Testing

Fatigue testing can simply be defined as cyclically applying a load, whose maximum amplitude is much lower than the yield point of the material, to a test specimen until it fails to understand how it will perform under similar conditions to actual usage. (28)

The load can be applied cyclically in 3 different ways. The simplest way is when the load is applied in either a sinusoidal/triangular fashion with the minimum and maximum stress/load of equal magnitude but of opposite sign, such that the mean is zero. This type of stress cycle is called a reversed stress cycle, illustrated in Figure 17. When the maximum and minimum are not symmetric, it is a repeated stress cycle shown in Figure 18. The repeated stress cycle is the most common stress cycle in engineering.

Finally, it is possible to have the load applied with a random frequency and load, called a random stress cycle, illustrated in Figure 19. In this type of stress cycle only cycles that exceed a certain threshold will contribute to the growth of a fatigue crack. The loads can be compressive in a random stress cycle, which is not shown in Figure 19. (4)

For fatigue failure to be initiated, there are three factors that must be considered. Firstly, the maximum values of the stress levels must be high enough to exceed the fatigue limit of the material; otherwise the fatigue failure will not be initiated. The magnitude and direction of these values is irrelevant to some extent, may even change with time, so long as the loading cycles are sufficiently large to allow fatigue to initiate.

Secondly, the material must undergo a large number of cycles under the applied stress cycle. If this is not the case it suggests there is either a defect in the sample causing a stress concentration and thus the sample to fail early or the experimental conditions have been set incorrectly.

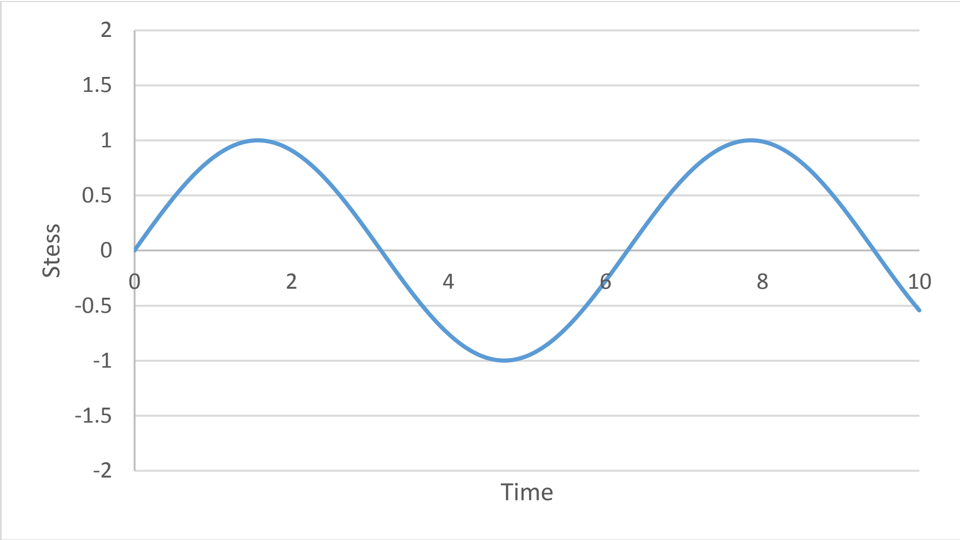

Figure 17 - Diagram of a reversed stress cycle

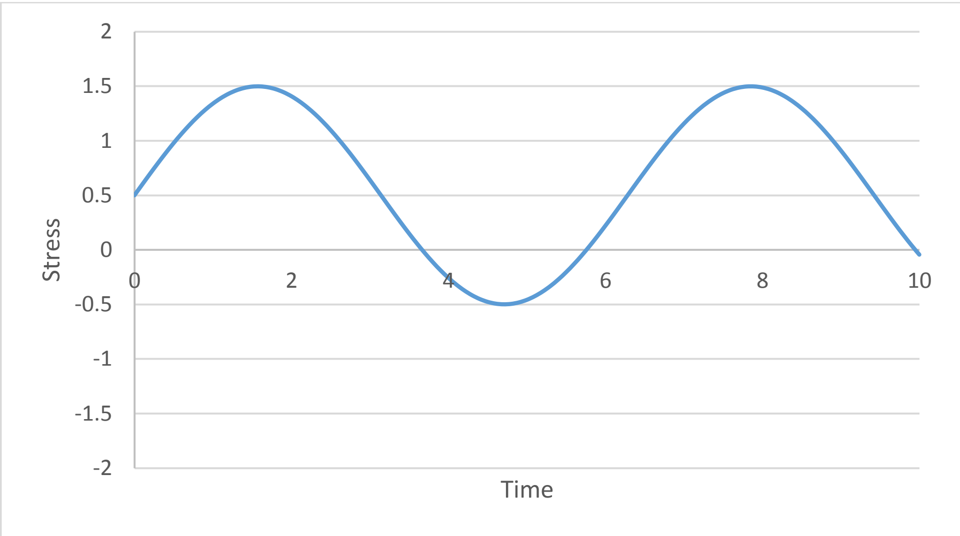

Figure 18 - Diagram of a repeated stress cycle

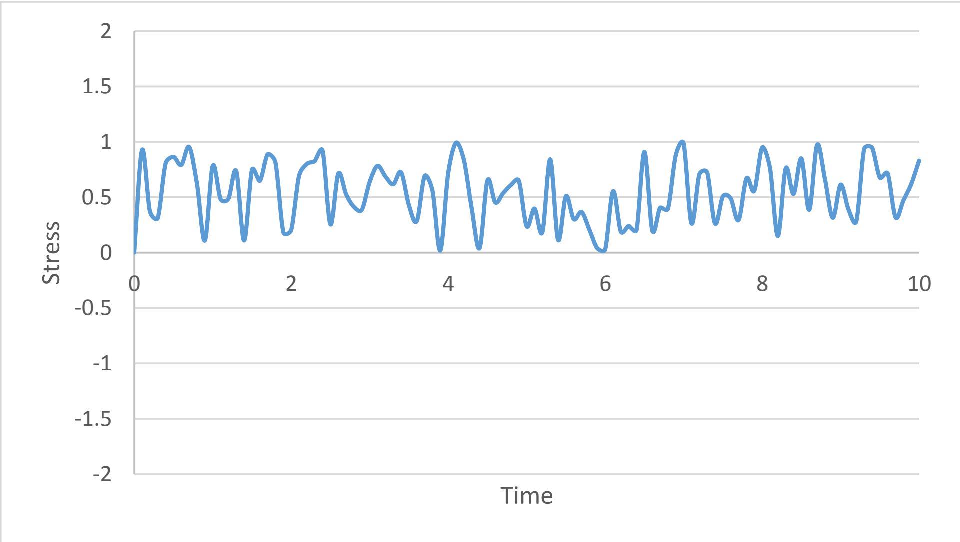

Figure 19 - Diagram of a random stress cycle

A fatigue failure occurs in the following five stages.

1. Sub structural and microstructural changes which cause nucleation of permanent damage.
2. Creation of microscopic cracks
3. Growth and coalescence of microscopic flaws to form dominant cracks.
4. Stable propagation of the dominant macro crack.
5. Structural instability or complete fracture.

During stage 1 the stresses on the material cause the permanent damage to form, which then causes stage 2 with further stress cycles. With more cyclic stresses the cracks generated in stage 2 become dominant cracks (stage 3). During stage 4 the dominant crack steadily grows through the sample, which ultimately leads to stage 5 and failure of the material.

Typically the data from a fatigue test is presented by plotting the stress against the logarithm of the number of cycles to failure N_f, called an S-N curve, shown in Figure 20. There are two types of behaviour that can be observed, which depend on whether the material being tested has a fatigue limit.

When a material has a fatigue limit, the gradient of the S-N curve will gradually tend to zero, after which a fatigue failure will not occur, illustrated in Figure 20. A material that does not have a fatigue limit will continue down the S-N curve with increasing N illustrated in Figure 21. For these materials, the response to fatigue is called fatigue strength and is classified by the stress level at which failure occurs at a specified number of cycles, known as the endurance limit.

Fatigue is statistical in nature. Not every sample of a given material will fail after precisely same number of cycles, therefore a large testing regime with some statistical analysis is needed to quantify the fatigue behaviour of the material in question.

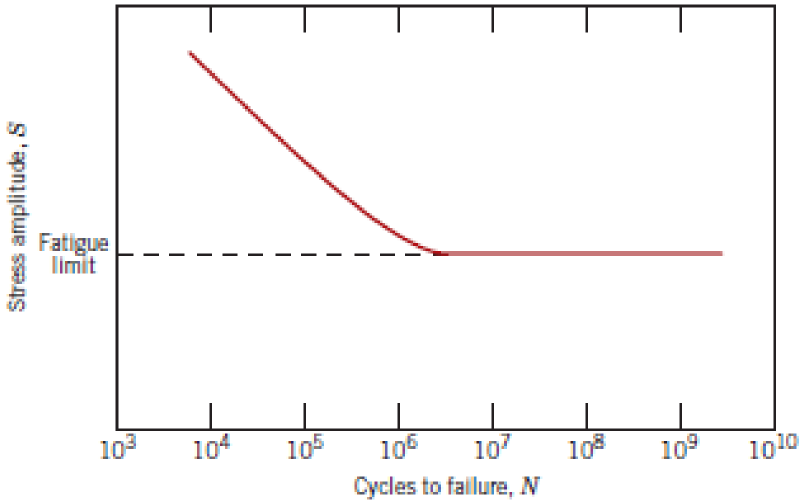

Figure 20 - Typical S-N curve of a material that exhibits a fatigue limit, reproduced from (27)

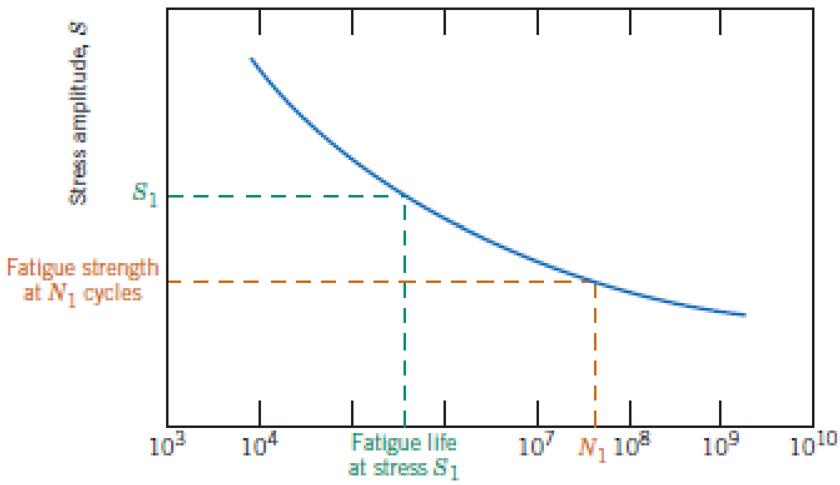

Figure 21 - Typical S-N curve of a material that does not exhibit a fatigue limit, reproduced from (27)

There are 3 ways of applying the stress to a sample. Tension – compression fatigue testing where the load is applied axially has been employed. It also possible for the applied stress to cause a flexural (bending) or torsional (twisting), however these modes of loading have not been considered in this project, although the literature did show that the foot of an athlete can impart a torsional load.

The factors which can influence a fatigue test are similar to the factors that can affect a tensile test; these factors are specimen shape, specimen dimension, grip and face selection, specimen alignment, specimen preparation as well as the type of stress cycle and more.

Paris's Law relates the stress intensity factor range to sub-critical crack growth under a fatigue stress regime, and in its simplest form is;

$$\frac{da}{dN} = C\Delta k^m$$

Equation 2 – Paris's Law

Where a is the crack length, N is the number of cycles (da/dN is the crack growth rate), C and m are material constants, and k is the stress intensity factor given by;

$$k = \sigma Y \sqrt{\pi a}$$

Equation 3 - Stress intensity factor

Where Y is a dimensionless constant that depends on the geometry of the system and the other symbols have their usual meaning. (29)

With integration and rearrangement, it is possible to calculate the number of cycles to failure N_f, which is given by

$$N_f = \frac{2\left(a_c^{\frac{2-m}{2}} - a_i^{\frac{2-m}{2}}\right)}{(2-m)\, C\, (\Delta\sigma Y \sqrt{\pi})^m}$$

Equation 4 - Rearrangement of Equation 2 and Equation 3 to give N_f

Where a_c is the critical crack length and a_i is the initial crack length.

2.3.3.1 Fatigue Behaviour and Failures of Polymers

With the exception of some modes of deformation such as craze formation or the rotation of molecular chains, the mechanisms for deformation and failure in polymers exhibit many similarities to other materials. Under cyclic loading, polymers display deformation modes (such as stress strain hysteresis and cyclic softening) and subcritical crack growth analogous to atomic (i.e. not polymeric) solids.

In polymers, the deformation can be manifested as crazing, shear band formation, rotation or other changes in the orientation of molecular chains, or a combination of these mechanisms.

A craze is a region of very localized plastic deformation causing micro voids to occur, shown in Figure 22, which can lead to crack formation, Figure 23. Unlike a crack, a craze can support a load across itself causing the micro voids become elongated. (29)

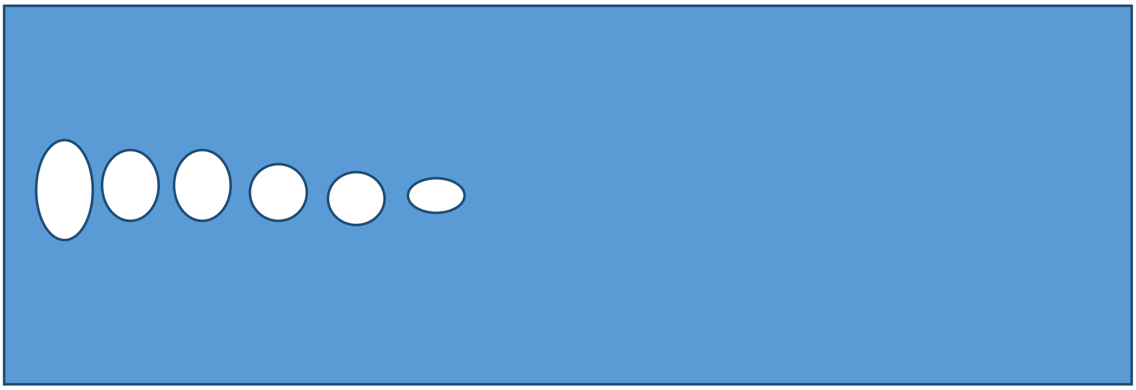

Figure 22 - Diagram of craze formation, reproduced from (29)

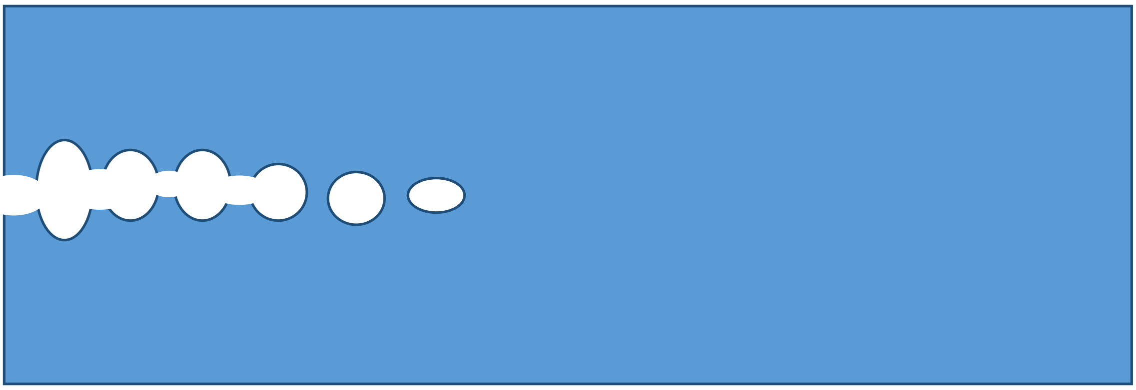

Figure 23 –Diagram of craze formation preceding a crack, reproduced from (29)

Polymers differ in fatigue performance from metals in that polymers are more sensitive to loading frequency, as high frequencies and/or relatively large stresses can cause localised heating and as such failure may be due to a softening of the polymer rather than as a result of a typical fatigue process. (4)

2.3.3.2 Fatigue Behaviour and Failures of Composites

The fatigue behaviour of composite materials depends on the fibre arrangement, volume fraction and the properties of the reinforcing component and matrix, as these factors determine how the applied load is distributed throughout the composite. Under cyclic stresses little damage is done until fibre fracture is initiated, at which point the load becomes slightly redistributed with each cycle within the region of the damaged fibres, leading to fatigue damage. As this only occurs at high stresses, fatigue performance can be very good for composites. For randomly distributed fibre composites, micro cracking by debonding can occur in regions of transverse fibres at relatively low stresses. During the cyclic loading these micro cracks grow and propagate through the matrix.

2.3.4 Wear Testing

Wear testing is a general term for many methods of assessing the lifetime of a component and the wear mechanisms the component experiences. Wear itself is a process by which material is progressively removed from a surface due to relative motion. (30)

There are three different contact situations that may cause any of the wear mechanisms described below to occur in the artificial sports turfs during their lifetime. These contacts situations are sliding, rolling and impact.

Sliding is defined as the relative motion of two surfaces in contact. The motion is tangential to each surface, which has more potential to cause wear than motion normal to the surface. Very severe sliding conditions may lead to high heat generation and seizure in the contact, potentially causing a thermal breakdown of the surface.

For an artificial sports pitch sliding is likely to occur when the fibres become pressed against each other beneath a footstep or other event, very severe sliding conditions are unlikely to occur without the influence of external factors, such as high ambient temperature.

Rolling is defined as one surface rotating against another; as either non-slip conditions where both surfaces move at the same velocity, or slip conditions where the surfaces move at different velocities. Slip causes some sliding motion to occur within the contact. In rolling situations, wear usually occurs through fatigue mechanisms acting perpendicular to the surface. The force acts perpendicularly, the subsurface crack may form and propagate parallel to the surface, normal to the applied load.

Rolling might occur briefly if a fibre becomes twisted beneath a footstep, but prolonged rotation is unlikely to occur.

Impact is defined as two separate surfaces coming into contact. It may occur as either percussive (where a large body impacts against another large body) or erosive (where many small bodies impact against a large body). Percussive impact may occur in three different ways, depending on the relative motion of the bodies. If the impact is normal between the surfaces (with no relative motion) there should be no sliding. This can be the least severe form of percussive wear, depending on the damage mechanism and impacted body. For example, erosion of metals is low when the impact is normal to the surface but high at decreasing angles of impact; conversely wear on a ceramic material is highest when the impact is normal to the surface. If the impact is normal with relative motion the wear is more severe and sliding may occur. Tangential impacts will cause sliding to occur.

Percussive impacts are guaranteed to occur between the fibres impacting against other fibres underneath a footstep. Erosion may occur between the sand particles and the fibres/backing materials under foot. (31)

There are seven different types of wear mechanism. These are abrasive wear from contact with hard granular materials, abrasive wear from hard particles trapped between moving surfaces, adhesive wear from the rubbing together of smooth surfaces, fretting, cavitation erosion, particle erosion and surface fatigue. (30)

Of these seven different types of wear mechanisms, two are expected to dominate the tribological behaviour of the artificial sports turfs. These are;

Abrasive wear which occurs when material is removed from a surface by a cutting action, where one body is harder than the other. For example, filing a surface down. It can also be caused by hard particles being trapped between two smooth surfaces rubbing against each other, shown in Figure 24. This is expected to occur in the artificial sports turfs, as sand particles are present. Abrasive wear can typically be identified by damage ranging from fine scratches to deeper gouges occurring on the surface. For more ductile materials, the debris could be removed in a spiral form, however in the case of more brittle materials the debris tends to be in the form of chips, caused by localised brittle fractures.

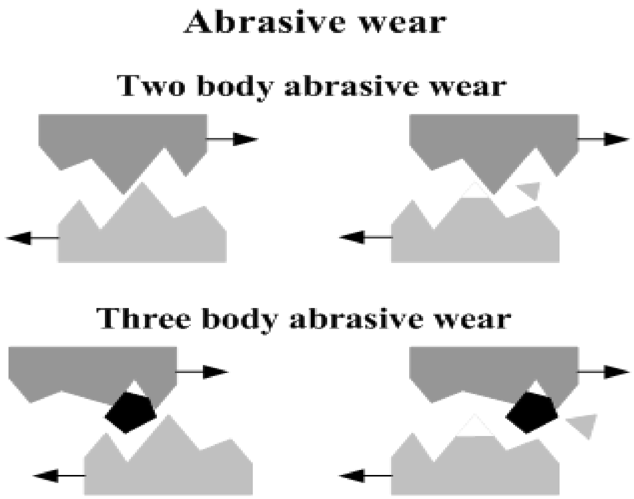

Figure 24 - Diagram of abrasive wear reproduced from (32).

Adhesive wear is where material is removed from a smooth surface due to polishing against another smooth surface. No surface is “perfectly” smooth, and thus two surfaces rubbing against each other have peaks where concentrated loading occurs. As a result these peaks adhere to each other and pull material away and along the surface, illustrated in Figure 25. This mechanism could occur in the artificial sports turfs being tested, if the fibres in them slide past each other underfoot. Adhesive wear can be identified by surface polishing on the sample, with debris being removed as fine flakes, or can show severe surface damage due to the surface dragging or even seizure.

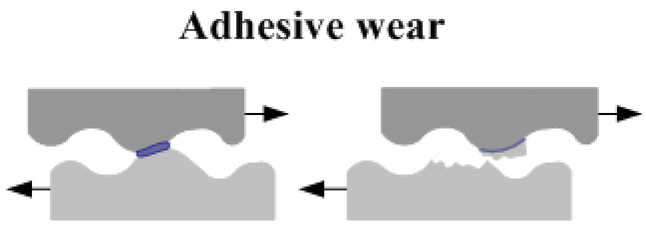

Figure 25 - Diagram of adhesive wear, reproduced from (32)

Additionally, there are three more types of wear mechanism that could affect the tribological performance of the sample. These are;

Fretting, a form of adhesive wear which occurs when there are small oscillatory movements between two surfaces. An example of this is the wear on gear couplings. Fretting often produces fine powdered and oxidised wear debris, which leads to surface damage and roughening of joint surfaces. It is assumed fretting does not occur in the artificial sports pitches.

Erosion is a process by which material is removed by a high speed impact of a liquid or a stream of hard particles carried by the liquid. This is not investigated in the project.

Finally, surface fatigue is a mechanism in which material is lost due to fatigue cracks in the surface connecting, creating loose particles, as illustrated in Figure 26. This mechanism occurs due to either contact or thermal fatigue, so cracks may form either on or under the surface depending on the tribological/environmental conditions. The contact fatigue mechanisms can occur to the artificial sports turf in use, due to the rolling of a ball or foot causing alternating tensile and compressive stresses.

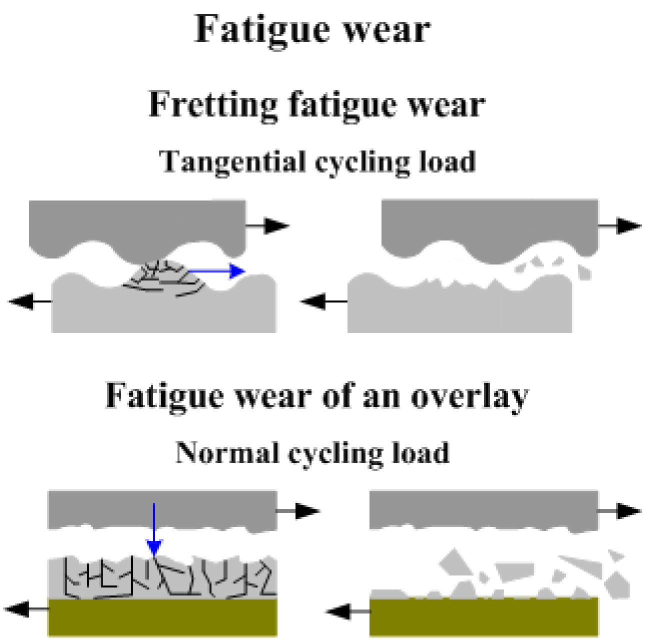

Figure 26 - Diagram of fatigue wear reproduced from (32).

Wear testing may cause a wear track to form. This is the area affected by the wear event, and is typically a groove worn into the surface of the material. The dimensions of the wear track are determined by the specific parameters of the rub. (33)

2.3.4.1 Polymer Tribology

The main mechanisms of wear for polymers are adhesion, abrasion, and fatigue. (34)

Adhesive wear occurs when the surface of a polymer is wearing against either a like or an unlike surface, for example, a polymeric sole of a football shoe or a metal stud. When adhesive wear occurs in polymers, the strength of the adhesive bonds formed between the counter face and the polymer (friction joints) can be greater than the cohesive strength of the polymer. The cohesive forces in polymers are Van der Waals forces, which hold the molecular chains together, can be stronger against an unlike material, e.g. a metal stud. When this happens, some material is transferred from the softer polymer to the hard counter face and forms a transfer film, whilst other material is removed as wear debris, shown in Figure 25. If the polymer film is continually removed and reformed, the wear rate significantly increases. When the film is held in place, friction occurring between the like surfaces may cause seizure. Spreading of the film across the counter face may cause an abrupt jump in frictional force, but the wear rate will not change significantly. The affect the transfer film has on the friction is largely dependent on the material. For example, a transfer film from ultra-high molecular weight polyethylene (UHMWPE) has the tendency to decrease the friction.

When a transfer film forms on a counter face, it will normally accumulate on asperity ridges, which are areas of highest adhesion. The transfer films build up in layers, aligning with the direction of propagation. (35)

This film transfer also affects the roughness of the two surfaces. The surface of the polymer will undergo large variation during the running in stage, whilst the roughness of the counter face is altered by the addition of the transfer film.

It is possible for material from the hard surface to transfer to the softer material under certain conditions, in which particles become embedded into the softer surface and then act as an abrasive against the harder material. An example of this is bronze on polymer. Sand particles in the artificial sports pitch may cause a similar phenomenon, and become embedded in a polymeric counter face.

Abrasive wear occurs in two distinct modes of deformation, plastic grooving (ploughing) and cutting. Ploughing is when a prow is pushed ahead of a particle resulting in material being continually displaced sideways forming a distinct groove. Material is not removed from the surface during this mode, and forms ridges either side of the groove. Cutting is when the material displaced is removed as wear debris.

Fatigue wear of polymers, as with metals, occurs when cracks propagating through a surface due to cyclic stresses connect, and material is released.

As with metals, three stages of wear can be observed. These are running in, steady state regime and catastrophic wear. During the running in stage the film transfer occurs, followed by steady regime wear (in which material is steadily removed) until catastrophic wear which may cause a component to fail. (34)

2.3.4.2 Tribology of Composite Materials

Studies investigating the wear of composite materials have shown four different processes dominate the process of material removal. These are matrix wear, fibre wear, fibre cracking and fibre/matrix separation at the interface (delamination). It is often assumed that these last two occur sequentially and are considered as one combined process. (36)

Matrix wear is typically due to standard wear mechanisms such as plastic deformation, ploughing, cutting and cracking caused by the counter face being in contact with the matrix.

Fibre wear becomes important once enough of the matrix has been worn away. It is dependent on the orientation of the fibres. Wear of the matrix and fibre occurs at the same rate until the depth of approximately half of the diameter of the fibre, at which point the fibres start to detach and release debris. For parallel/anti parallel fibre orientations, this debris can be of the form of small particles or larger pieces of fibre. This debris also causes an additional matrix wear process because these fibre particles can act as third body abrasives. Wear debris from the matrix is typically a fine powder.

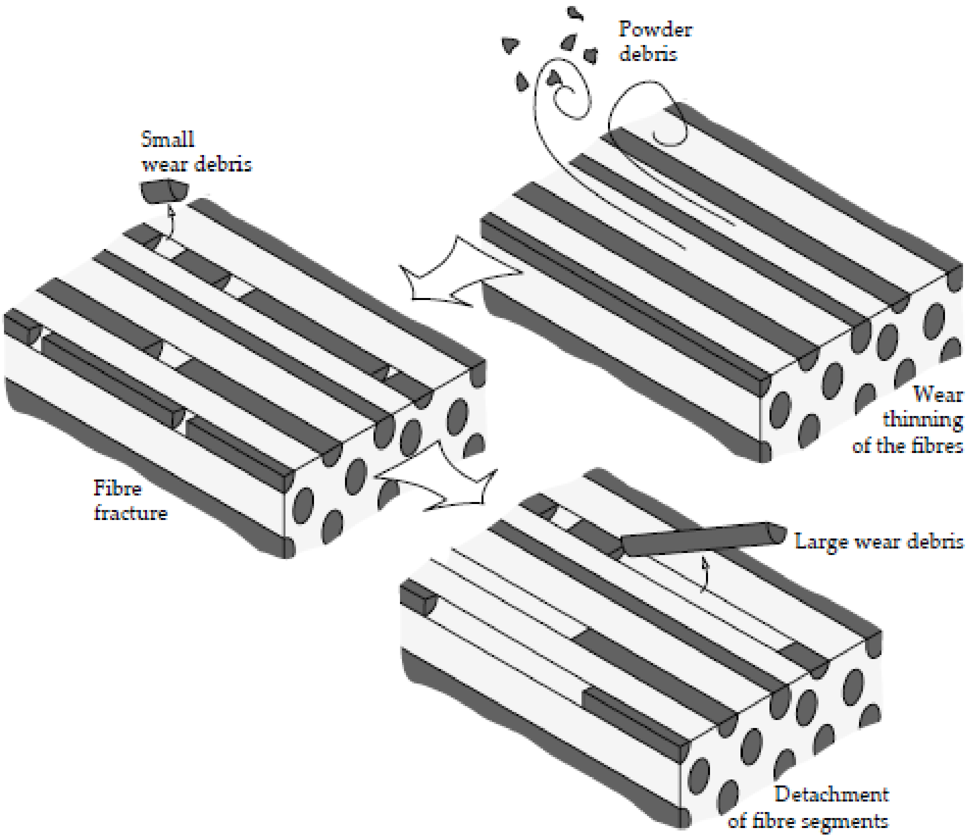

Figure 27 - Diagram showing a wear process in a composite, reproduced from (37)

The wear mechanism of normally oriented fibres is different because partially worn fibres remain firmly attached in the matrix. The wear process subjects the fibres to repeated bending, which gradually creates a crack between the fibres and the matrix, in a fatigue type process. As such, a simultaneous process of fibre/matrix cracking and fragmentation of the fibre ends allows material to be released as wear debris.

Polymer composites with parallel fibre orientation are the most preferable followed by the anti-parallel types. Polymer composites with the normal fibre orientation give a low wear rate but risk sudden seizure, because the exposed normal fibres tend to gouge into the counter face and initiate severe wear or seizure.

Unidirectional and woven reinforcements do not offer greatly improved wear resistance over short fibre reinforcements for wear against smooth steel counter faces. Wear rates under these conditions are usually controlled by crack propagation between fibres and matrix. These reinforcements offer far more favourable crack propagation conditions than short fibre reinforcements, where many cracks are formed for each fibre. This causes rapid wear due to crack propagation releasing wear particles into the wear system.

Fibre reinforcements are effective in reducing the matrix wear so long as there is strong adhesion between the matrix and fibres. In a matrix with a lower wear rate, this beneficial effect is not as pronounced. (38)

Polymer composites often exhibit good wear resistance when in contact with a smooth counter face where adhesive or fatigue wear would prevail, however show inferior wear resistance compared to the unimproved polymer under conditions of abrasive or erosive wear. (37)

2.3.5 Imaging

The imaging of worn samples is not trivial, and so multiple different methods of imaging the artificial sports turfs to analyse the structure of the specimens, the wear and tribological performance of the specimens were employed.

Optical microscopy is a method of imaging samples on a larger scale which was used in this project to investigate properties such as the fibre density in the artificial sports turf. In particular, factors such as focal length, magnification and ambient lighting affect the quality of the images. (39)

Obviously, if the sample is outside the focal length, then any images taken will be out of focus. If the magnification is set too high then two issues occur. Firstly, getting enough light on to the area of interest becomes troublesome, and secondly, due to the structure of the samples being investigated it becomes difficult to get the entire image in focus.

Environmental scanning electron microscope (ESEM) imaging is a method of imaging smaller structures and surface details, such as the damage on individual fibres. ESEM differs from SEM in that an environment is present in the vacuum chamber, which both prevents charge build up on the sample and helps conduct the signal generated to the detector. Factors that affect the use of an ESEM are beam voltage, filament current, generated secondary electron (GSE) gain, pressure and the pressure limiting apertures (PLA).(40)

If any of these factors are set too high, for example the beam voltage or filament current, then flaring can occur where the "tear drop" interaction (shown in Figure 28) occurs at an edge of the surface resulting in bright edges and a loss of image quality, illustrated in Figure 29. The greater depth of field ESEM imaging has overcomes some of the issues the optical microscopy encounters.

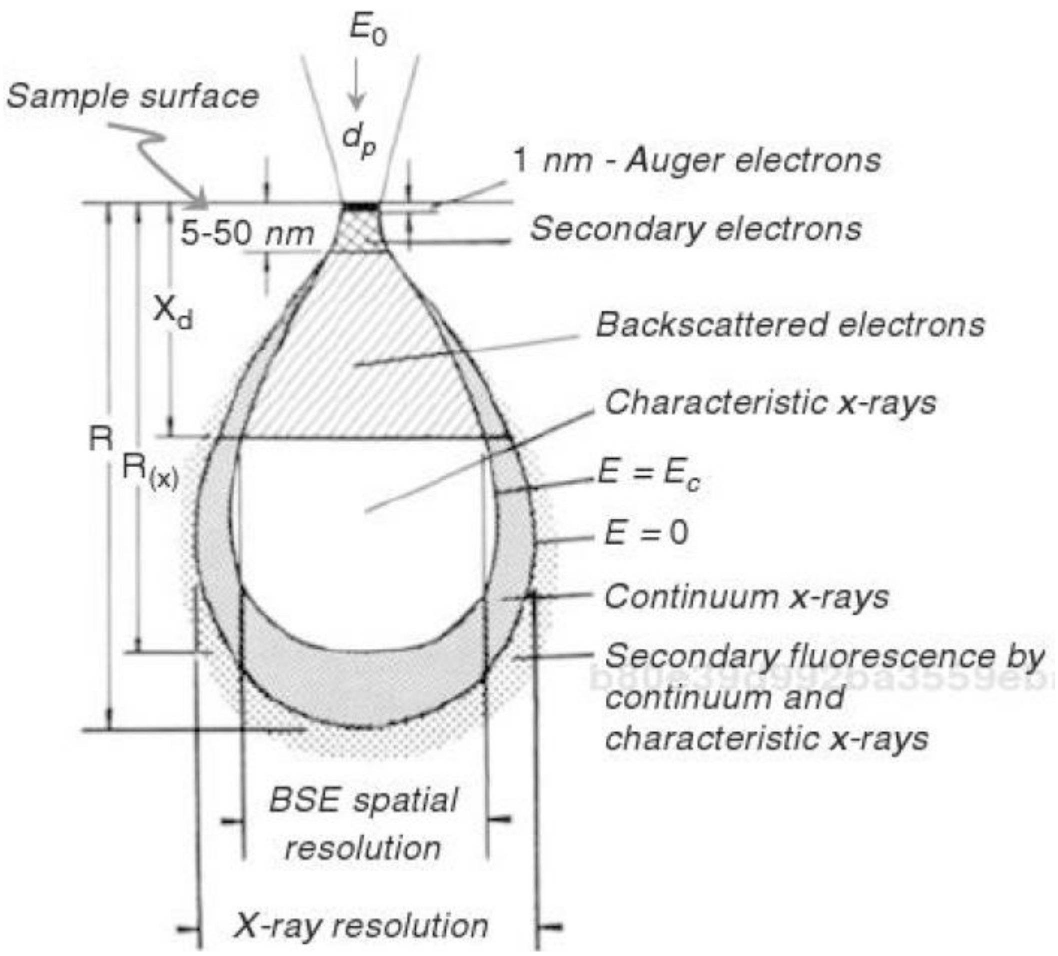

Figure 28 - Schematic of SEM interaction volume, reproduced from (41)

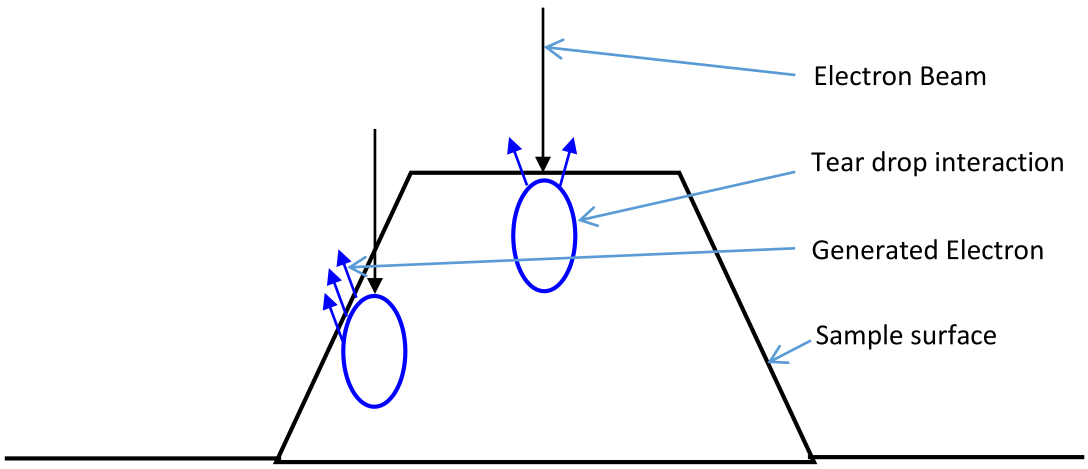

Figure 29 - Schematic drawing of flaring

In addition to these factors, the conductivity of the samples needs to be considered, as charging of the samples will negatively affect the images. The contrast and brightness of the images also affects the quality of the ESEM image.

ESEM was used because the polymeric nature of the samples means they are likely to become damaged by the electron beam, in that scission may take place at random along the polymer chain giving the production of smaller molecules, potentially depolymerisation causing “unzipping” of the polymers to occur. Therefore a lower energy beam is required and an environment to remove any charge build up. Additionally the nature of the samples requires low contrast and high brightness with a reasonable pressure of atmosphere is required to produce an image. (40)

X-ray computed tomography (CT) and micro X-ray CT are methods of imaging that were used as a method of imaging the distribution of the latex within the artificial sports turfs. Factors that affect the images taken are resolution of the scanner, the focal length, the size of the sample, the X-ray absorption/permeability of the samples and more.

Nuclear Magnetic Resonance Imaging (NMRI, aka MRI) is a method of in vivo imaging in medical applications. The MRI was also used as a method of imaging the distribution of the latex within the artificial sports turfs.

MRI uses the magnetic properties of spinning hydrogen atoms to generate a signal to produce an image. A strong magnetic field, of the order of 1.5 T to 3 T, is applied to the object being imaged. This forces the hydrogen atoms to align predominately parallel to the field lines. A second magnetic field is then applied at a frequency in the range of radio waves in the EM spectrum (the radio frequency pulse, aka RF pulse), which knocks the hydrogen atoms out of alignment and into a transverse plane. This induces a current which is used as the basis for the image.

Some of the key factors that affect the performance of an MRI scan are the proton density (number of hydrogen atoms present in the sample), the chemical environment of the hydrogen atoms, the magnetic susceptibility, and the T1 and T2 relaxation times. T1 relates to the time the net magnetisation vector takes to rotate back to the longitudinal direction and T2 relates to the spin of the hydrogen atoms and the time it takes for them to de-phase after the RF pulse. (42)

2.4 Literature Review Summary

Subchapter 2.1 covered the forces involved in the interaction between the foot and the artificial sports turf as well as the time the foot is in contact with the artificial sports turf, which are the most important variables for the testing conducted in this project. This subchapter also covered the testing some sporting bodies have had conducted. The major findings from these works are the loading phase, duration and forces involved, which the testing regime was built upon.

Section 2.2, covered how the wear may appear, that the resilience of a carpet is governed by the pile, the inelastic mechanisms and carpet fatigue mechanisms and that the carpets with a higher weft density should perform better in the wear testing. Voids/pores are expected to be observed in the carpets. It is also known that the mechanisms of deformation under load will vary depending on the age of the sample, and that the compliance modulus will affect the perceived comfort of the sample. The major findings from these works are how fibre failures are characterised, how they appear under SEM, and how wear accumulates in carpets, which allowed for comparison of samples imaged in this project.

In subchapter 2.3, the types of composite materials, the theory behind tensile and fatigue testing, and the factors that are important in the tensile and fatigue behaviour of polymers and composites has been covered. The fundamentals of wear testing and wear mechanisms in addition to the important factors relating to the tribology of polymers and composites are also discussed. Finally this subchapter has discussed the fundamentals of imaging the samples investigated in this project. The major findings from these works are what responses are expected from different materials during testing, and how to conduct the experiments correctly.

3 - Experimental Methods and Procedures

3.1 Recap of artificial sports turfs tested

Table 4 details the artificial sports turfs tested, as discussed in 1.2.

Manufacturer	Average Pile Yarn Weight	Colour	Usage	Sample number/name	Notes
Leigh Spinners	1150	Blue	New	1.x, 2.x	Not large enough to cut 6 samples.
	1300	Orange	New	3.x, 4.x	Not large enough to cut 6 samples.
	1150	Grass green	New	18.x, 19.x	
	1300	Grass green	New	7.x, 8.x	
Rawsons	1150	Grass green	New	14.x, 15.x	
	1150	Lavender	New	16.x, 17.x	
	1300	Terracotta	New	9.x, 10.x	
	1300	Green	New	11.x, 12.x	
American		Green	New	22.x, 23.x	
Unknown	1300	Green	13 years	P1 and P2 P1Hx, P1Vx P2Hx, P2Vx	1 m by 2.56 m.
Unknown	1300	Green	13 years	Worn in situ (square sample) 24.x, 25.x	1 m by 1 m.
NottsFilm stiff		White	New	5.x, 6.x	
No latex		Blue	"New"	20.x, 21.x	

Table 4 - Artificial sports turfs tested

3.2 Optical Imaging

Circular samples with a diameter of 77 mm (the largest diameter the pin on disc machine could hold), were cut by pressing a cylindrical tube with a sharpened edge through the artificial sports turf, and imaged under an Olympus SZX12 optical microscope. This was to investigate the structure of the fibres, the fibre density, the shape and size of the fibres within the artificial sports turfs and the damage on the fibres both before and after wear testing. Optical imaging was also employed to assess samples of the artificial sports turf that had been worn in situ. For each sample, images were taken at 9 points, shown in Figure 30, with suitable magnification.

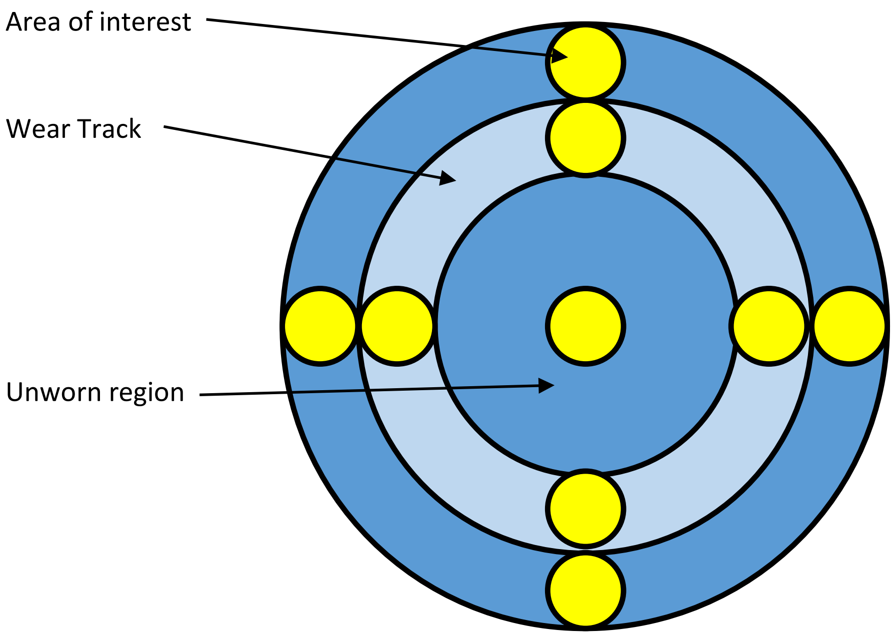

Figure 30 - Diagram showing positions of images on a 77 mm diameter disk

3.3 Environmental Scanning Electron Microscope

Samples were imaged with a Philips XL30 ESEM before and after wear testing to assess the structure of the fibres, their size and shape within the artificial sports turfs and the damage on the fibres. There were some minor issues as the samples were slightly too large for the stage in the ESEM, however these issues were overcome by carefully securing the underside of the sample to the stage in the desired position.

Other samples were simply cut into squares, with a Stanley knife, approximately 40 mm by 40 mm and placed in the ESEM. Care was taken to ensure no loose particles that could damage the turbofan in the ESEM were put in the chamber.

10 individual fibres, chosen by random selection, from the worn in situ square sample artificial sports turf were removed with tweezers and a scalpel from the same section, stuck to a carbon tab and imaged in the ESEM to see how the wear accumulates along the length of the fibres.

The pressure of the water vapour atmosphere was set to 0.9 Torr (0.11999 kPa). The beam voltage was typically set to 10 kV, sometimes 15 kV, and the filament current set to 40 amps. Spot size 5 was used for all images and the working distance was approximately 10 mm. No PLA were used for any image.

3.4 Resin ESEM

To investigate how well the latex/powder backing had bonded to the fibres, some samples were imaged in cross section. Portions of artificial sports turf (approximately 5 mm by 5 mm) were mounted into a general purpose low shrinkage epoxy resin that cured overnight. The resin was made by pouring 100 grams of epoxy resin and 23 grams of epoxy hardener (as recommended by the instructions) into a cup and then stirred thoroughly for 5 minutes before being carefully poured on to the samples, which had been placed into moulds. To ensure that the resin fully permeated the samples, the samples were vacuum impregnated with the resin. This was achieved by placing the moulds inside a vacuum chamber and repeatedly depressurizing the chamber to -0.8 atm (-81.06 kPa).

After the resin had set, the samples were removed from the moulds using a manual press. The resin was then ground back by use of a grinding/polishing machine and various silicon carbide abrasive papers of reducing grit levels (Table 5) before being polished to 0.25 µm diamond grit give a good imaging surface. The mounted sample was periodically observed under optical microscopes to assess the surface during polishing.

Stage	Grit level
1	240
2	320
3	600
4	800
5	1200
6	6 µm diamond
7	3 µm diamond
8	1 µm diamond
9	0.25 µm diamond

Table 5 - List of grit levels of SiC abrasive papers

3.5 Filler Materials

The filler materials (sand and egg shell particles) were imaged both under an optical microscope and ESEM. The particles were mounted on to a stand via a carbon tab, which was dipped into a container of the respective particles, to ensure the particles remained stationary under the microscope. Excess particles were removed with the use of a compressed gas duster.

3.6 Hardness Testing of Filler Materials

The Vickers hardness of the sand and egg shell particles was measured using a Mitutoyo MVK-G1 micro-hardness tester. The particles tested were set in resin, which was then ground back to uncover the particles before micro hardness testing. The procedure for setting the particles in the resin is described in section 3.4, without vacuum impregnation. The resin was only ground back using 240 grit paper, as the samples were not going to be imaged polishing was deemed unnecessary.

13 indents were taken on the egg shell sample, 10 in the regions where the egg shell particles were present and 3 on the resin. 11 indents were taken on the sand particle sample, 8 on sand particles and 3 on the resin. A 200 gram load was used for all indents, as this was sufficiently large to form a clear indent on the particles whilst not too large to press the particles in to the resin.

3.7 X-Ray CT

A portion of both the Leigh Spinners 1150 grass green and Rawsons 1150 green were cut, with a circular saw, into a 150 mm by 150 mm square (with one corner removed to give a reference point) and scanned in a Metris Xtec xt h225 X-ray CT machine in an attempt to image and map the voids observed visually in the backing. 150 mm by 150 mm was selected because the artificial sports turfs were provided in strips 150 mm wide. These samples were mounted in the X-ray CT at an angle of 45 degrees to allow for an even distribution of X-rays through the samples. The scans used a beam energy of 70 kV for 3 hrs, whilst the sample rotated throughout 1 complete rotation.

3.8 Micro X-ray CT

Micro X-ray CT scans were attempted using a Quantum FX micro CT from Caliper Life Sciences on four samples (an unworn sample from each manufacturer and the sample without SBR applied), also to image the distribution of the voids in the samples. The samples were cut to 40 mm by 40 mm to match the field of view of the micro x-ray CT. The resolution of these scans is higher than the scans taken in the micro X-ray CT.

Some dog bone samples of the American artificial sports turf (vertical orientation) that had undergone both tensile and fatigue testing were scanned in the micro X-ray CT to observe and compare the damage believed to occur in the backing latex.

A range of X-ray beam energies (50 kV, 60 kV, 70 kV and 90 kV) were used depending on the sample being scanned. This range of energies was required as some energies were too high for some samples, whilst some were too low for others. All the samples were scanned with a field of view (FOV) of 40 mm diameter, which leads to an axial FOV of 40 mm and a voxel size of 80 µm. The samples were scanned with an exposure time of 17 seconds.

Some post-processing, primarily thresholding was applied to the images to reduce the noise in the images.

As the machine used was normally used for medical applications, it was housed on the clean side of a medical building and as such the samples had to undergo a cleaning procedure called “VHP” – vaporised hydrogen peroxide. This is used to protect the animals against any potential viruses or bacteria on the samples which may cause them health problems. During this process, VHP is produced from a solution of liquid H_2O_2 and water (typically 30% to 35% concentration), by generators specifically designed for the purpose. These generators initially dehumidify the ambient air, then produce VHP by passing aqueous hydrogen peroxide over a vaporiser, and circulate the vapour at a programmed concentration in the air, from 140 parts per million (ppm) to 1400 ppm, by the use of either a slightly positive or negative pressure depending on the infectious agent to be cleared. For comparison, a concentration of 75 ppm is considered to be "Immediately Dangerous to Life or Health" in humans. After the VHP has circulated in the enclosed space with the sample for a pre-defined period of time (30 to 45 minutes), it is circulated back through the generator, where it is broken down into water and oxygen by a catalytic converter until concentrations of VHP fall to safe levels, <1 ppm. (43) This cleaning process is also used to clean UHMWPE linings on biomedical implants, such as hip replacements. (44)

3.9 Nuclear Magnetic Resonance Imaging

Nuclear Magnetic Resonance Imaging (NMRI) scans were attempted on 4 samples (the same samples that were imaged in the micro x-ray CT) to image the distribution of the latex in the samples. The samples were placed in the MRI machine and scanned, and with the samples placed inside a water bath, to take a negative image of the samples.

The VHP process detailed above was also conducted on these samples.

3.10 Tensile Testing Procedure

For the tensile testing, the artificial sports turfs were tested in batches of 6 samples in accordance with the industry standard. The samples were cut to the dimensions as shown in Figure 31 which are taken from the industry standard BS EN 12230:2003 (45). In Figure 31, the units are millimetres, D is the distance between the clamps, and L is the gauge length. Some apparent directionality has been observed in the backing, and so 3 of each batch of samples were cut such that the gauge length was oriented vertically – following the directionality (Figure 32) and the other 3 cut such that the gauge length was oriented horizontally – perpendicular to the directionality (Figure 33, Figure 34). The industry standard does not mention orientations, so 3 of each is assumed to meet the requirements. The samples were cut using a Stanley knife from underneath a template which was clamped in place by the use of standard G clamps pressing down on the heads of the template.

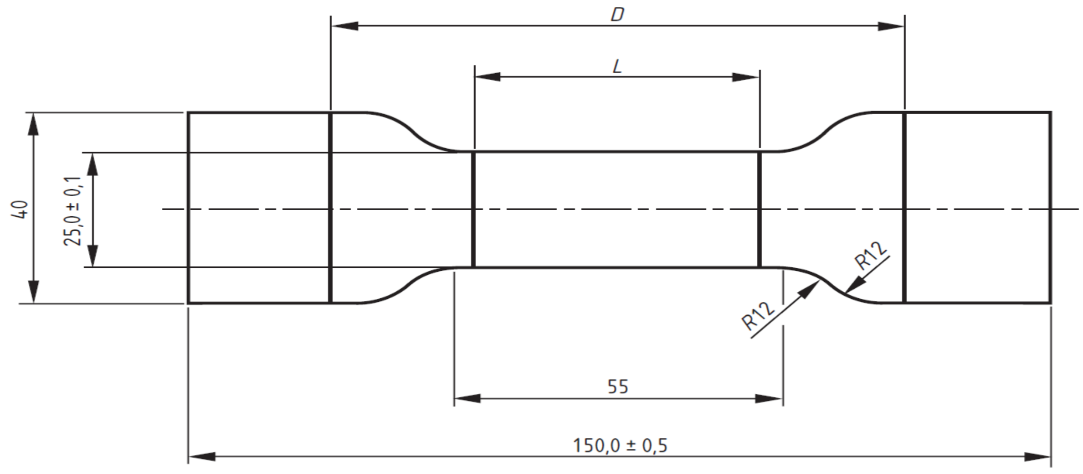

Figure 31 - Diagram of tensile test dog bone, reproduced from (45)

Figure 32 - Diagram illustrating the vertical orientation

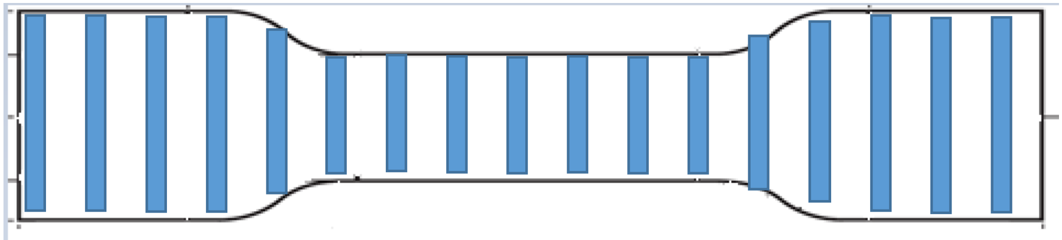

Figure 33 - Diagram illustrating the horizontal orientation

Figure 34 – Macro photo of a tensile dog bone – horizontal orientation.

Before and after each test, each sample was photographed. Photographs were taken of both the fibre side and underside (backing) of the samples. The photographs were all taken against a white background with a 10 Megapixel Nikon Digital SLR camera securely mounted on a tripod. Figure 34 is an example of the photographs taken. Some samples were weighed with a Mettler Toledo ME204 analytical balance before and after the tests, to measure any material loss.

The data acquired from these tests was used to generate force extension graphs for each sample tested. This was then used to calculate the UTS and stiffness of the samples after the experiments had run, as the software on the load frame was believed to be inaccurate.

The samples were clamped in accordance with BS EN 12230:2003 into a (UKAS accredited) Hounsfield HTE load frame with a 5000 N load cell. Initially the apparatus was set up with a load range of 5000 N, a speed of 50 mm/min (in accordance with the industry standard) and an until load (the amount the load has to drop by for the load frame to automatically stop the test) of 50 N. This is not in the industry standard, but the control software required the setting. Care was taken to ensure the samples were aligned correctly.

For the majority experiments the body of the clamps were C shaped with the clamp faces having serrated faces fastened with the tightening of bolts to prevent the sample slipping during testing, shown in Figure 35. The torque applied to the bolts was not measured, but the samples were observed for slip during the tests.

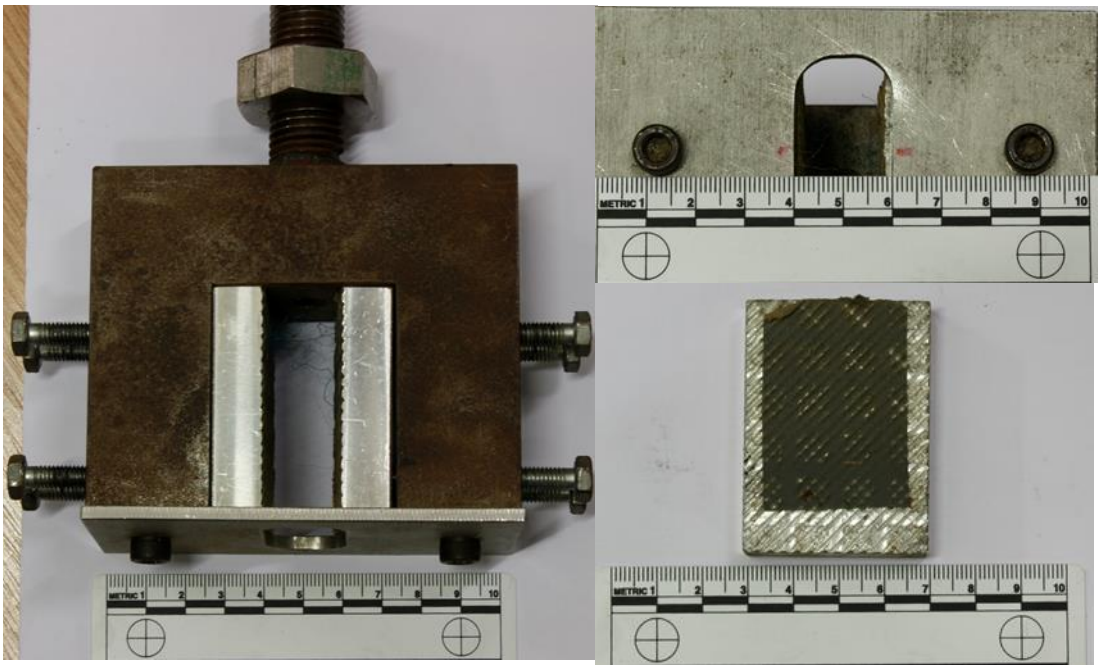

Figure 35 - Clamp used for tensile testing

For the preliminary experiments the extension range was set to 25 mm. After this test the until load setting was removed and the extension range was increased to 50 mm. The extension range was later increased again to 150 mm when the samples did not fail completely within the distance, and increased another time 250 mm for similar reasons. Samples that did not fail within the extension range were not included in analysis and repeated.

3.11 Tensile Testing of Worn In Situ Samples

When testing the worn in situ samples described in 1.2, care was used to ensure that as much sand as possible was removed before testing. The sand was removed by gently shaking the samples, followed by using a compressed gas duster to remove as much as possible. The mass change was not measured, assumed to be minimal.

Tensile testing of the worn in situ (square sample) was conducted in accordance with BS EN 12230:2003, following the procedure described in 3.10.

Additionally, tensile testing the rectangular sample of worn artificial sports turf was also conducted. The aim of this testing was to see if the properties of the artificial sports turf changed along its length, and so two batches of samples labelled position 1 and position 2 (P1 and P2) were cut from extreme edges of the artificial sports turf. As the artificial sports turf was 2.56 m long, the separation between these two samples was approximately 2.40 m. Again, the samples were cut and tested following the procedure described in 3.10.

3.12 Tensile Testing of American Samples

Samples of the American artificial sports turf were limited, so only 4 samples underwent tensile testing. A directionality was observed in this artificial sports turf, and so 2 samples were cut for each orientation. In addition to this, the 2 cut in the horizontal orientation had to be cut from different pieces of artificial sports turf. The samples were tested following the procedure described in 3.10.

3.13 Tensile Testing of X-ray CT Scanned Samples

Tensile testing of samples cut from a piece of Leigh Spinners 1150 grass green that was scanned in the X-ray CT was also conducted.

5 samples were cut in the vertical orientation and 6 cut in the horizontal orientation. The samples were cut using a Stanley knife from underneath a template which was clamped in place. As the portion of turf was 150 mm by 150 mm, the samples had a total length of 75 mm and head width of 20 mm. The gauge length was 25 mm and gauge width was 10 mm.

A (UKAS accredited) Instron 3343 load frame with a 500 N load cell was used. The apparatus was set up with a load range of 500 N, a speed of 10 mm/min and an extension range of 250 mm.

Wedge grip clamps with serrated clamp faces tightened manually were used for testing of these samples, shown in Figure 36.

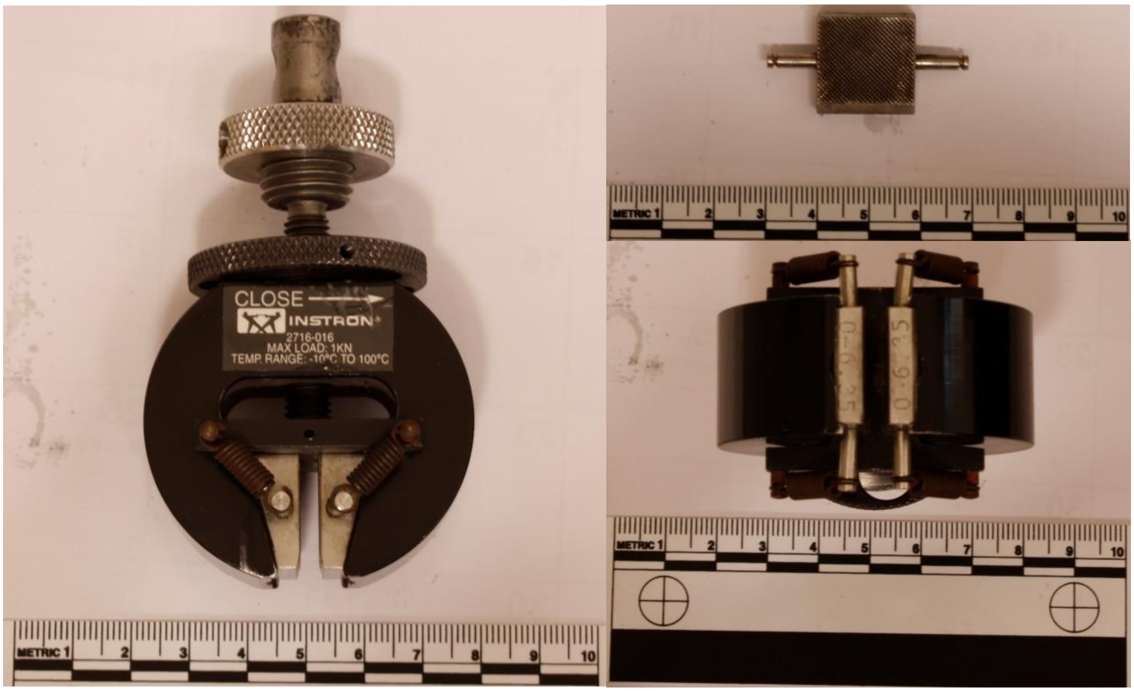

Figure 36 - Wedge grip clamp

3.14 Fatigue Testing Procedure

Tension – compression repeated stress cycle fatigue testing (where the load is applied axially) has been employed as a method of replicating the usage of the artificial sports turf in order to quantify the lifetime of the artificial sports turf in terms of footsteps. Loading in the tensile direction is considered positive, compressive loading is considered negative. Thus, tensile loading is equivalent to the loading experience during the braking and drive phase of a footstep.

3.15 Fatigue Testing – Small Samples

Samples of Rawsons 1150 green were cut such that the gauge length was 30 mm long and 4 mm wide using a specialised cutting tool, where the cutting blade was pressed through a sample of the artificial sports turf. The samples were all cut in the vertical orientation. In later experiments the samples were cut using a Stanley knife from underneath a template which was clamped in place, as the cutting tool was suspected of introducing defects into the samples. The samples were clamped into a (UKAS accredited) Instron 3343 load frame with a 500 N load cell, using the clamps shown in

Figure 36. The samples were cyclically loaded in a repeated stress cycle between 1 N and 6.15 N at a rate of 1 N/s until the sample fails. See 9 for the complete calculation.

The clamps used were the wedge grip clamps used for testing the samples cut from the piece of artificial sports turf scanned in the X-ray CT machine, shown in Figure 36.

3.16 Fatigue Testing – Large Samples Preliminary

Inconsistent results, (discussed in 6.3) lead to the need for larger samples to be tested. The samples were cut to the same dimensions and in the same manner as the samples used for tensile testing.

The increased size of the samples necessitated a change of clamp design, shown in Figure 37. These samples were fitted into clamps that were of a similar design to the clamps used in the tensile testing; only differing in the attachments to the load frame, such that the same Instron 3343 load frame used earlier could be used. Initially the load frame was programmed to run continuously until the sample failed, however the data files being produced caused the control systems to run slowly, and so this was changed so that the machine was reset every 12 hours, to ensure a consistent load rate.

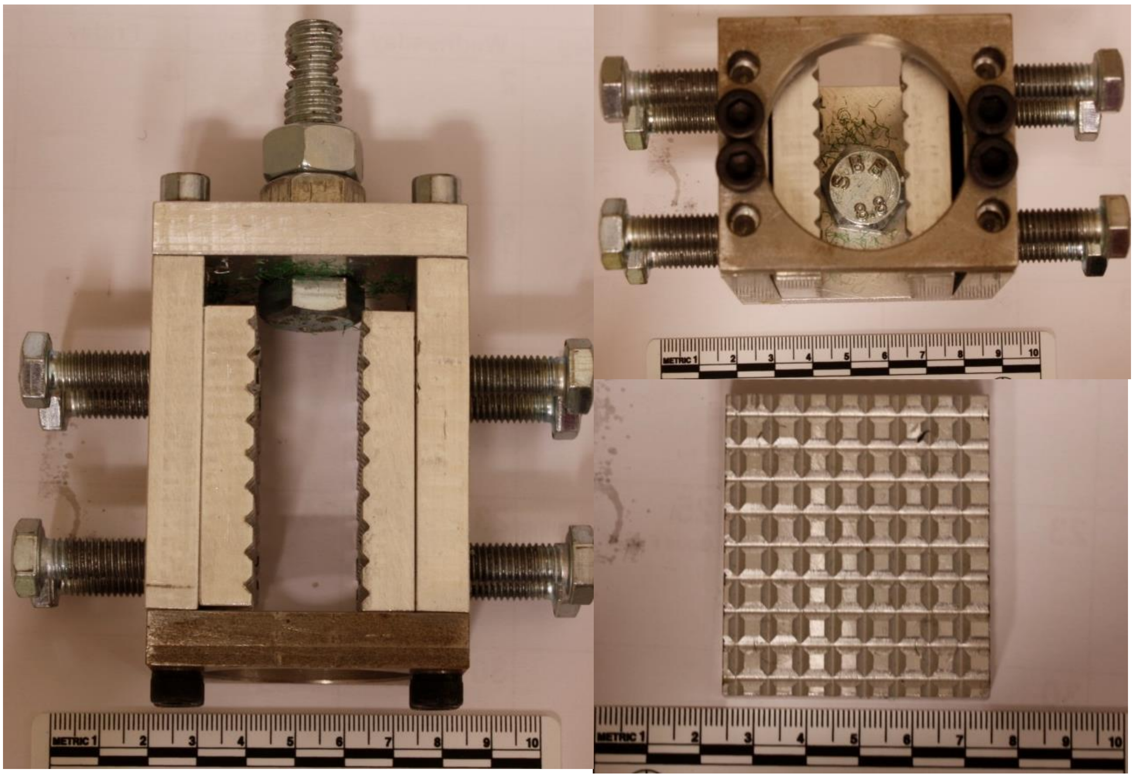

Figure 37 – Clamp for initial fatigue testing of larger samples

This sample was cyclically loaded in a repeated stress cycle between 1 N and 40 N at a rate of 6.15 N/s until it failed. The load rate was chosen such that this represented a realistic load rate determined from the literature, without compromising the validity of the fatigue test (46). See 9 – Appendix 1 for the complete calculation.

The load frame that was being used for this testing did not perform well with these increased variables as this model is not dynamic, so another load frame was used for the testing.

3.17 Fatigue Testing – Large Samples

This required increasing these variables further, to reduce systematic errors in the new load frame (as this load frame used a 100 kN load cell). The sample was clamped into a UKAS accredited MTS 810 load frame and again underwent a repeated stress cycle between 1 N and 80 N at a rate of 80 N/s (1 Hz) until failure. See 9 – Appendix 1 for the complete calculation.

When it came time to test the vertical orientation of the American sample, this sample had to be cut to slightly shorter dimensions owing to lack of material. As a result, the heads at either end of the test piece where 10 mm shorter than was wanted, thus giving a total length of only 130 mm. Despite this, there was still enough head left to get a good grip on.

This change in load frame required another change of clamps. The clamps were blocks of metal with serrated faces tightened with nuts and bolts, shown in Figure 38. Similar to the fatigue testing, the torque applied to the bolts was not measured, but the samples were periodically observed for slip during the tests. These differ from the tensile and fatigue clamps in that the blocks were attached to the frame vertically rather than horizontally.

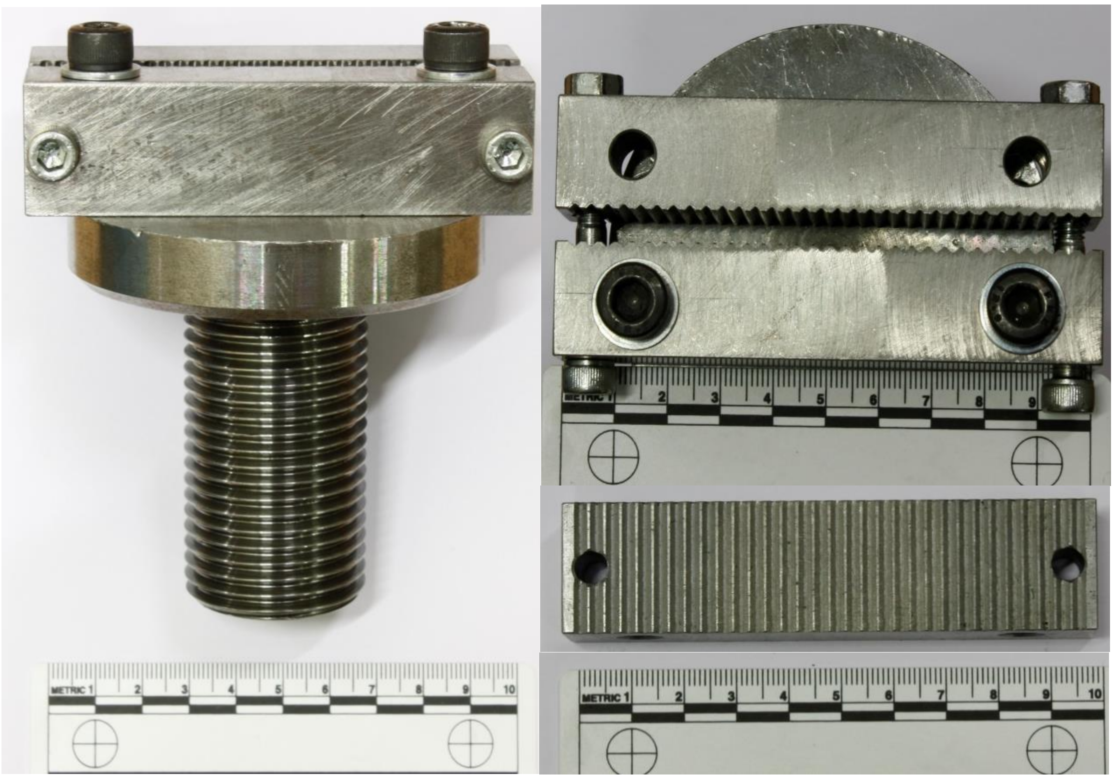

Figure 38 - Clamp used for fatigue testing of larger samples

3.18 Wear Testing

A series of pin on wheel tests were conducted on the artificial sports turfs. The apparatus rotated a circular sample 77 mm in diameter (the size of the sample holder) about its centre, causing it to wear against a fixed counter face 35 mm from the centre of rotation, illustrated in Figure 40. Figure 41 shows the wear rig used for the testing. The samples were cut by pressing a cylindrical tube with a sharpened edge through the artificial sports turf.

For the preliminary experiments the counter face was a steel ball bearing of diameter 8 mm, pressed against the sample under a force of 16 N (full calculation in 10) rotating at 3 rad/s (tangential velocity at wear track 0.1 m/s). The type of steel is unknown, assumed to be stainless steel. This experiment ran for 7200 seconds.

The main experiments were a series of tests investigating the effect of the sand within the backing has on the wear rate of the artificial sports turfs, and how the mechanical properties change across the experiment. Samples were tested with and without approximately 40 grams of sand (discussed in 1.2) applied (0.086 kg m^{-2}) such that approximately 2 mm of pile was visible, in accordance with recommendations from Notts Sport Ltd (2). These experiments all ran for 1800 seconds.

The force on the stud was either 2.55 N (referred to as the lower load) or 7.65 N (referred to as the higher load) depending on the experiment, and the sliding speed was in the range of 3.14 rad/s to 4.5 rad/s (giving a tangential velocity of 0.1 m/s to 0.15 m/s at the wear track) for all the samples. This range in speed is due to a rather crude speed controller. These variables were chosen to prevent the sample being pulled from the holder, as the coefficient of friction was expected to be higher than in the previous experiment.

For the main experiments, the counter face was a polymeric stud removed from a commercially available shoe (Sondico flair TF, size 11.5, rrp £49.99 Figure 39) used for play on artificial sports turf. This counter face was secured in place using epoxy resin glue. Due to time constraints, it was not possible to use a new counter face for each wear test and so the same stud was used for multiple different artificial sports turf samples, although it was replaced periodically when other parameters (such as load on the sample) where changed, as shown in Figure 117 and Table 9.

Figure 39 - Shoe from which counter faces were cut. Lower right shows shoe with studs removed.

Force exerted against the beam was measured with a linear variable differential transformer (LVDT) (not pictured in Figure 40) which enabled the measurement of friction between the counter face and the sample. As such, a calibration run was conducted before the experiments were conducted where a series of increasing weights were attached to the LVDT by system of string and pulleys. The data from this, given in 11 enabled the conversion of the voltage output from the LVDT into Newtons.

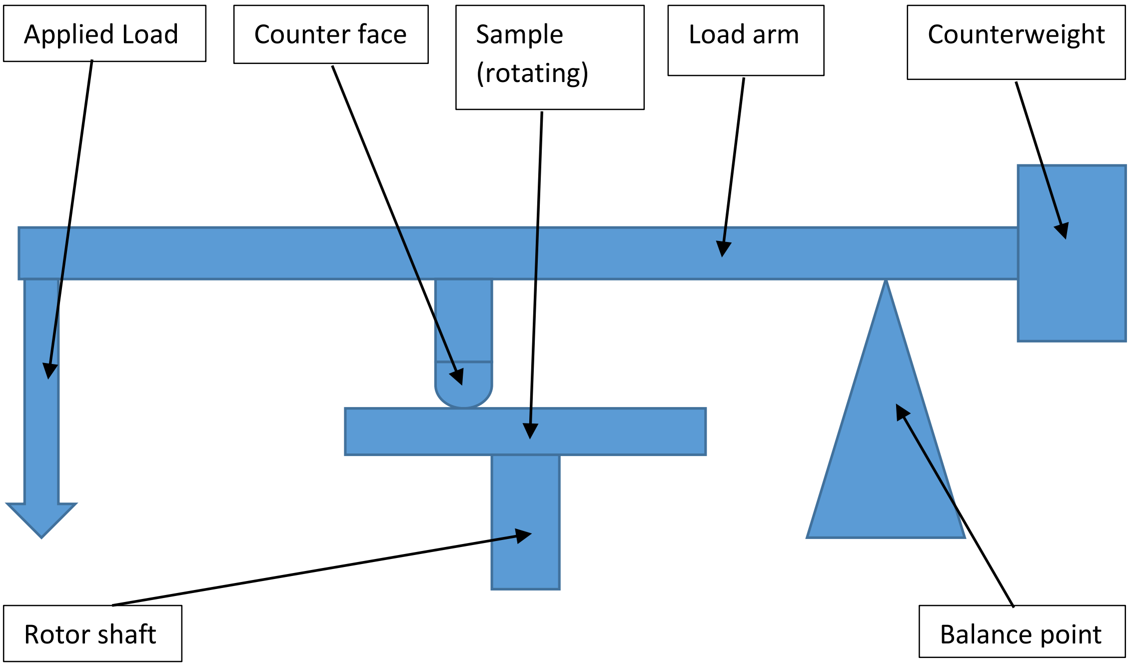

Figure 40 - Schematic of wear rig

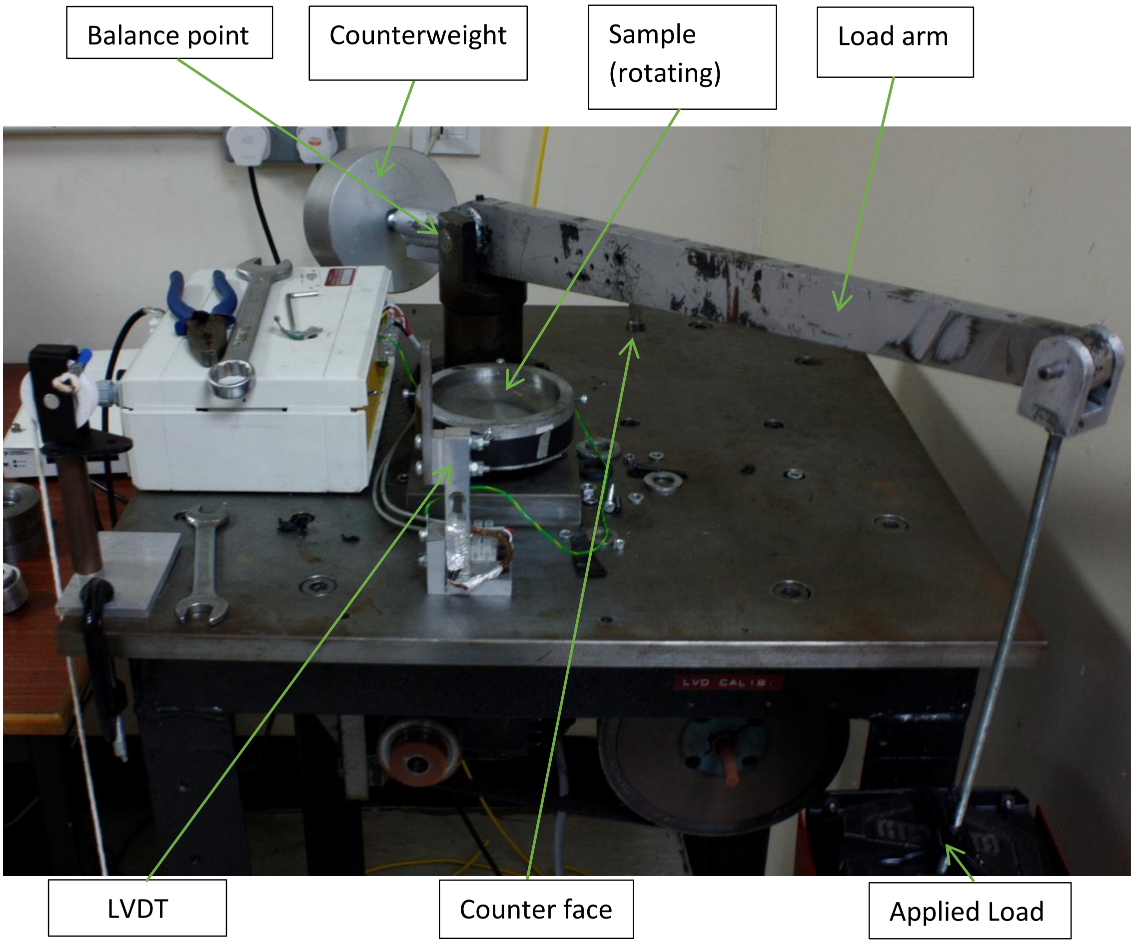

Figure 41 - Macro photo of wear rig

3.19 Experimental Methods and Procedures Summary

From this chapter it can be taken that the many different techniques used to analyse the tensile, fatigue and wear performance of artificial sports turfs, and four different methods used to investigate and image the structure of the artificial sports turfs and the PP fibres in the artificial sports turfs.

The imaging techniques used settings that were determined in situ, whilst the tensile testing was conducted in accordance with the industry standard, fatigue testing used the same sample preparation as the tensile testing, and variables determined from the literature. Wear testing also used variables determined from the literature. Where appropriate, single factor analysis of variance (ANOVA) and t-Tests were used to analyse the data.

4 - Characterisation

4.1 Optical

In Figure 42, the directionality observed in the backing of the American artificial sports turf is shown running vertical, highlighted white. Figure 43 shows this directionality is not present in the pile of the artificial sports turf.

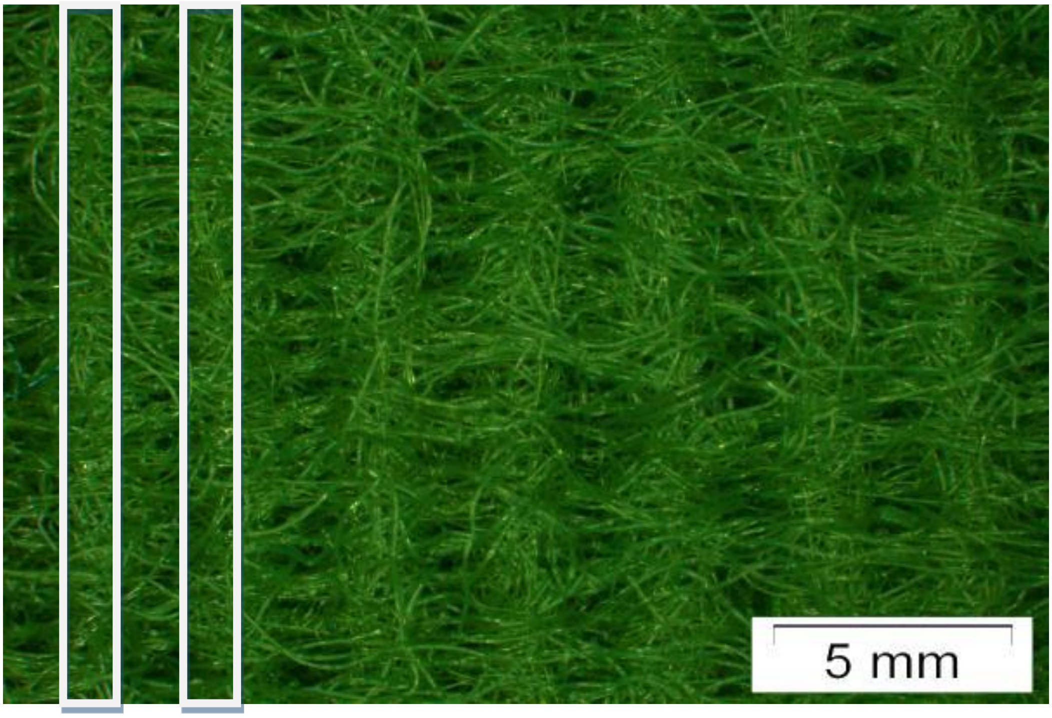

Figure 42 - Optical Image of the backing on the American artificial sports turf.

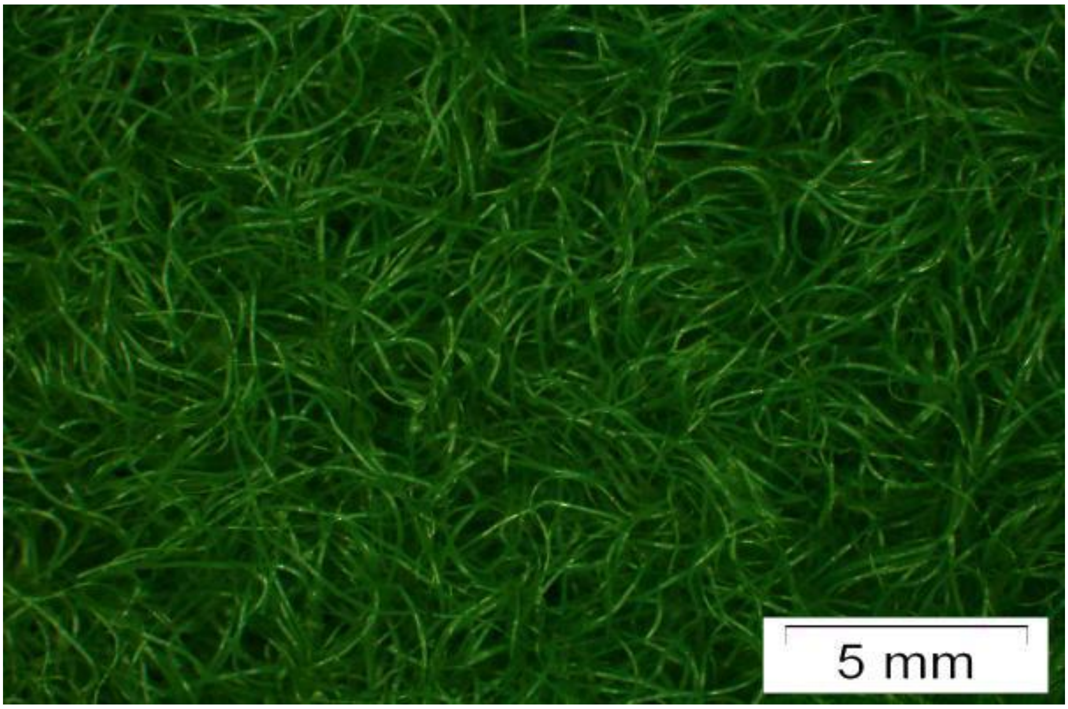

Figure 43 - Optical Image of the fibres on the American artificial sports turf.

Figure 44 and Figure 45 show the backing and fibres of a sample of the worn in situ square sample artificial sports turfs. The observed directionality is no longer visible in the backing and the pile fibres are noticeably damaged.

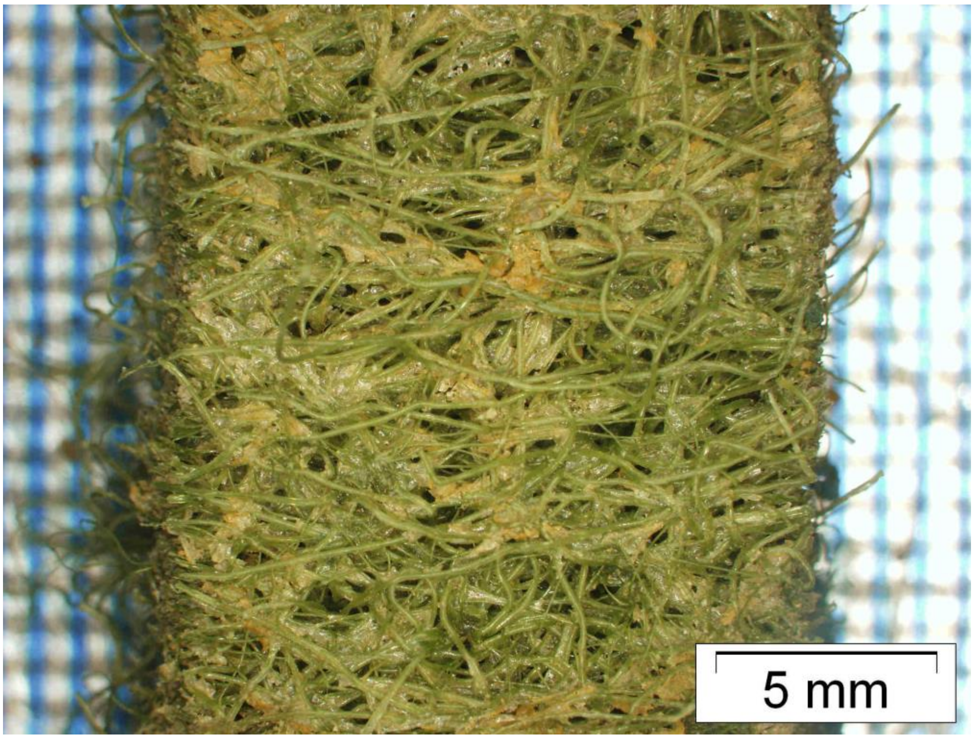

Figure 44 - Optical Image of the backing on the worn in situ square sample

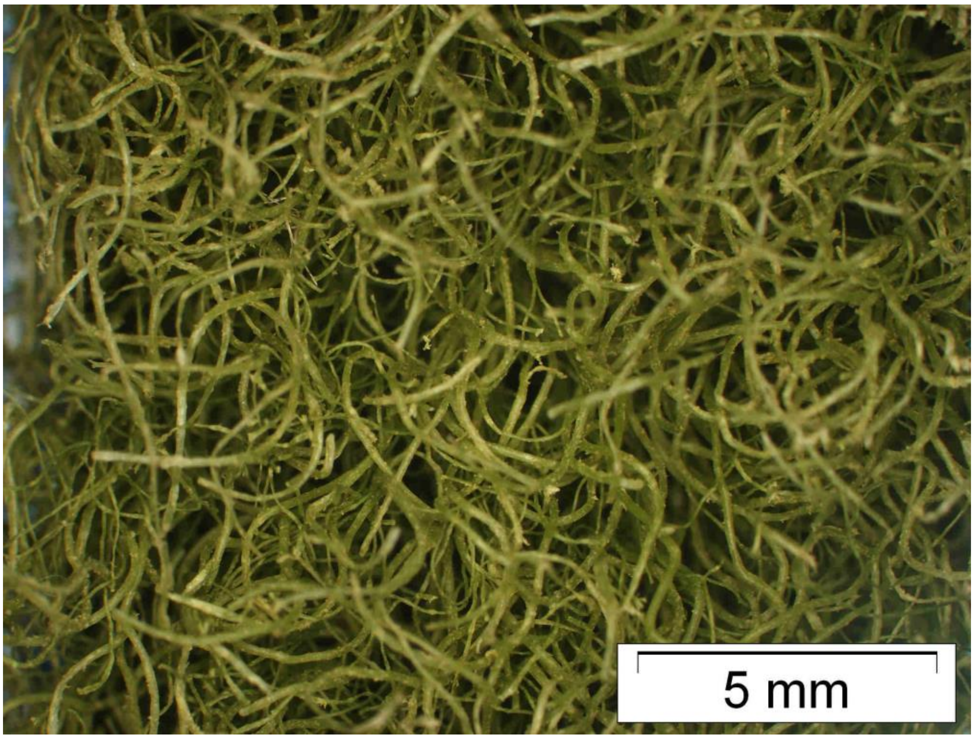

Figure 45 - Optical Image of the fibres on the worn in situ square sample

Figure 46 and Figure 47 show the backing and pile of a sample of Leigh Spinners 1300 grass green. The observed directionality is visible in the backing as indicated, but less apparent than in the American artificial sports turfs.

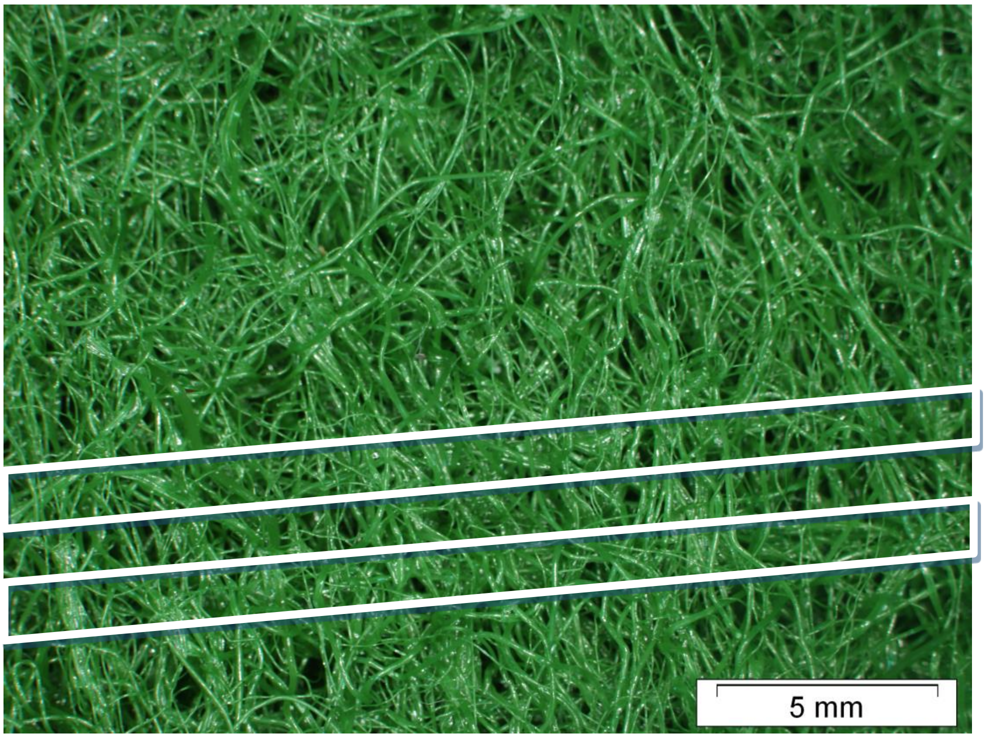

Figure 46 - Optical Image of the backing on the Leigh Spinners 1300 artificial sports turf

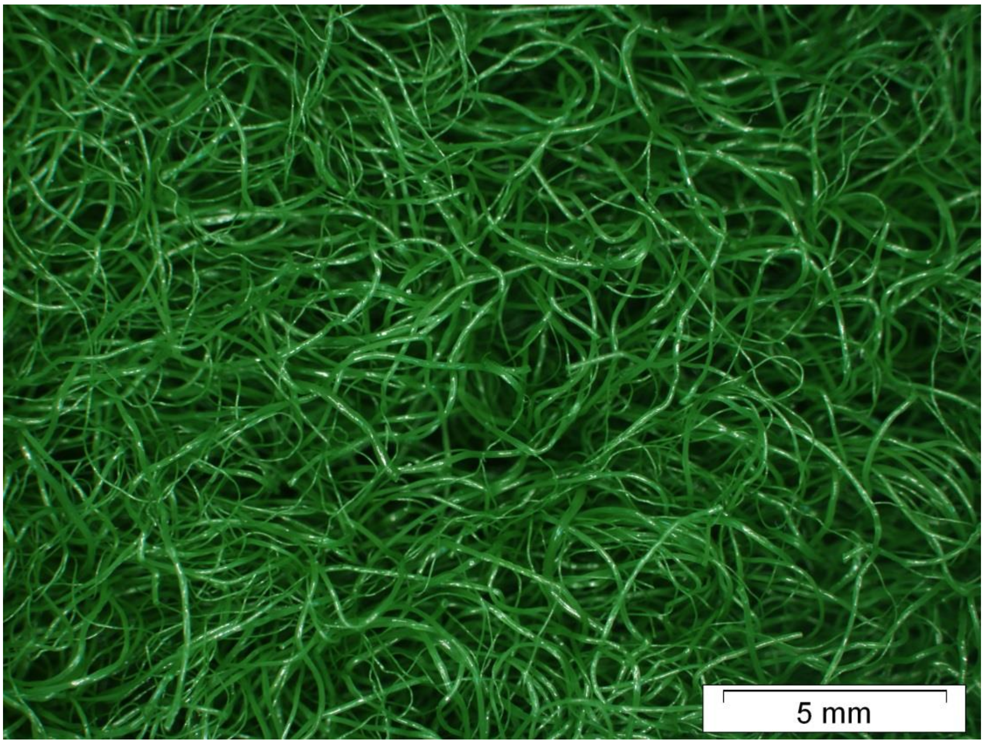

Figure 47 - Optical Image of the fibres on the Leigh Spinners 1300 artificial sports turf

Figure 48 and Figure 49 show the backing and pile of a sample of Leigh Spinners 1150 grass green. The observed directionality is visible in the backing as indicated, but it is still less apparent than in the American artificial sports turfs.

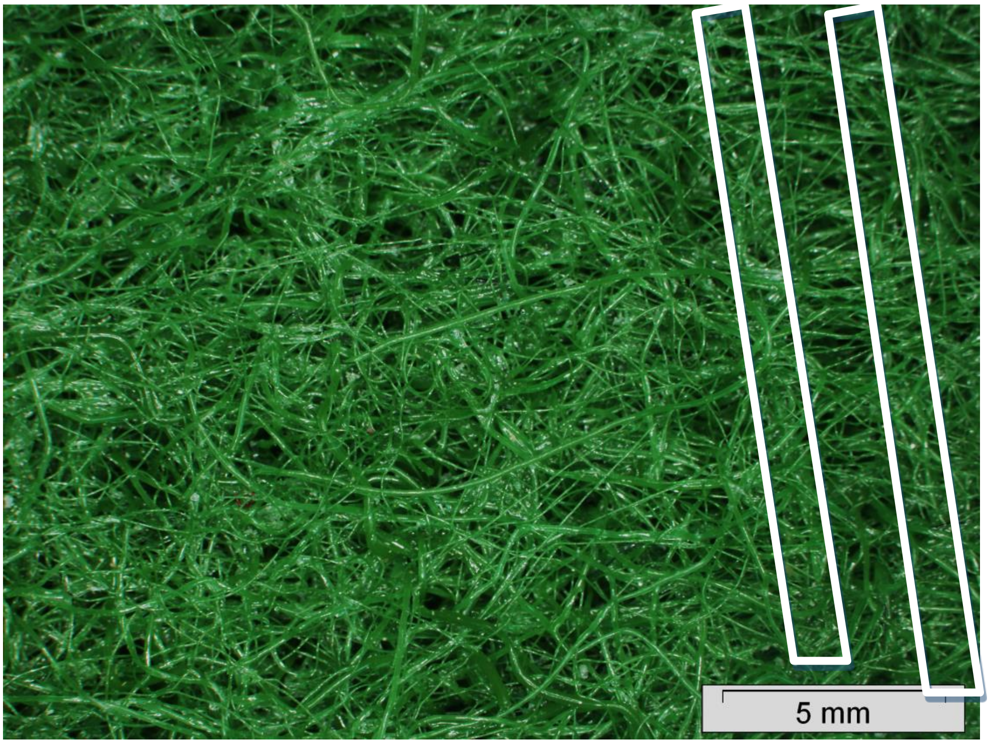

Figure 48 - Optical Image of the backing on the Leigh Spinners 1150 artificial sports turf

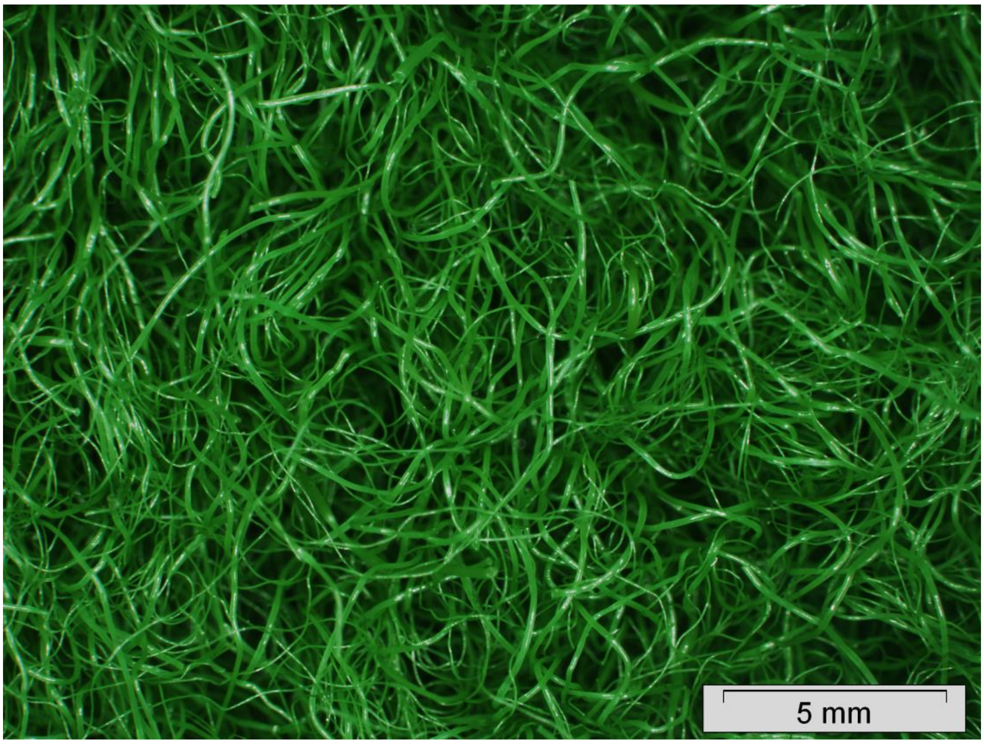

Figure 49 - Optical Image of the fibres on the Leigh Spinners 1150 artificial sports turf

4.2 ESEM

4.2.1 Unmounted Samples

4.2.1.1 Unworn

Figure 50 and Figure 51, chosen as example images, show little damage on the fibres in the pile and underside of the American artificial sports turfs as a result of the manufacturing process. Some type E/F damage can be seen on the fibres in the form of flakes of material removed (circled), believed to be caused by the needling looms impacting the fibres during manufacturing.

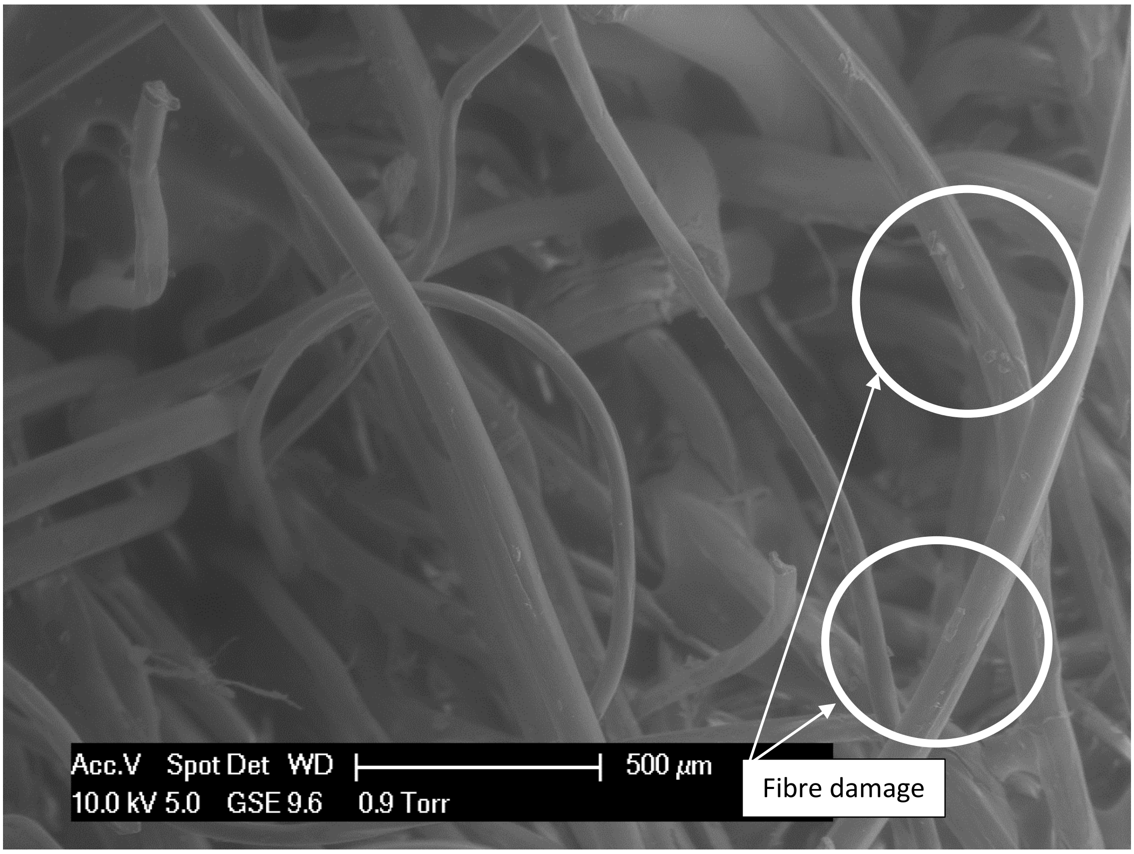

Figure 50 – Typical ESEM image of the fibres in the American artificial sports turf.

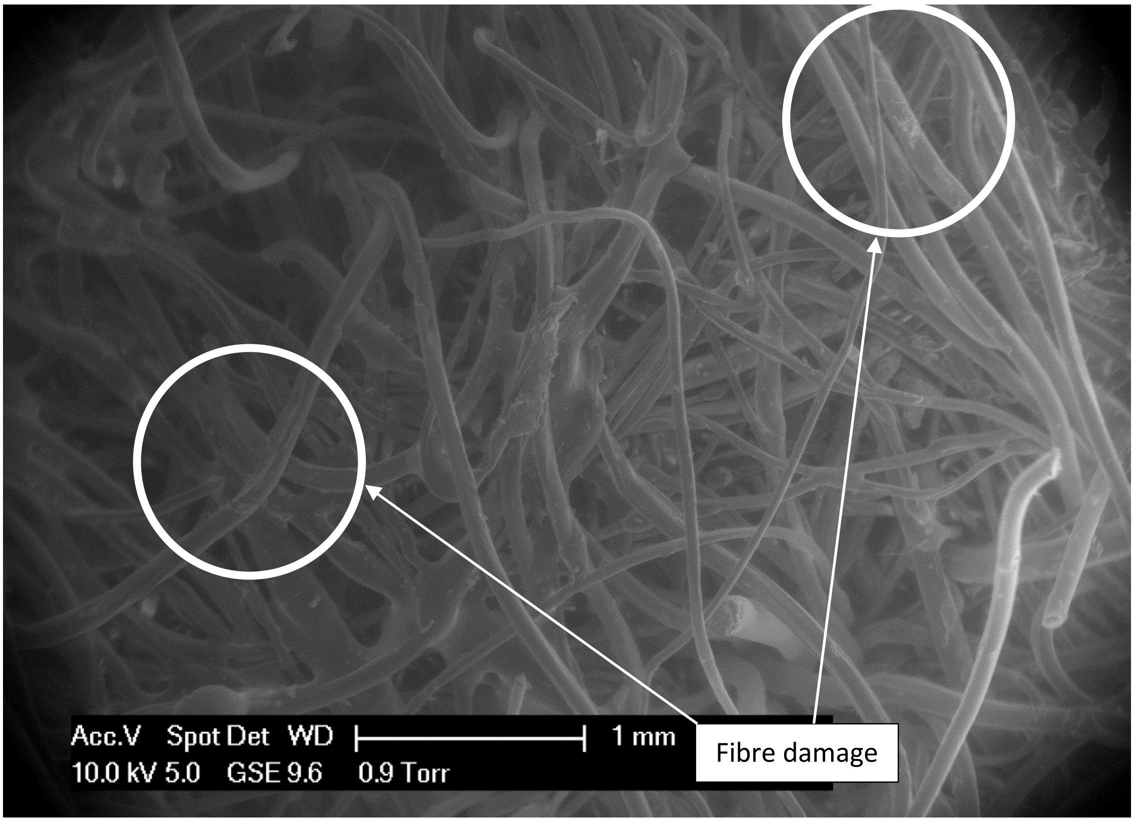

Figure 51 - Typical ESEM image of the backing fibres in an unworn sample of the American artificial sports turf.

Figure 52 and Figure 53 show little to no damage to the fibres in the pile and underside of the Leigh Spinners 1300 grass green artificial sports turf, although again some small flakes of material have been removed (circled). Both show signs of damage type A, incipient distortion.

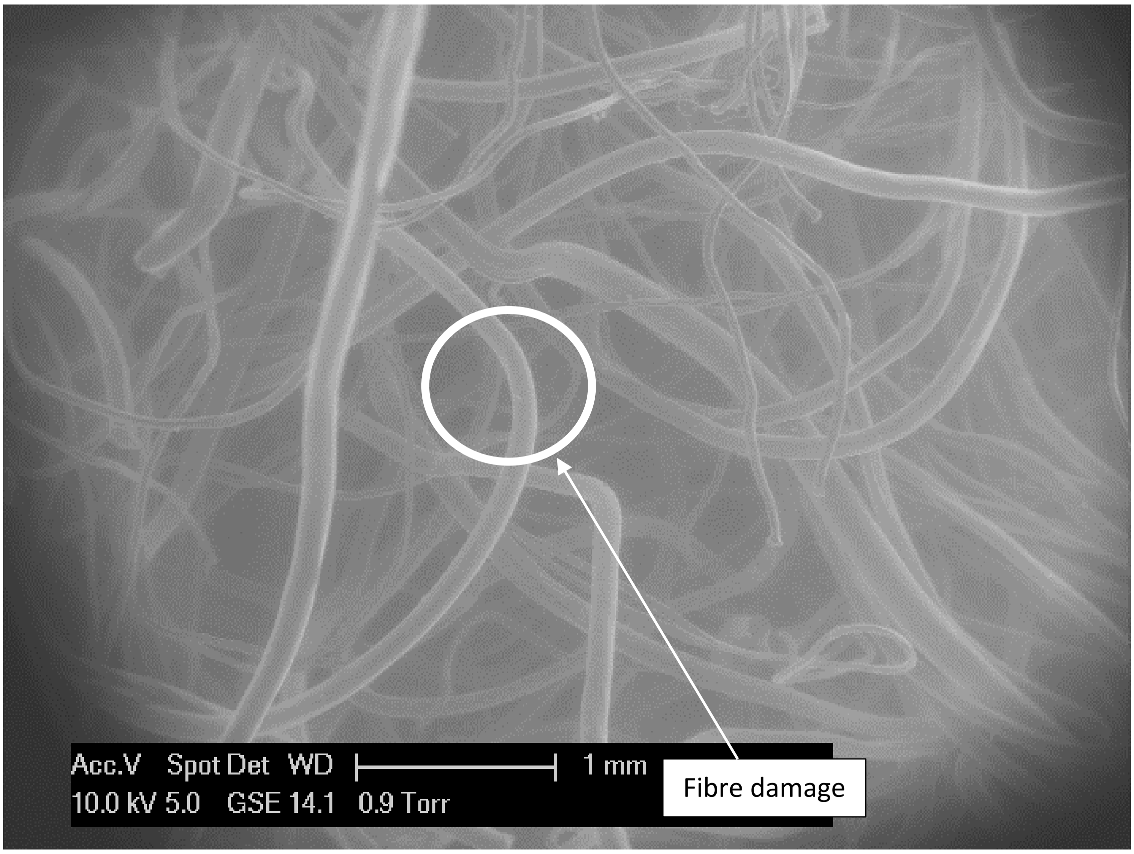

Figure 52 - ESEM image of the pile of a Leigh Spinners 1300 grass green

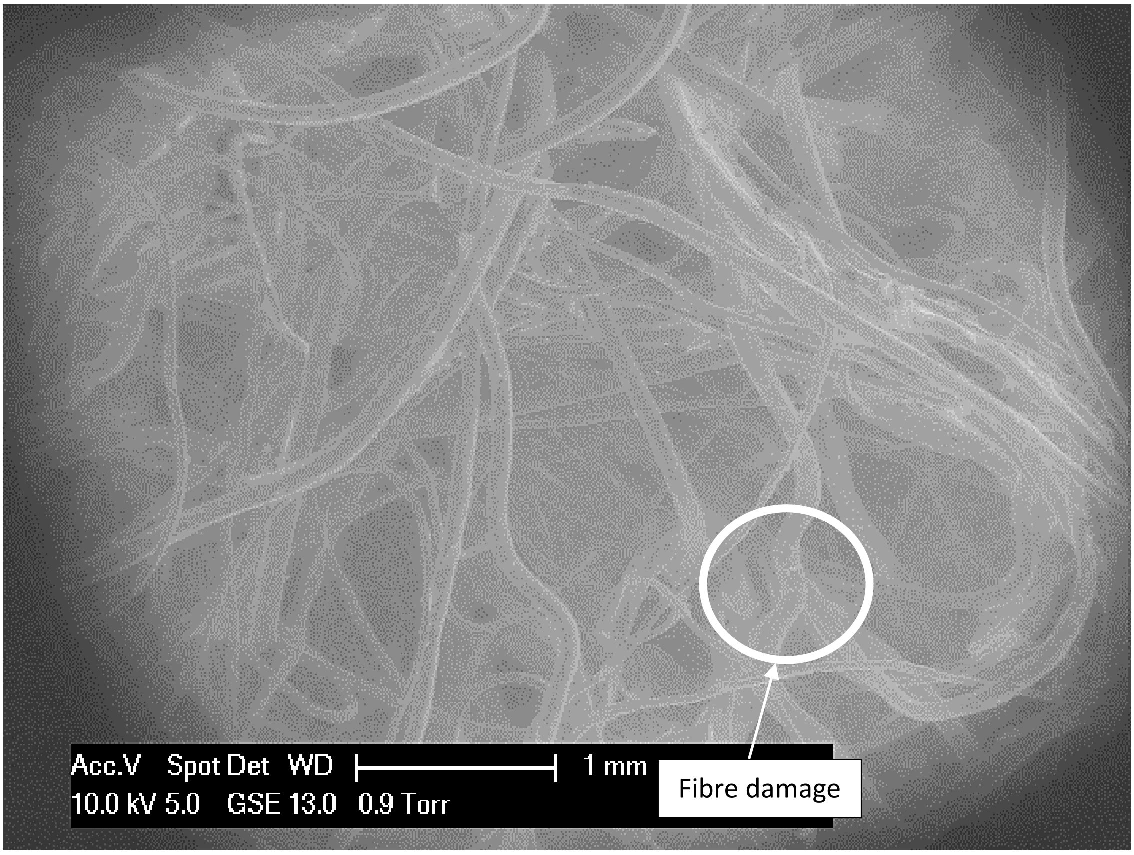

Figure 53 - ESEM image of the backing of a Leigh Spinners 1300 grass green

4.2.1.2 Worn in situ

Figure 54 shows thinning and flattening of a fibre from the worn in situ rectangular sample artificial sports turf. There are no smooth fibres that were seen in Figure 50, and indeed all of the fibres in that image show signs of either adhesive or abrasive wear mechanisms occurring, such as flattening of the fibres along a significant length (<1 mm) towards a frayed and broken end, highlighted. Damage types A B and C as well as type G can be seen, also highlighted.

Figure 55 shows failure of a fibre, also from the worn in situ rectangular sample. A biaxial split has occurred, and the remnants have been worn. This would suggest that as well as gradual wear working on the artificial sports turf; catastrophic wear events may occur.

Figure 56, an image of the back of the worn in situ rectangular sample, artificial sports turf, again there is no unworn surface remaining, although the flattening observed in the pile cannot be seen here. There appears to be cracks in the latex forming, circled.

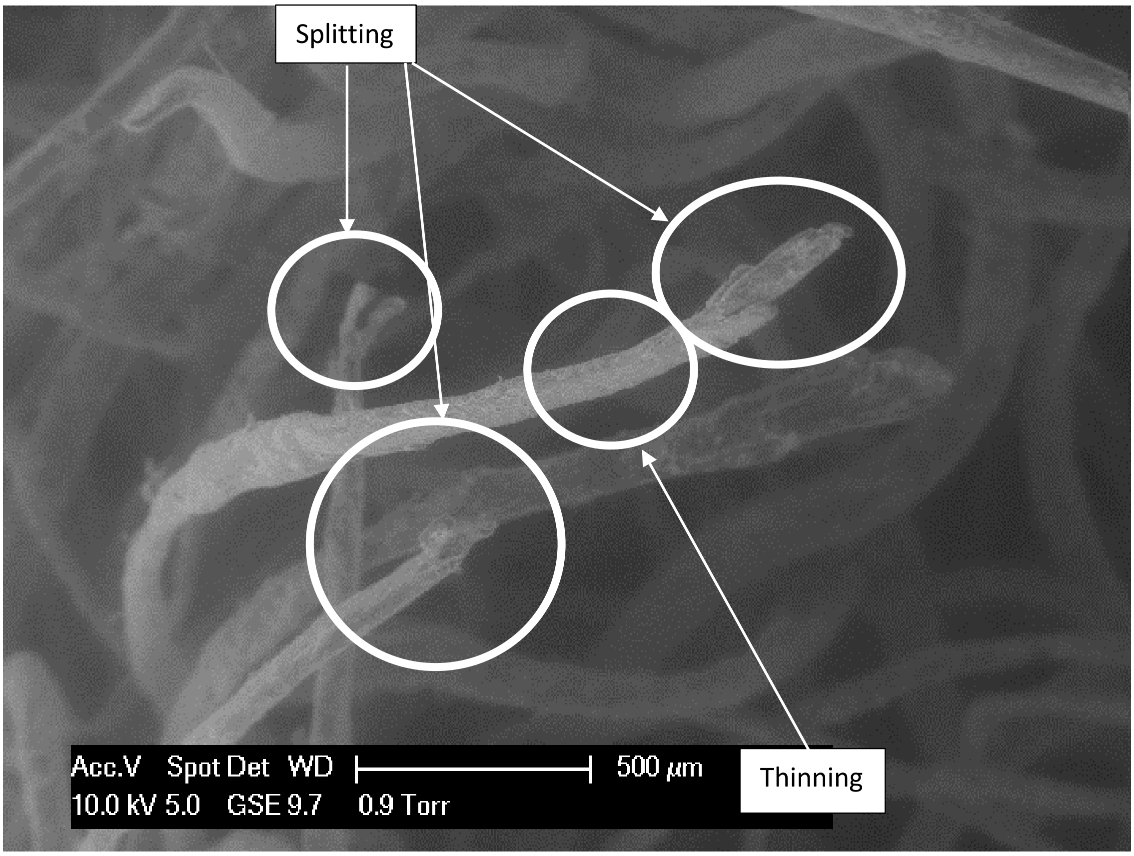

Figure 54 - ESEM Image of fibres from worn in situ rectangular sample, position 1.

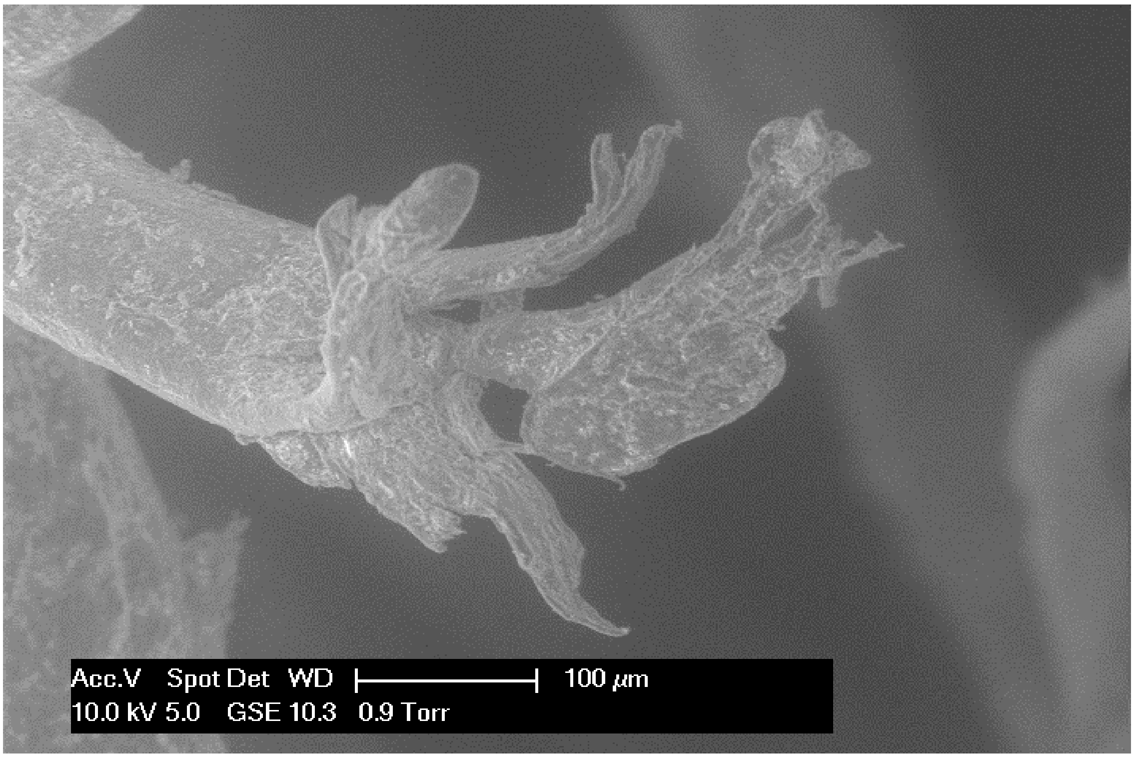

Figure 55 - Close up of a broken fibre end from the worn in situ rectangular sample, position 1.

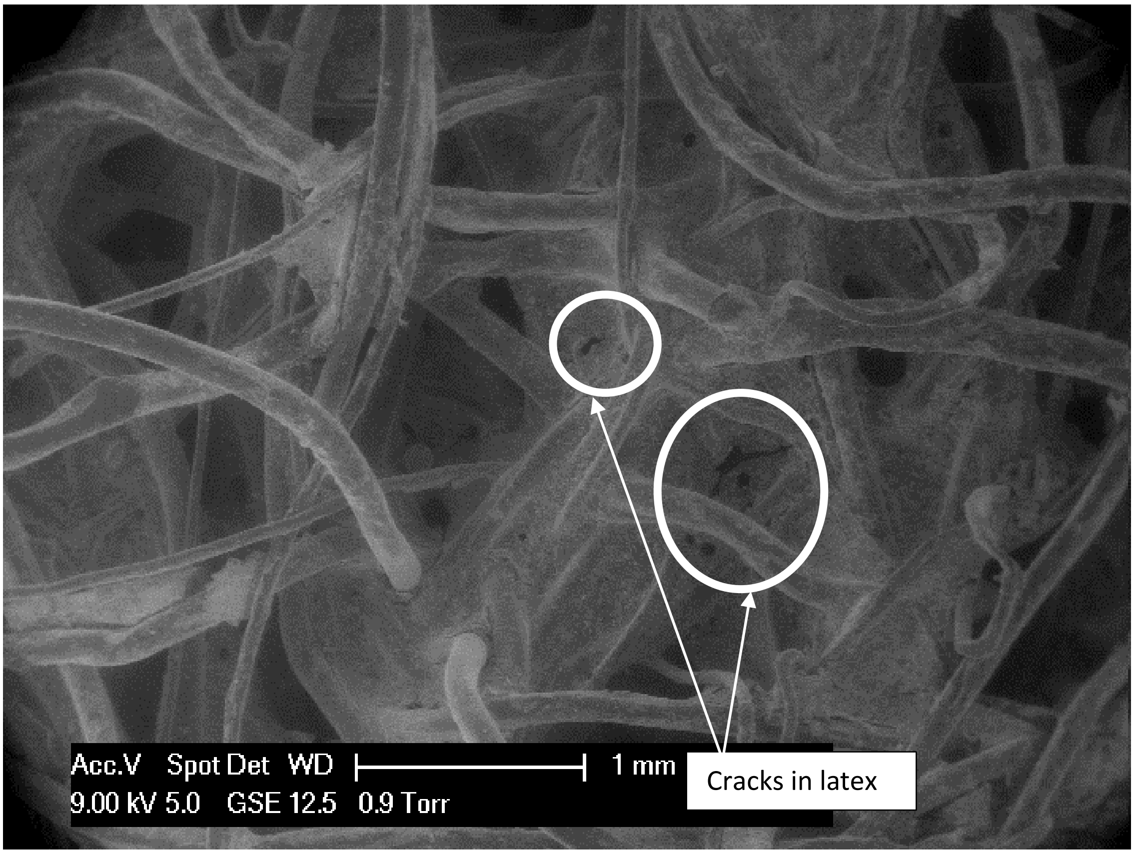

Figure 56 - ESEM image of the backing of a sample worn in situ rectangular sample.

4.2.1.3 Wear testing worn fibres

Figure 57 is an ESEM image of a fibre damaged from the wear testing. Damage type d (High degree of fibrillation) is present and highlighted.

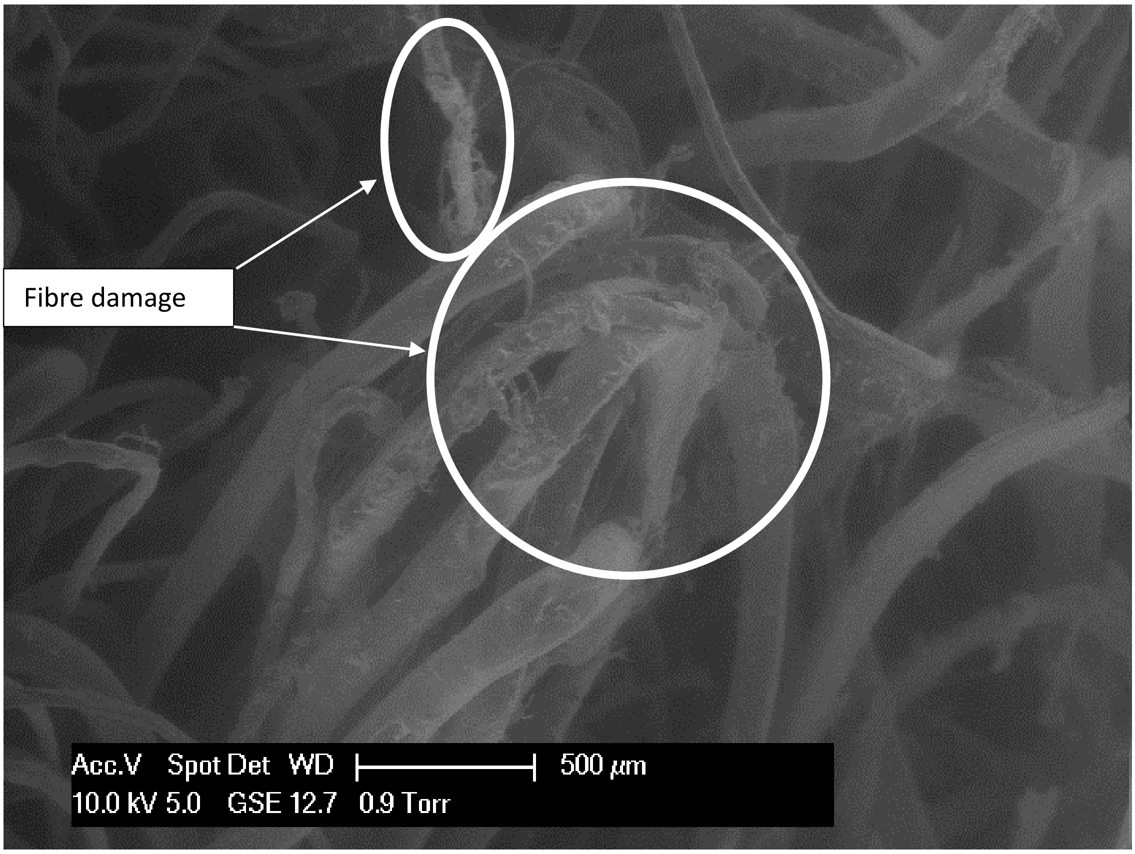

Figure 57 - ESEM image of a worn sample of a Leigh Spinners artificial sports turf.

4.2.2 Worn fibre length

Figure 58 shows a fibre from the worn in situ square sample, and Figure 59 shows a fibre from the backing of this sample. The wear appears to be least at the end of the fibre closest to the backing (upper section), worsening along the length (midsection) and worst at the very end (lower section), which is different to what was seen in some of the other fibres. The narrowing observed in Figure 54 can be seen in the lower section of Figure 58. The images shown in Figure 58 are taken approximately 5 mm apart; overall length this fibre is approximately 10 mm. The wear on the backing appears to be less than the wear on the fibres in the pile, and roughly equal along the length of the fibre. Flattening/thinning of the fibre is absent. A kink band, circled, can be seen in the left most portion. Damage types A or B appear to be present.

Figure 58 - Image of individual worn in situ fibre

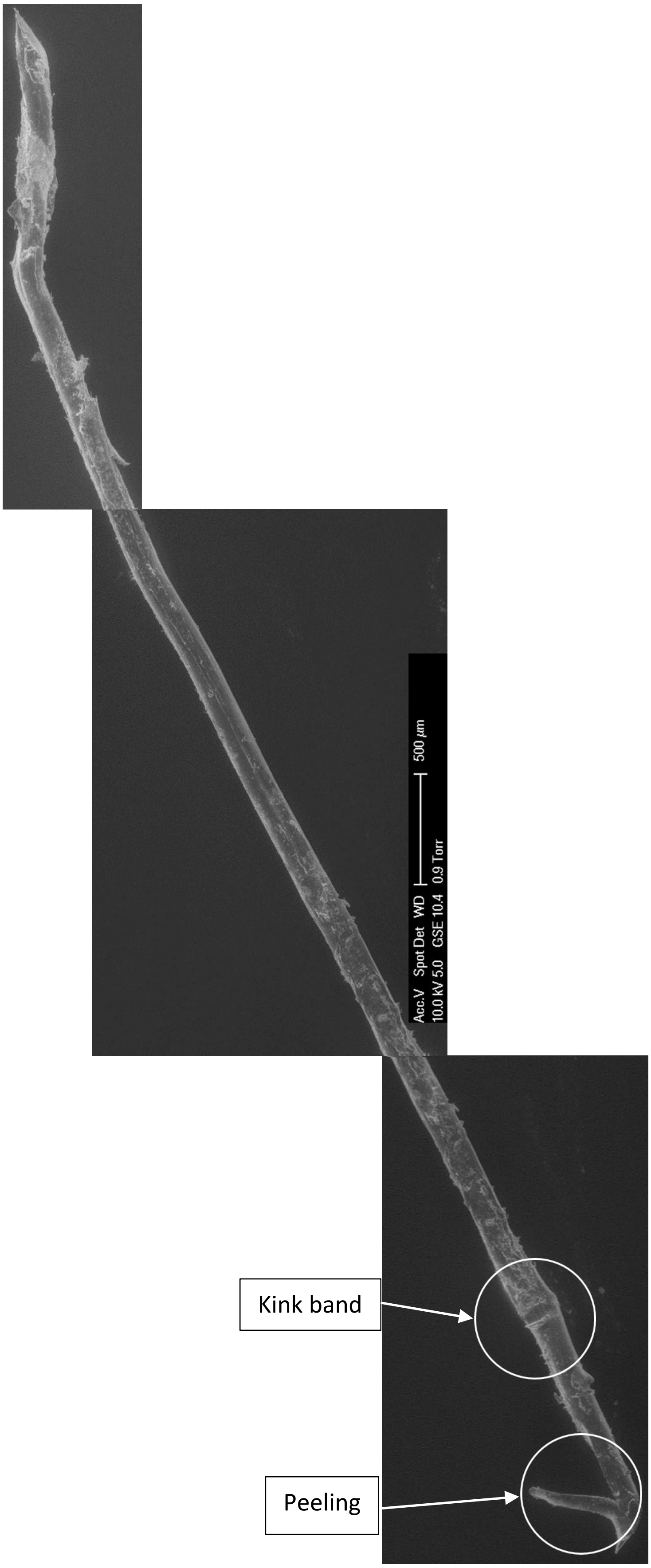

Figure 59 - Image of individual worn in situ backing fibre

4.2.3 Mounted in Resin

From Figure 60 we see in comparison to Figure 61 the latex in the 1150 Leigh Spinners artificial sports turf appears to be present in roughly the same volumes as in the American artificial sports turf, with both having regions of differing sizes. Figure 61 has been altered such that the scale of the image matches Figure 60.

Secondly, it is clear there is a variety of fibre sizes. It has been determined that there appears to be 3 sizes of fibres, ranging from between 20 µm to 40 µm, then 40 µm to 100 µm and finally greater than 100 µm in diameter.

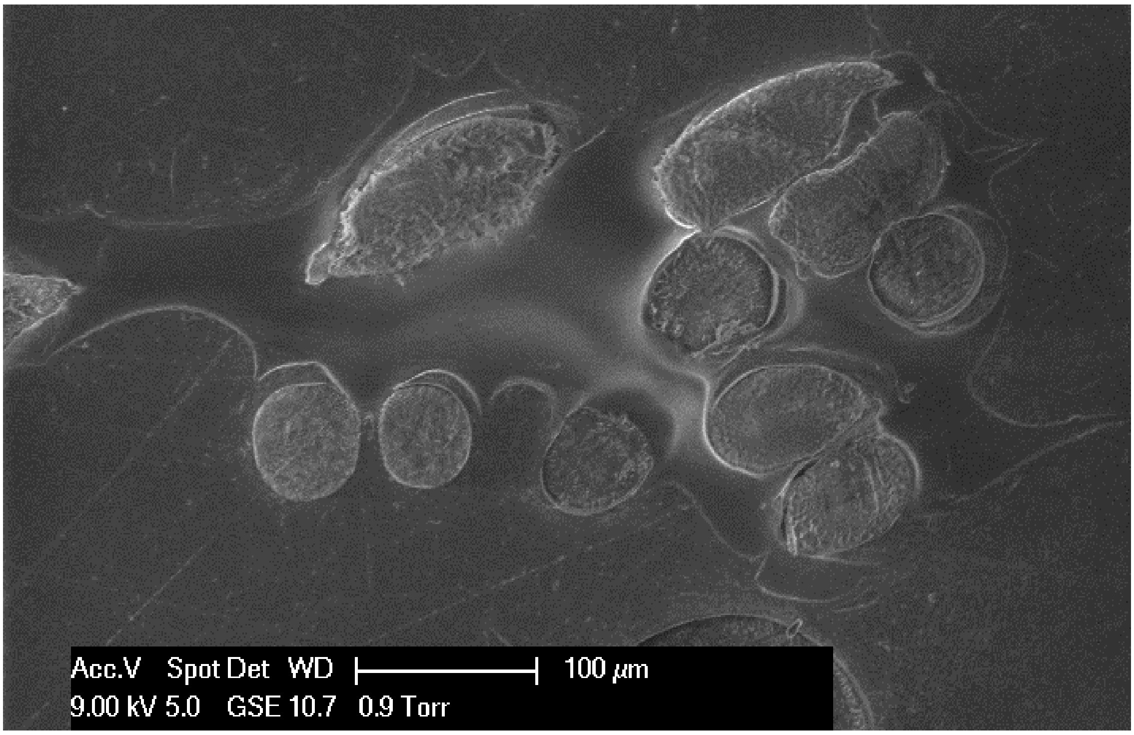

Figure 60 - An ESEM Image of fibres and latex in the 1150 Leigh Spinners artificial sports turf

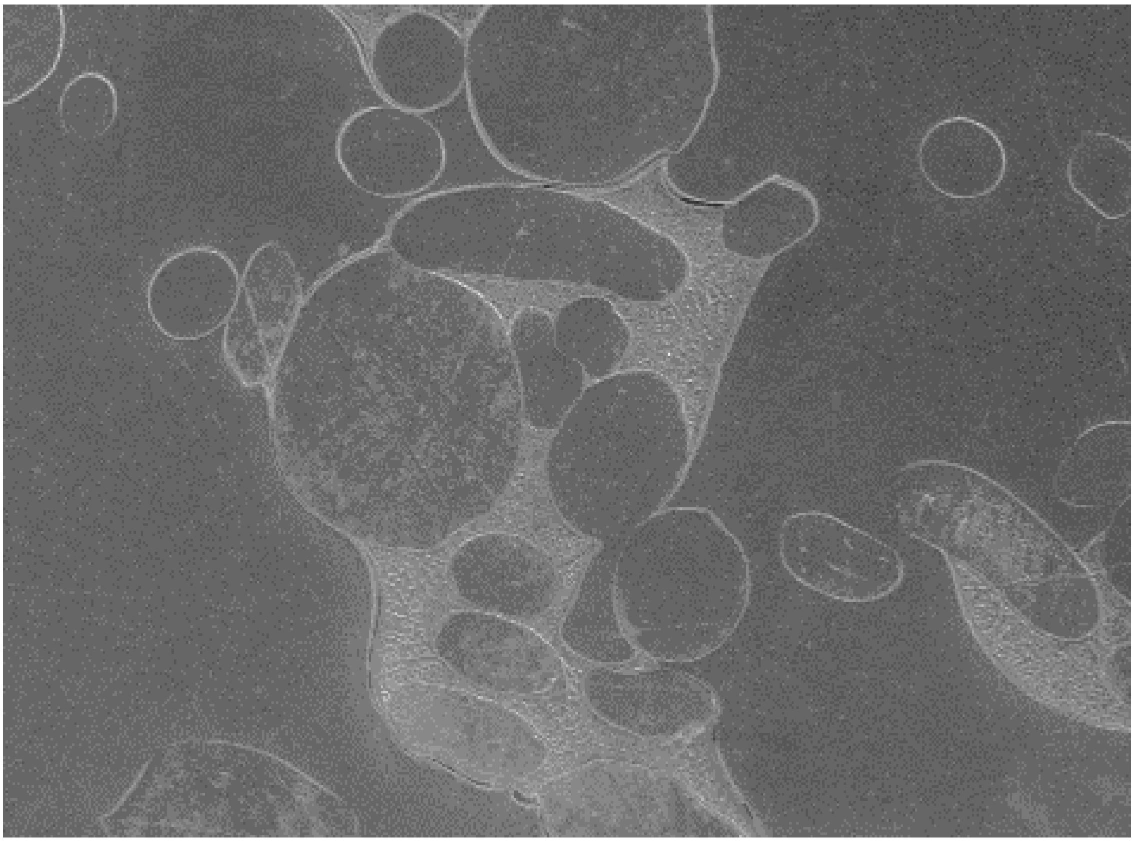

Figure 61 - ESEM Image of a region of latex in the American Sample

4.2.4 Sand Particles

Figure 62 and Figure 63 show the shape of the sand can vary drastically. All the sand particles imaged where of the size shown in these figures, 100 µm to 300 µm.

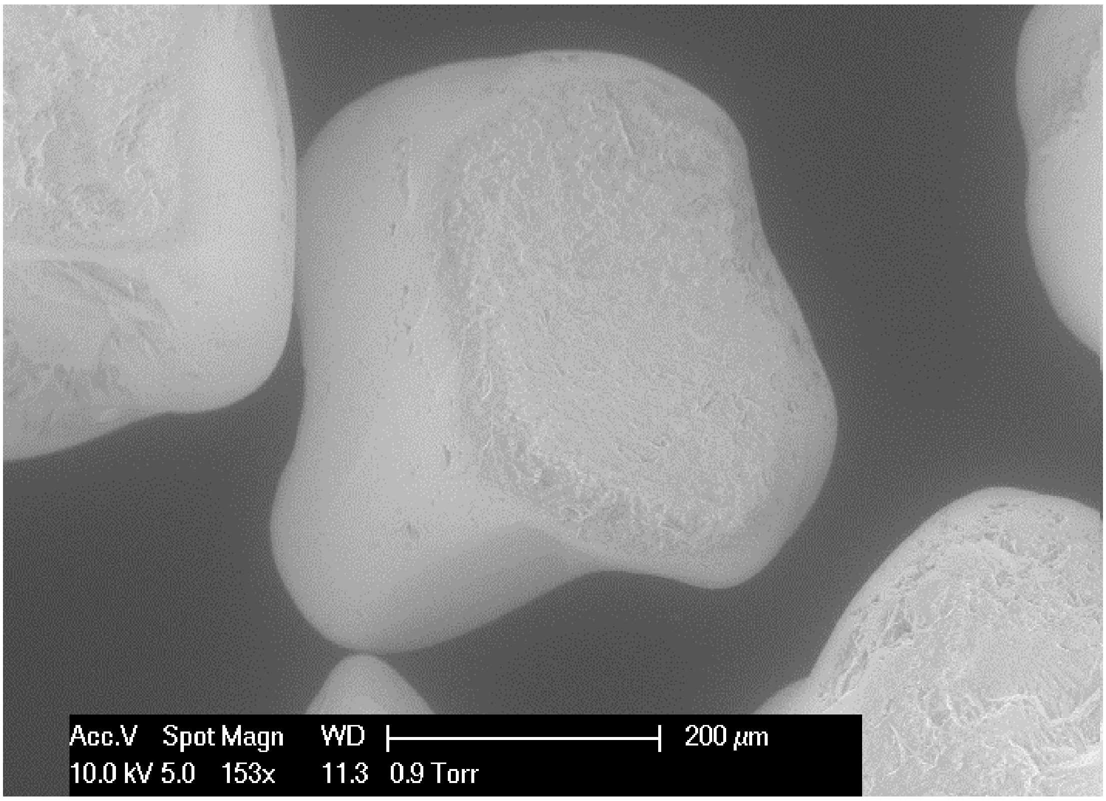

Figure 62 - SEM Image of a sand particle with rounded edges and surfaces

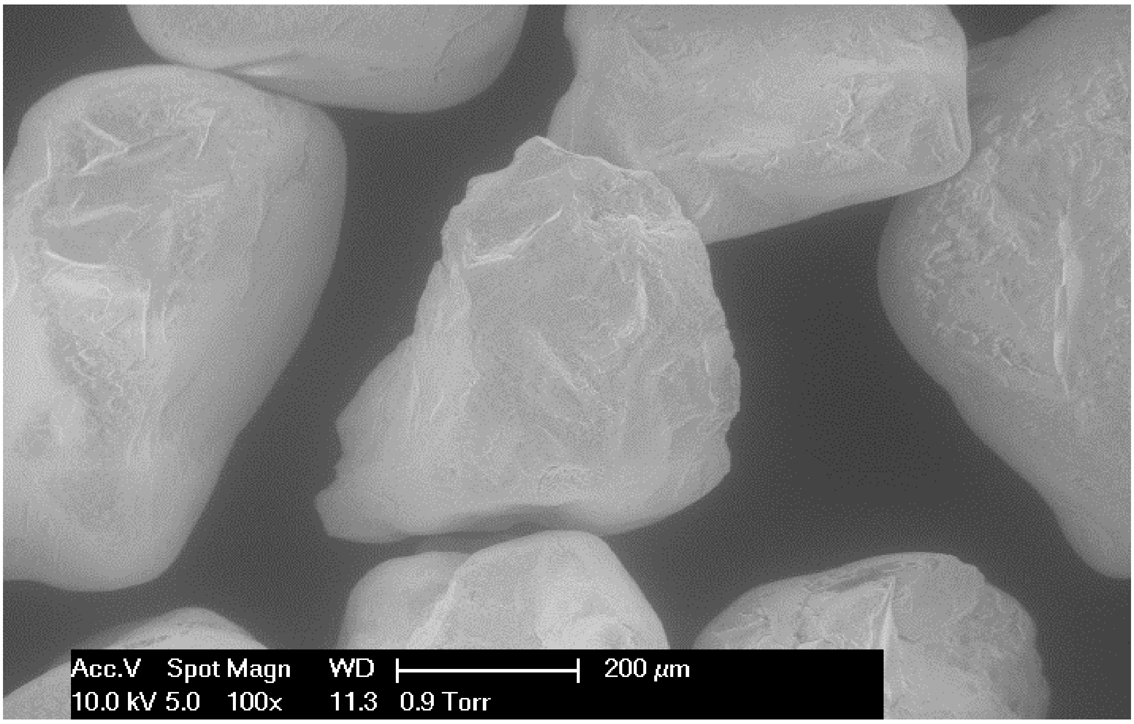

Figure 63 - SEM Image of a sand particle with angular edges and surface of grain

4.2.5 Egg Shell Particles

Figure 64 shows the egg shell particles are predominately small particles approximately 5 to 10 µm in size, with some larger particles approaching 100 µm in size. All the particles appear to have sharp edges.

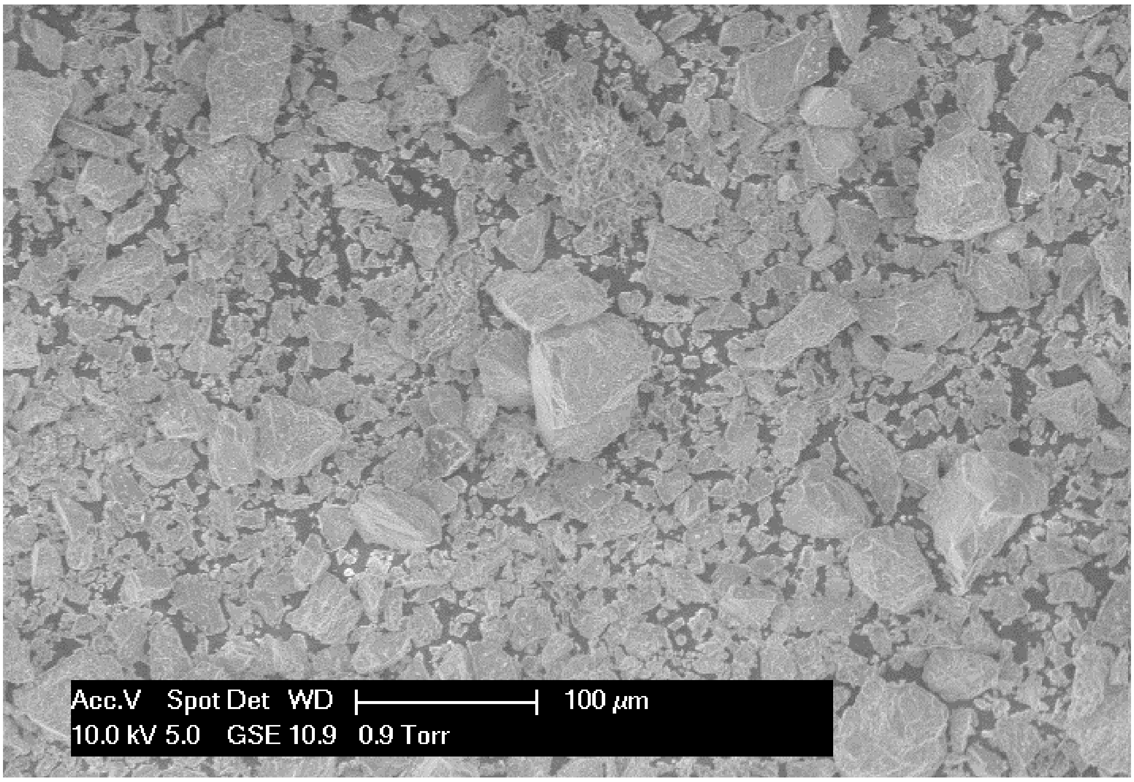

Figure 64 - ESEM Image of egg shell particles

4.3 X-ray CT

Figure 65 and Figure 66 are X-ray CT images of a section of Leigh Spinners 1150 grass green and Rawsons 1150 artificial sports turf respectively. Both show dark/light regions in the artificial sports turf. These regions are believed to be voids in the latex backing showing up as air gaps.

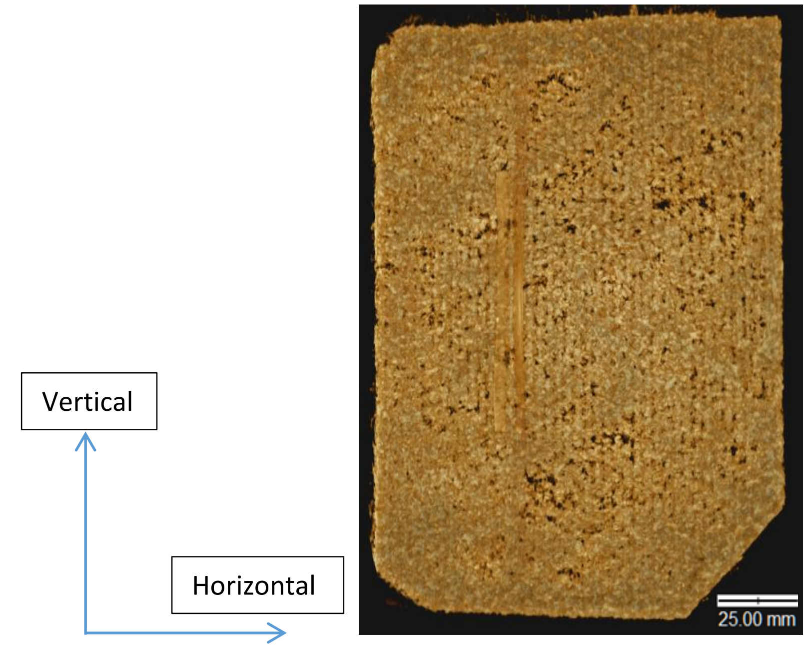

Figure 65 - X-ray CT image of Leigh Spinners 1150 grass green artificial sports turf.

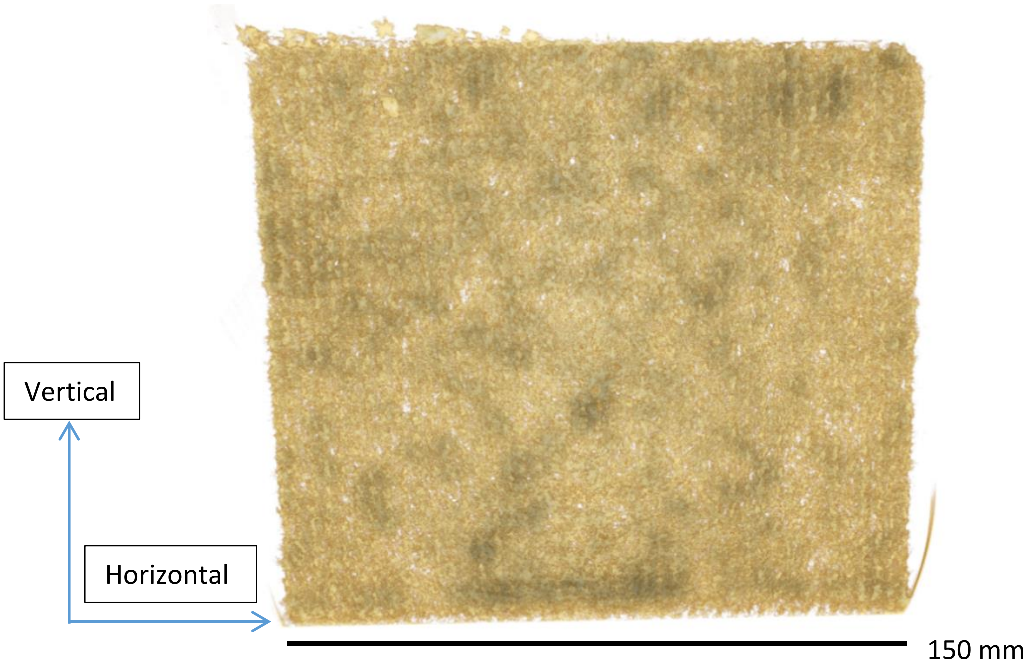

Figure 66 - X- ray CT image of a Rawsons 1150 artificial sports turf

From Figure 67 shows the distribution of the latex in the various samples cut from the latex. Samples 6 to 11 have been cut in the horizontal orientation, and 1 to 5 in the vertical orientation.

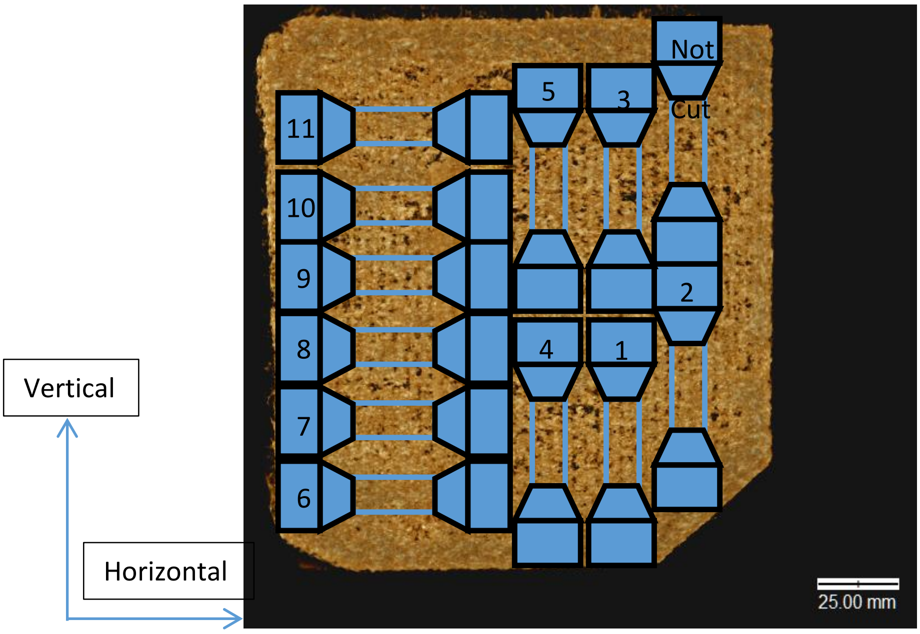

Figure 67 - X ray CT image overlaid with positions of tensile "dog bone" shapes.

Figure 68 shows the force extension curves for the samples that were cut as shown in Figure 67. There is a clear elastic region up to approximately 2 mm/50 N followed by plastic deformation to failure, and some fibre response. The difference between orientations is apparent (discussed in 5). The mean fracture point for the horizontal orientation (223.18 N (18.13)) occurs at 15.80 mm (2.85) extension, whilst the vertical orientation has a mean fracture point of (75.15 N (21.36)) and fails at 16.58 mm (5.96). ANOVA gives a P-value of 5.61E-07 for the fracture points, but 0.78 for the extension values.

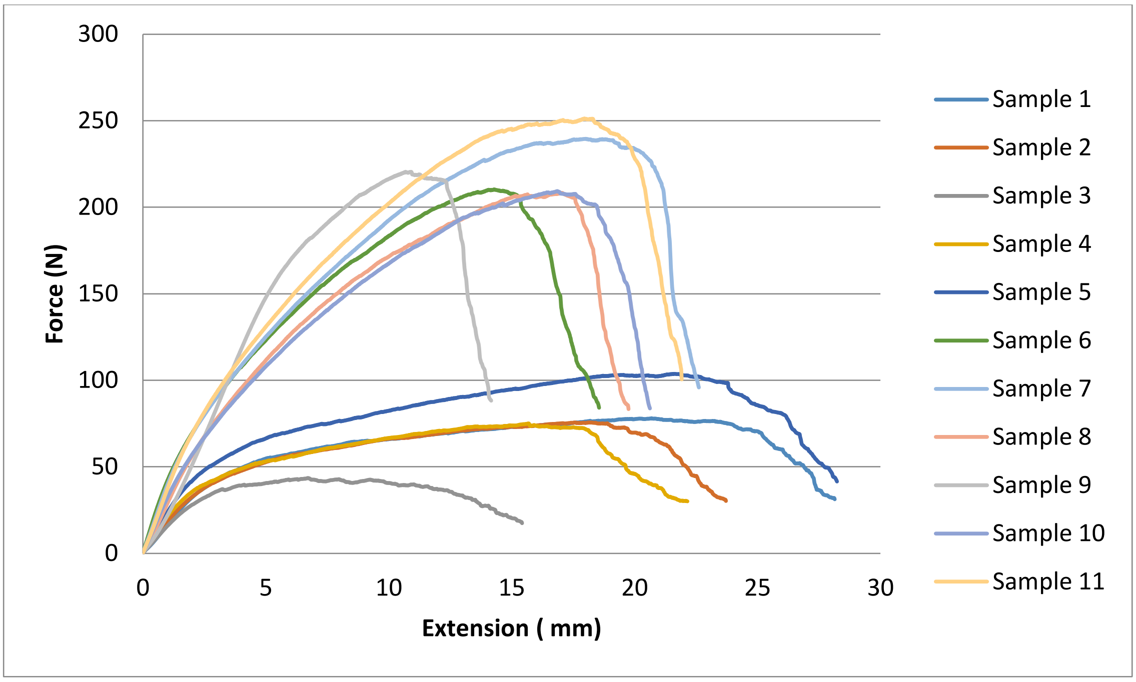

Figure 68 - A graph showing the performance of the 11 samples.

Figure 69 gives the relationship between the mass of a sample and its fracture point. It can be seen that there is some correlation, for the vertical orientation with increasing mass increasing the fracture point, but no correlation for the horizontal.

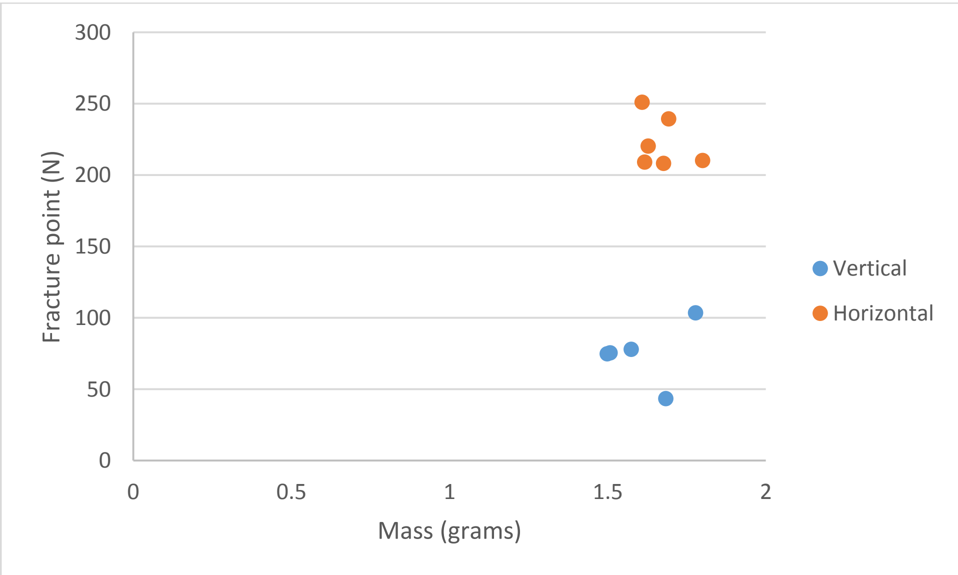

Figure 69 - Graph showing the relation of the Mass of a sample and its fracture point

4.4 Micro X-ray CT

Figure 70 to Figure 73 micro X-Ray CT images taken with a beam energy of 70 kV of a sample of turf without any latex backing applied, the American artificial sports turf, the Rawsons 1300 artificial sports turf and Leigh Spinners 1300 artificial sports turf respectively. In Figure 70 there is some loose structure to the fibres as evidenced by the orientation running across the sample and there are regions of voids. Figure 71 and Figure 72 show similar structure of fibres to the others, and randomly distributed voids in the backing. Figure 73 shows clear structure of the fibres, with some voids evident in the structure.

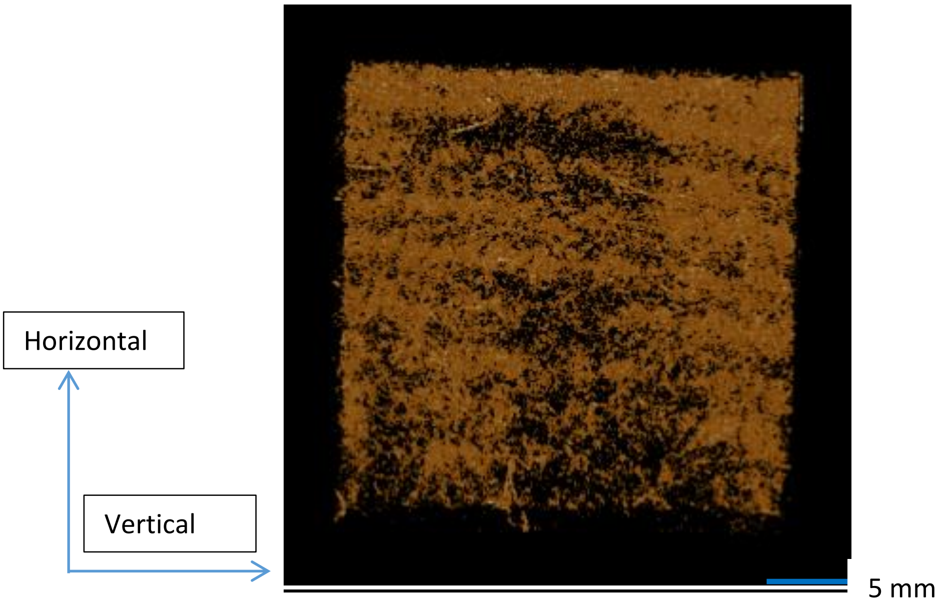

Figure 70 - No latex 70 kV

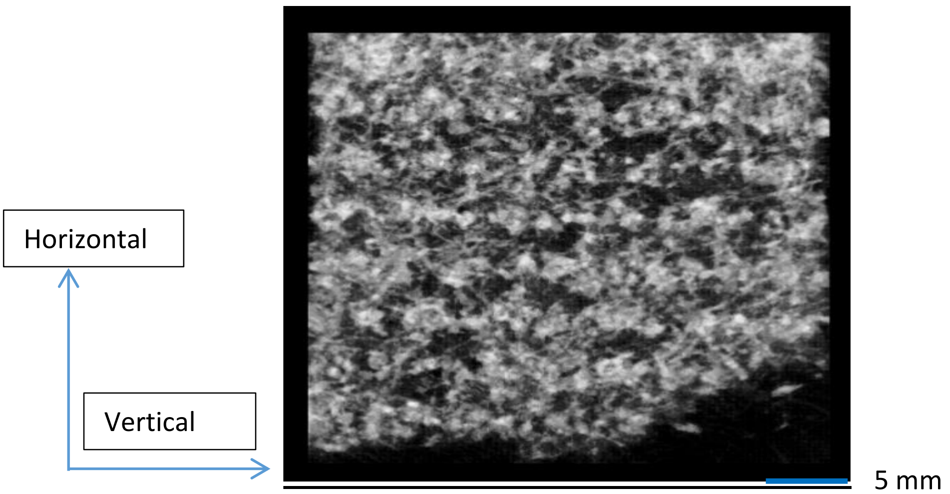

Figure 71 - American 70 kV

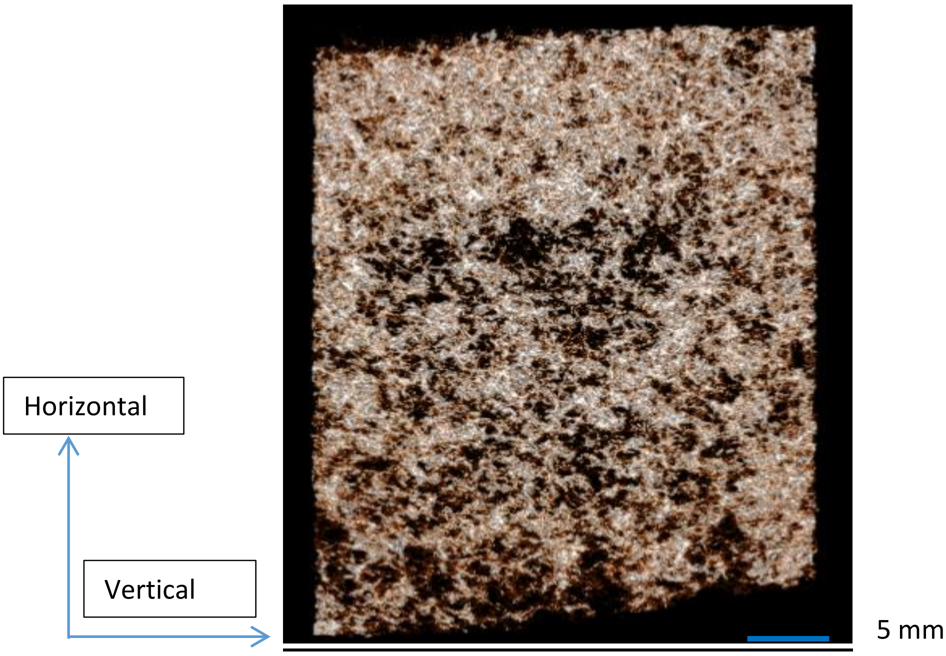

Figure 72 - Rawsons 70 kV

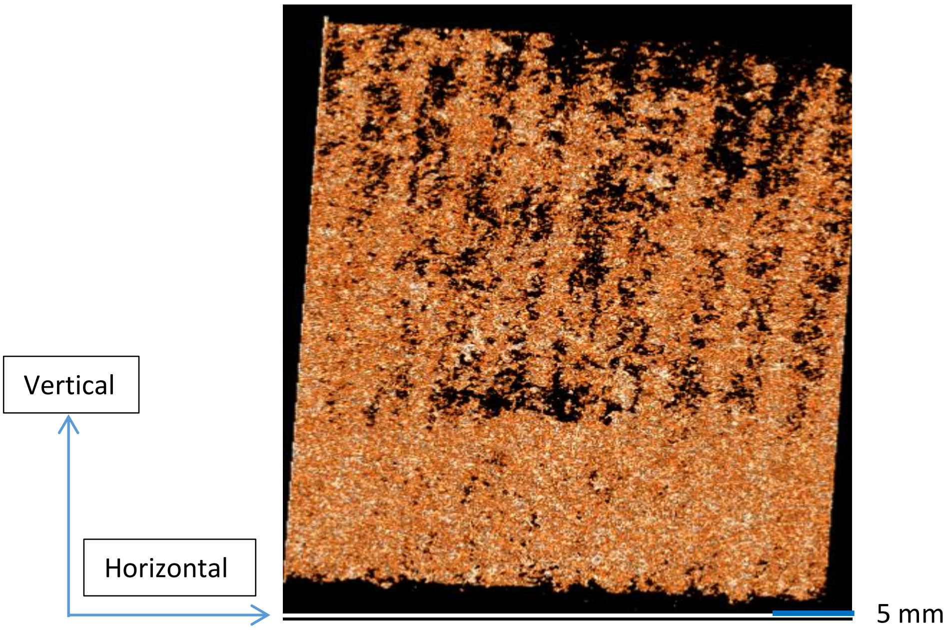

Figure 73 - Leigh Spinners 70 kV

Figure 74 and Figure 75 shows the damage incurred to a sample of the American artificial sports turf after fatigue and tensile loading to failure respectively. The fatigue damage is all along the length, and the structure observed on other experiments is no longer visible, however tensile loading did not cause much damage and the structure is still very apparent.

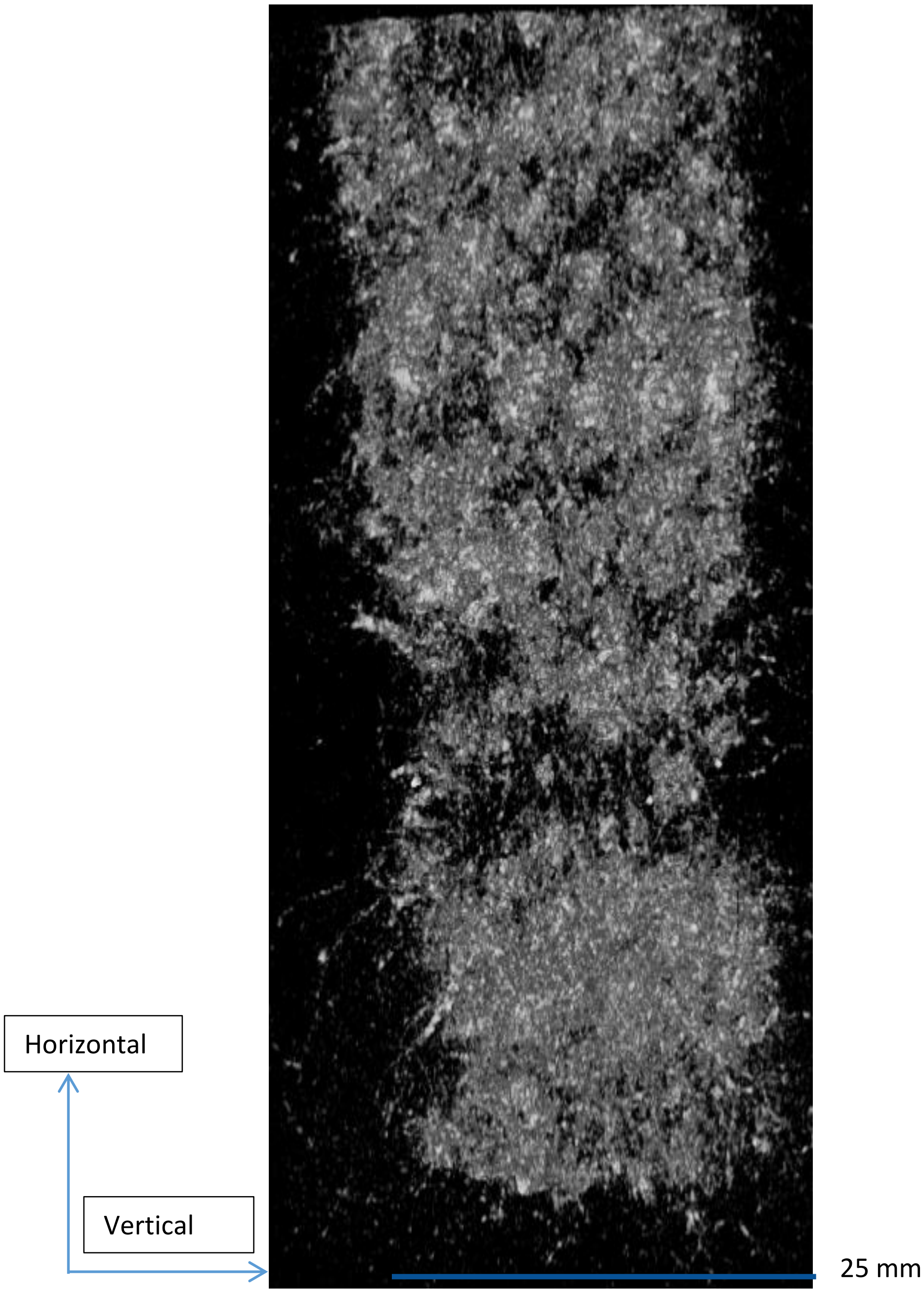

Figure 74 – X-ray CT Image of an American sample (vertical orientation) after fatigue testing

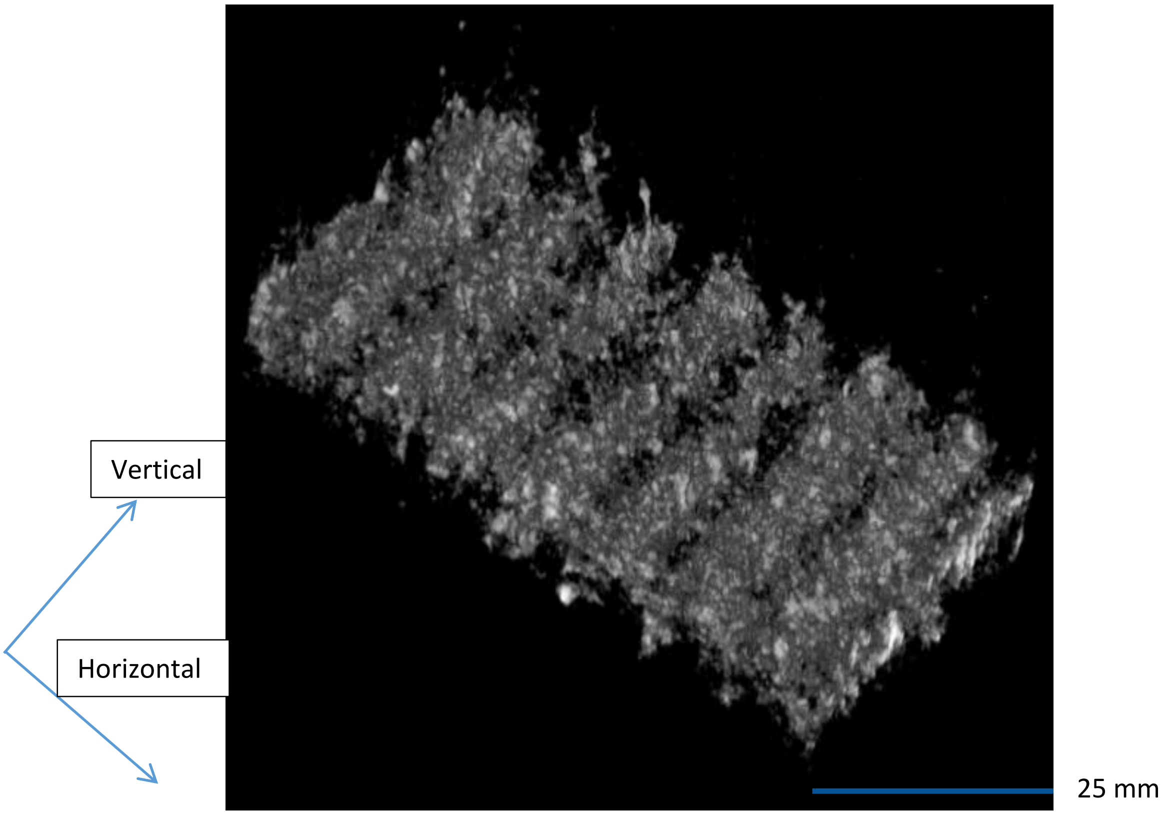

Figure 75 - X-ray CT of the American artificial sports turf after tensile testing.

4.5 MRI

Figure 76, the MRI image shows a thick band of backing (black) and an area of fibres. The MRI images of the other artificial sports turfs are of a comparable quality to Figure 76.

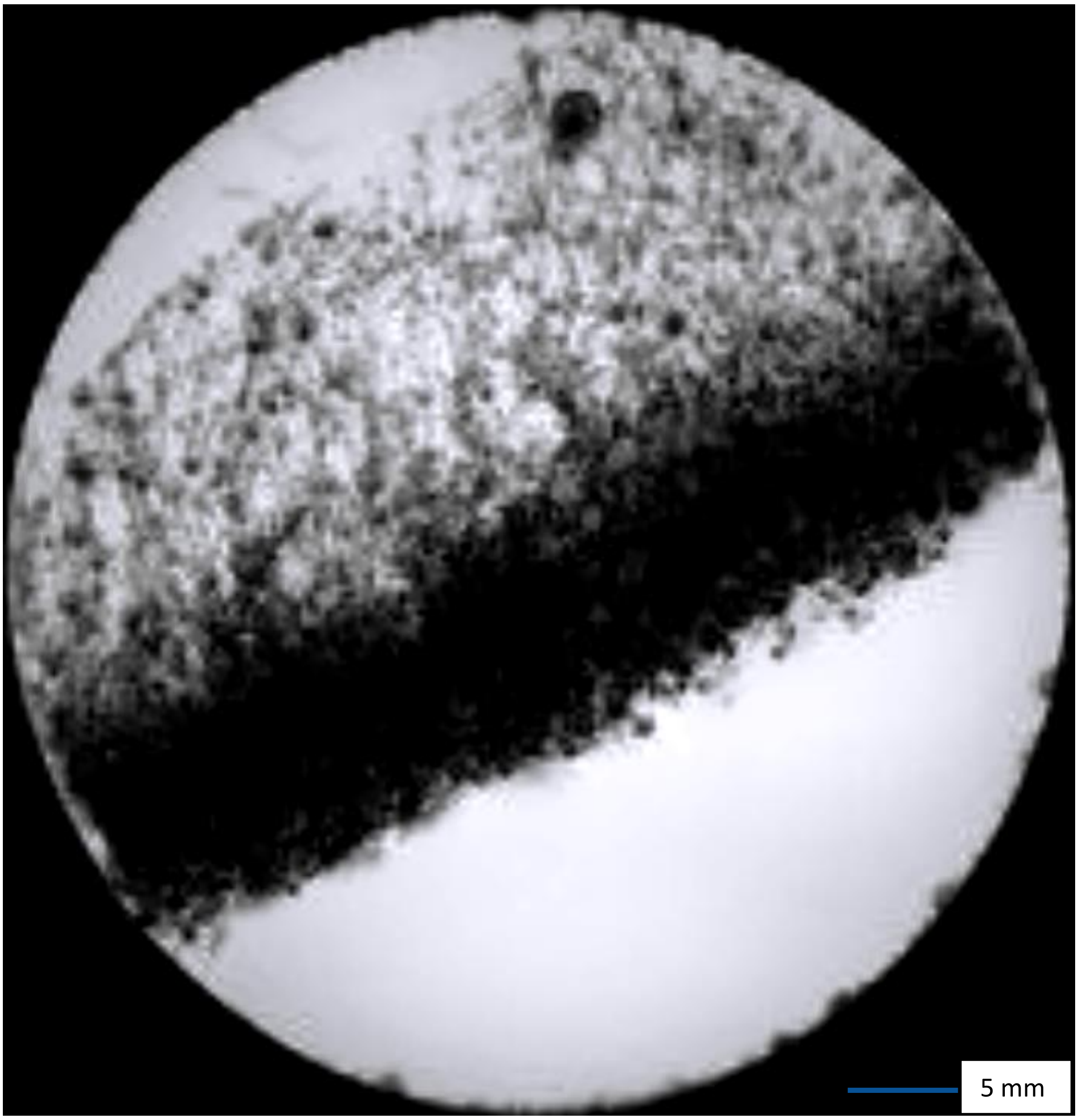

Figure 76 - MRI Image of a sample of Leigh spinners.

4.6 Characterisation Summary

The characterisation showed there is a directionality and voids/pores in the backing/structure of the fibres in all of the artificial sport turfs, that is similar between all the artificial sports turfs. Tensile testing was conducted to see if the directionality/voids affect the mechanical properties of the artificial sports turfs.

5 - Tensile Testing

5.1 Leigh Spinners artificial sports turfs

Figure 77 and Figure 78 show the force extension curves for the Leigh Spinners 1150 grass green artificial sports turf. In Figure 77 the different orientations were cut from different samples however in Figure 78 the differing orientations are cut from the same sample. Both show a clear elastic region up to approximately 10 mm/100 N followed by plastic deformation to failure, and some fibre response after the backing has failed.

In Figure 77 sample batch 1.x is the horizontal orientation which is stronger (mean fracture point = 546.67 N (33.04)) than the vertical orientation (mean fracture point = 360.93 N (11.87)), sample batch 2.x. The fracture occurs approximately 10 mm earlier for the horizontal orientation 67.79 mm (5.40) compared to 79.28 mm (3.05)

In Figure 78 sample batch 19.x is the horizontal orientation and there is a clear difference between the fracture points of this orientation (mean fracture point = 854.00 N (48.11)) and the vertical orientation (mean fracture point = 324.13 N (34.71)), sample batch 18.x. When the extension is considered, the horizontal orientation samples failed at 44.11 mm (5.82), and the vertical samples all failed at 56.89 mm (11.69), which for both orientations is much earlier than the samples shown in Figure 77.

Figure 79 and Figure 80 are the force extension curves for the Leigh Spinners 1300 artificial sports turf cut from different samples and cut from the same sample respectively. In both figures there is a clear elastic region up to approximately 10 mm/150 N followed by plastic deformation to failure, and the fibre response after the backing had failed, however in Figure 80 the elastic/plastic transition is not clear for the horizontal orientation.

In Figure 79 sample batch 3.x is the horizontal orientation which is stronger (mean fracture point = 497.67 N (30.92)) than the vertical orientation (mean fracture point = 298.13 N (15.31)), sample batch 4.x. The fracture occurs at approximately the same extension for these samples, 37.17 mm (2.96) for the horizontal orientation and 39.17 mm (7.16) for the vertical.

In Figure 80 sample batch 7.x is the horizontal orientation and this orientation is stronger (mean fracture point = 741.67 N (23.92)) than the vertical orientation (mean fracture point = 314.93 N (22.01)), sample batch 8.x. The fracture occurs approximately 12 mm earlier for these samples (horizontal orientation 36.35 mm (1.61), vertical orientation 48.37 mm (7.92)).

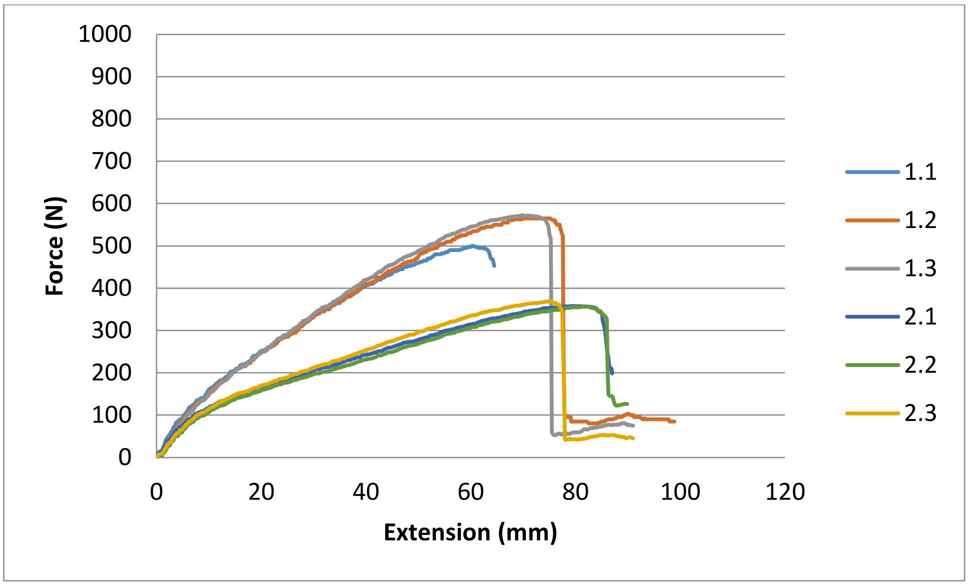

Figure 77 – Force extension graph of the Leigh Spinners 1150 artificial sports turf

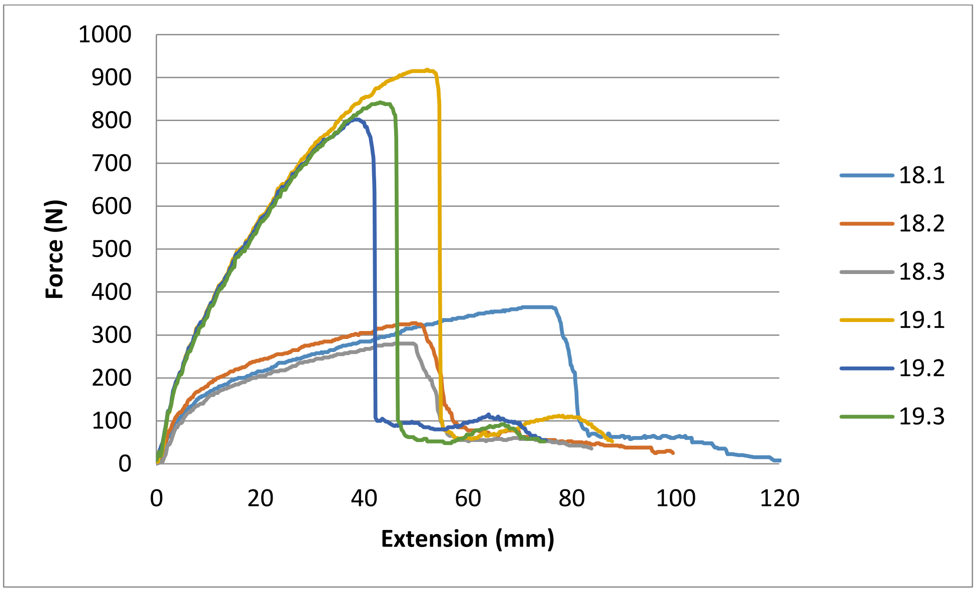

Figure 78 - Force extension graph for the Leigh Spinners 1150 grass green artificial sports turf

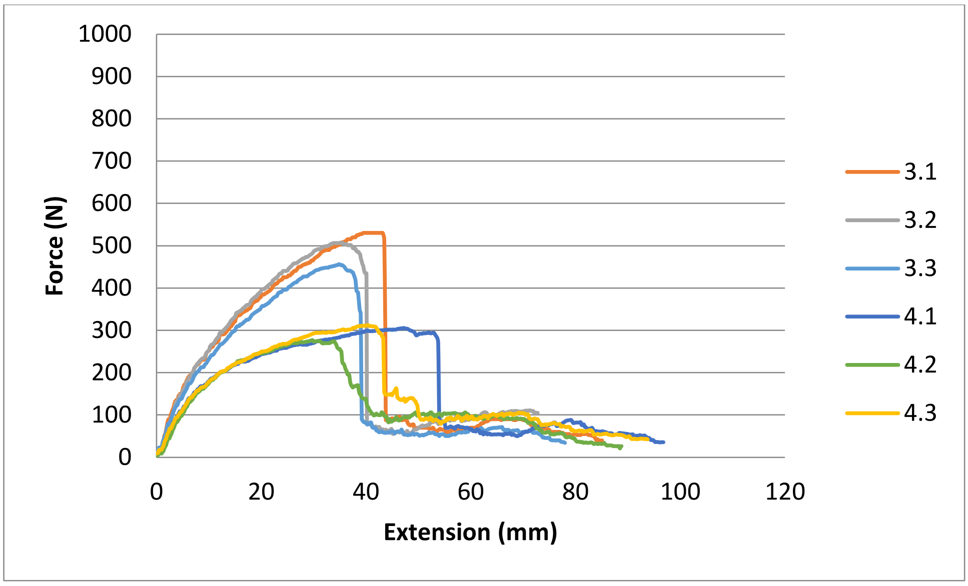

Figure 79 – Force extension graph of the Leigh Spinners 1300 artificial sports turf

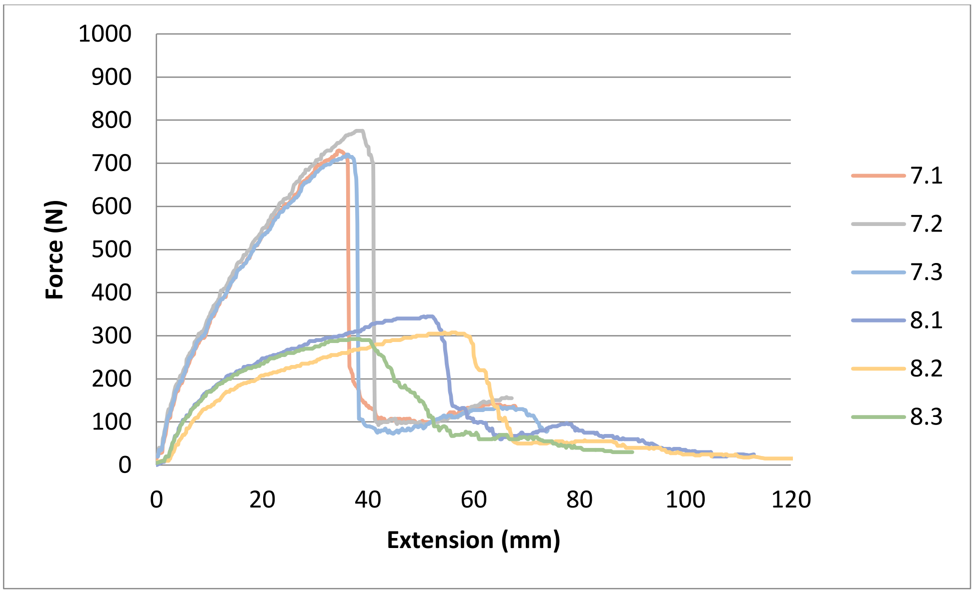

Figure 80 - Force extension graph of the Leigh Spinners 1300 grass green artificial sports turf

5.2 Rawsons artificial sports turfs

Figure 81 and Figure 82 are the force extension curves for the Rawsons 1150 olive green and Rawsons 1150 Lavender artificial sports turfs respectively. In Figure 81 there is a clear but short elastic region up to approximately 5 mm/100 N followed by plastic deformation to failure, and the fibre response after the backing had failed, which can also be seen in Figure 82.

Sample batch 15.x is the horizontal orientation (mean fracture point = 520.67 N (7.59)) of the Rawsons 1150 olive green which is stronger than the vertical orientation (mean fracture point = 399.2 N (28.87)), sample batch 14.x, although these samples do have distinct bands.

Sample batch 17.x is the horizontal orientation of the Rawsons 1150 Lavender. This orientation is stronger (mean fracture point = 719.0 N (30.69)) than the vertical orientation (mean fracture point = 571.0 N (20.85)), sample batch 16.x. When the extension is considered, both artificial sports turfs failed at similar extensions. The Rawsons 1150 olive green vertical orientation samples failed at 65.17 mm (1.41) and the horizontal 70.40 mm (5.63) whereas the Rawsons 1150 Lavender, horizontal orientation samples failed at 65.83 mm (4.52), and the vertical samples all failed in the 78.47 mm (0.24).

Figure 83 and Figure 84 are the force extension curves for the Rawsons 1300 terracotta and Rawsons 1300 olive green artificial sports turf respectively.

Both figures show a clear but short elastic region (up to approximately 5 mm/150 N for the Rawsons 1300 terracotta, up to approximately 5 mm/100 N the Rawsons 1300 olive green) followed by plastic deformation to failure, and the fibre response after the backing had failed.

Sample batch 9.x is the horizontal orientation of Rawsons 1300 terracotta and there is not a substantial difference between the fracture points of this orientation (mean fracture point = 371.13 N (46.01)) and the vertical orientation (mean fracture point = 328.83 N (56.13)), sample batch 10.x. When the extension is considered, the horizontal orientation all failed at 61.5 mm (3.29); however the vertical orientation failed at 47.74 mm (8.33).

Sample batch 11.x is the horizontal orientation of the Rawsons 1300 olive green (mean fracture point = 359.16 N (61.49)) and there is not a substantial difference between the fracture points of this orientation and the vertical orientation (mean fracture point = 269.3 N (23.92)), sample batch 12.x. The exception is sample 11.3, which failed at approximately the same force as the vertical orientation. With regards to the extension, all the samples failed in pairs. The first 2 horizontal samples failed at approximately 75 mm; however the last horizontal sample failed very near to one of the vertical samples, at approximately 40 mm extension. Finally, the other 2 vertical samples failed at 87.77 mm (1.88), therefore the standard deviation for these samples is large – horizontal orientations 59.25 mm (12.38), and vertical orientation 73.98 mm (19.56)

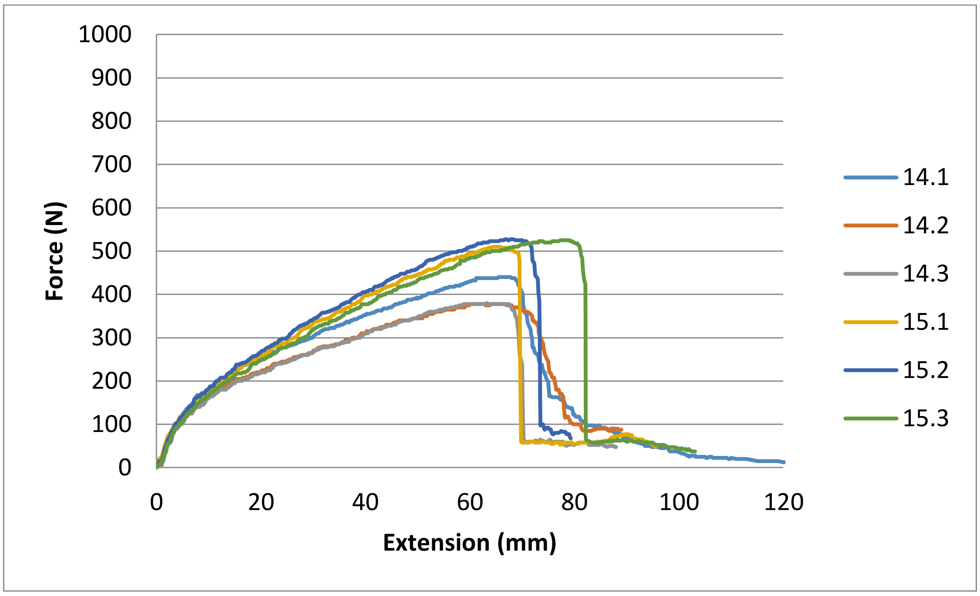

Figure 81 – Force extension graph for the Rawsons 1150 olive green artificial sports turf.

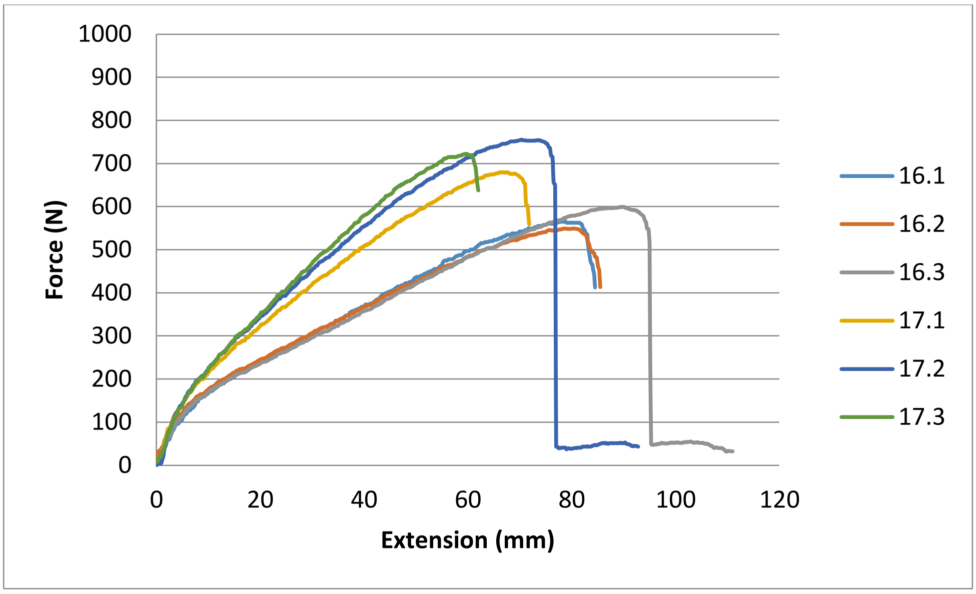

Figure 82 – Force extension graph for the Rawsons 1150 Lavender artificial sports turf.

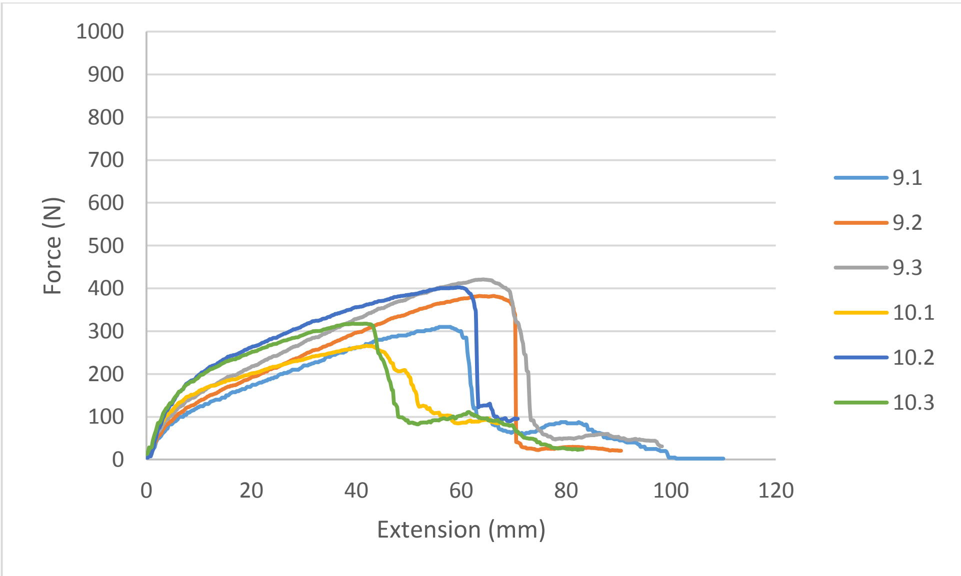

Figure 83 - Force extension graph for the 1300 Rawsons Terracotta samples.

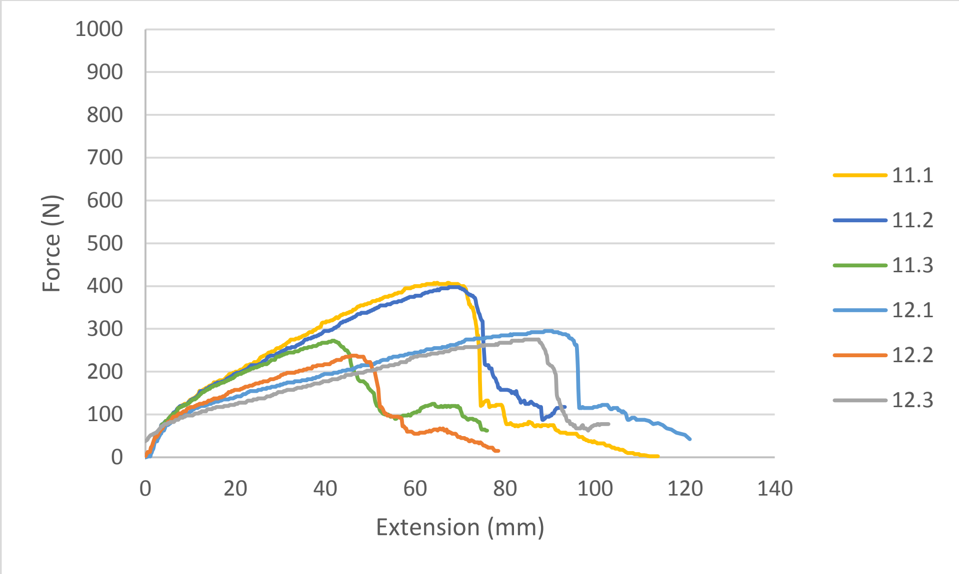

Figure 84 – Force extension graph for the 1300 Rawsons olive Green samples.

5.3 NottsFilm Stiff, No Latex and American Samples

Figure 85 shows the force extension curve for the NottsFilm stiff product. There is a short elastic region, less than 5 mm/100 N followed by plastic deformation to failure, and some fibre response after the backing had failed. Sample batch 6.x is the horizontal orientation (mean fracture point = 321.6 N (23.15)) and it is clear this orientation is stronger than the vertical (mean fracture point = 176.67 N (2.36)), sample batch 5.x. The fracture occurs at approximately 37.76 mm (0.43) extension for the horizontal samples, to 51.07 mm (2.31) for the vertical samples.

Figure 86 shows the force extension curve for the samples that did not have the latex backing applied. There is no clear elastic or plastic region, or even a clear fracture point; however there is a substantial difference between the tensile performances of the two orientations. The vertical orientation (sample batch 20.x) fails at 70.17 N (17.94) when the load is applied, whereas the horizontal orientation (sample batch 21.x) does take the load of 190.2 N (52.40) before the fibres are pulled apart.

Figure 87 shows the force extension curve for the American artificial sports turf. There is a clear elastic region up to approximately 5 mm/200 N followed by plastic deformation to failure, and some fibre response after the backing had failed for the vertical orientation (batch 22.x). The elastic region is less evident for the horizontal samples (batch 23.x). There is a clear difference between the fracture points between the 2 orientations. The mean fracture point for the horizontal samples is 625.4 N (77.65), whilst the mean fracture point for the vertical orientation is 265 N (2.6). When the extension is considered, the horizontal orientation samples failed at 60.84 mm (0.04), and the vertical samples all failed at 39.90 mm (18).

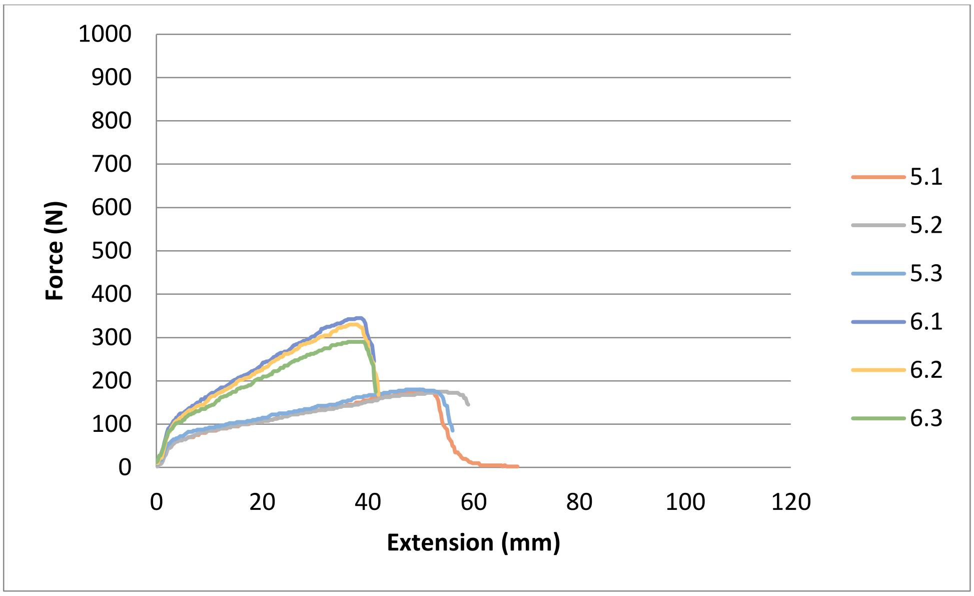

Figure 85 – Force extension graph for the NottsFilm Stiff samples.

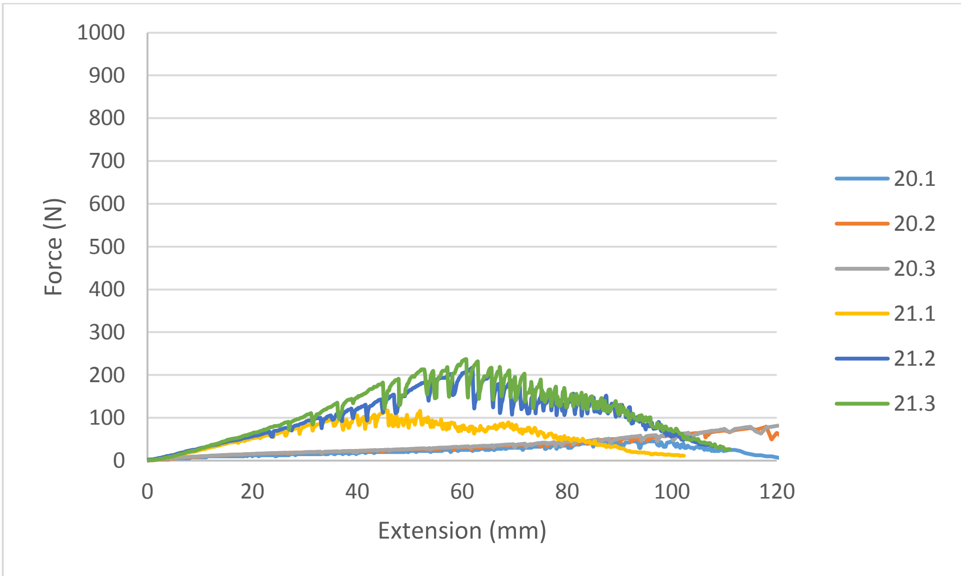

Figure 86 – Force extension graph of the "No latex" samples.

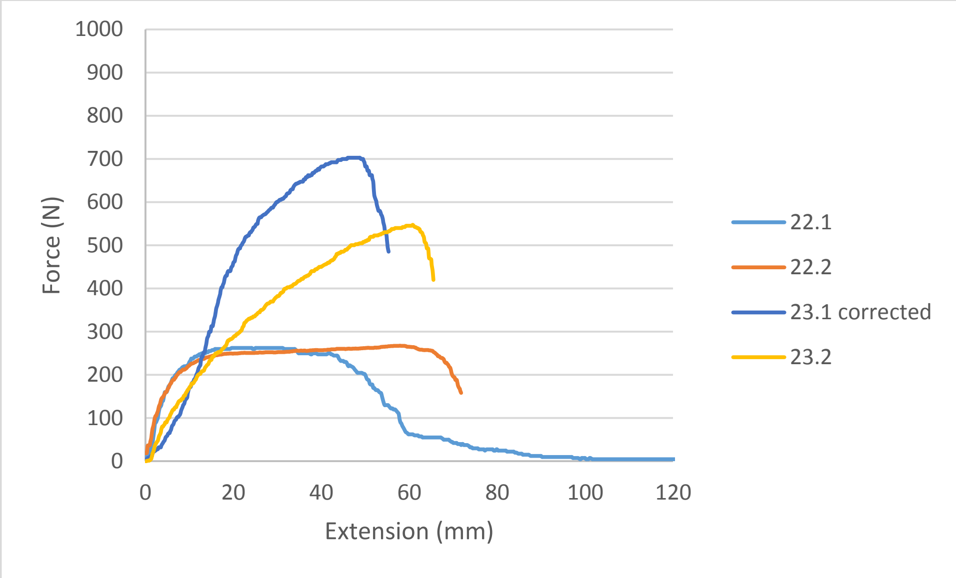

Figure 87 – Force extension graph of the American samples.

5.4 Worn in Situ Artificial sports turf

Figure 88 shows the force extension curve for the “worn in situ” samples cut from the square sample. Neither orientation shows a clear elastic region or plastic deformation to failure, nor had much fibre response after the backing failed. Sample batch 25.x is the horizontal orientation which has a mean fracture point of 884.3 N (74.68) vertical orientation, sample batch 24.x, has a mean fracture point of 273.6 N (6.75). When the extension is considered, the horizontal orientation samples failed at 28.33 mm (2.29), and the vertical samples all failed at 34.33 mm (5.10).

Figure 89 and Figure 90 show the force extension curve for the “P1” and “P2” samples respectively. For both the P1 and P2 samples the vertical orientation shows a clear elastic region followed by plastic deformation to failure and some fibre response after the backing had failed, the horizontal does not show such a clear distinction. Sample batches P1Hx and P2Hx are the horizontal orientation and there is a substantial difference between the fracture points of this orientation (mean fracture point of 853.33 N (17.46) and 848.00 N (13.37) respectively) and the vertical orientation (mean fracture point of 251.67 N (62.49) and 270.90 N (41.96) respectively), sample batches P1Vx and P2Vx. When the extension of the P1 samples is considered, the horizontal orientation samples all failed just after 20 mm extension, and the vertical samples all failed at approximately 40 mm. When the extension of the P2 samples is considered, the horizontal orientation samples again all failed just after 20 mm extension, and the vertical samples all failed at 35.00 mm (11.47).

Figure 91 shows the fracture points of the P1 and P2 samples. All the samples are grouped together within 100 N of each other.

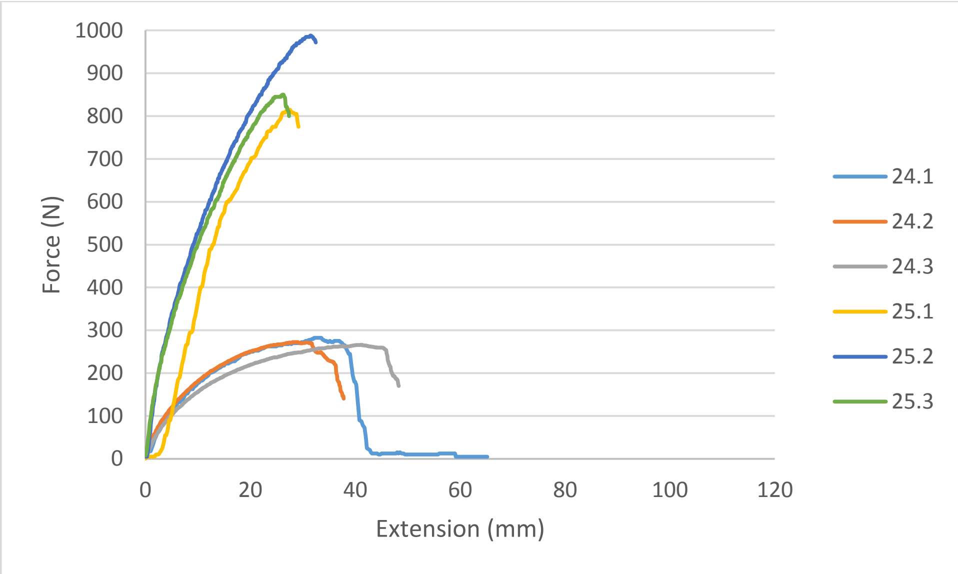

Figure 88 – Graph of the tensile testing of the samples of artificial sports turf worn in situ, square sample.

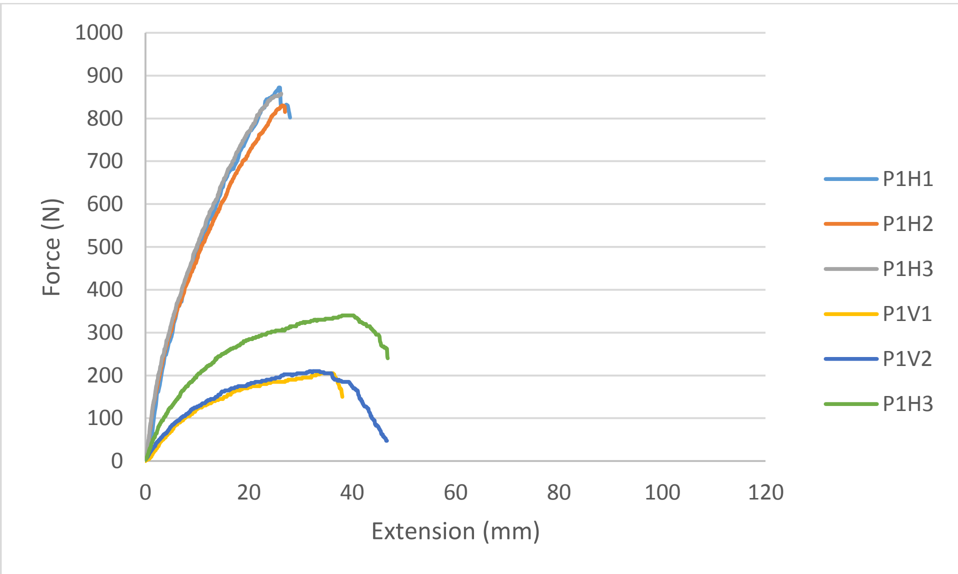

Figure 89 - Tensile results of the samples cut from position 1

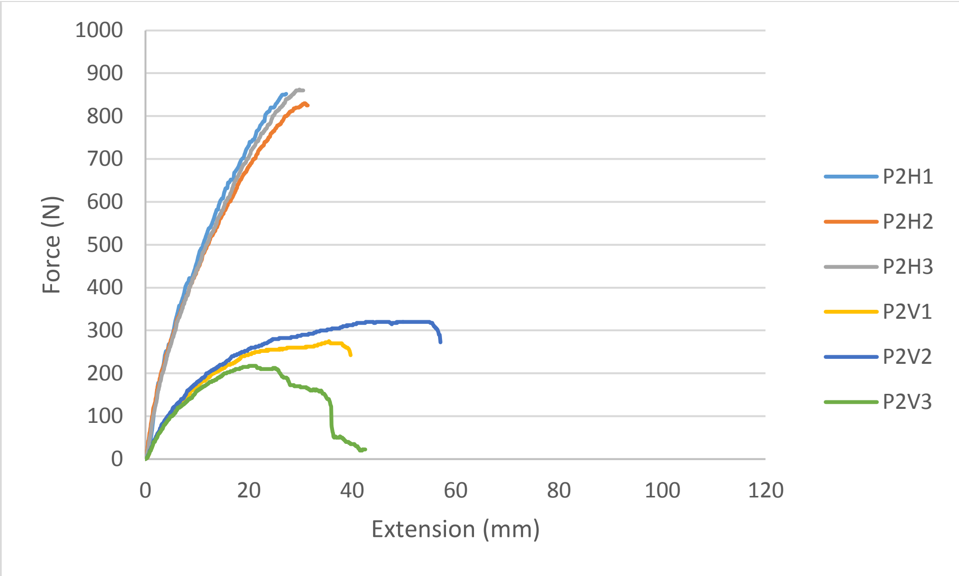

Figure 90 – Tensile results of the samples cut from position 2

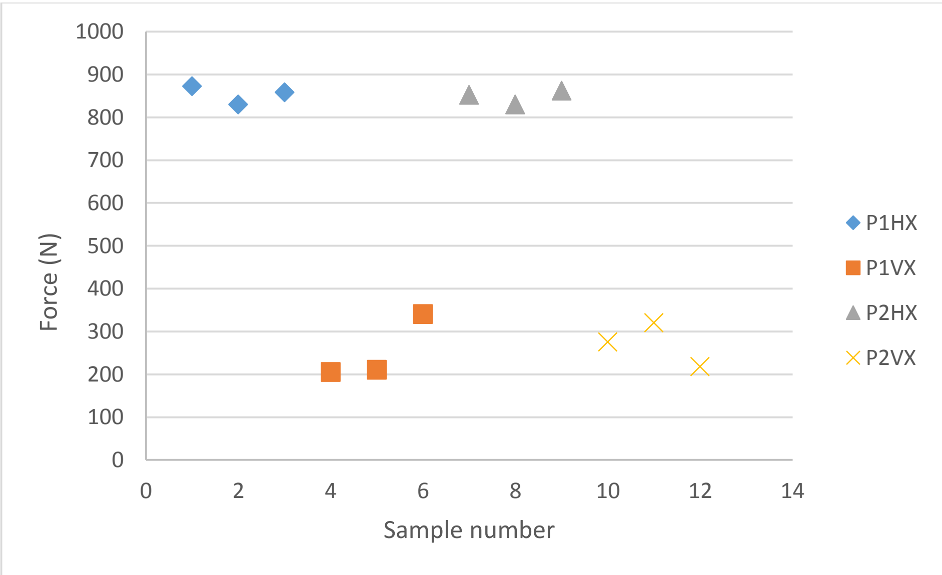

Figure 91 – Fracture points of the worn in situ artificial sports turf

5.5 Fracture Points All artificial sports turfs

Figure 92 shows the fracture points vary greatly with 3 distinct bands, indicated by the boxes. In the highest band, (greater than 650 N), are the Rawsons 1150 horizontal lavender, the Leigh Spinners 1300 horizontal green and the Leigh Spinners 1150 green horizontal. The second band, 450 N up to 650 N, contains mostly Leigh Spinners artificial sports turfs (2 thirds of the artificial sports turfs in this band are Leigh Spinners) and mostly 1150 artificial sports turfs (again, 2 thirds of the artificial sports turfs in this band are 1150 artificial sports turfs). The American horizontal orientation is in this band. The lowest band, 225 N up to 450 N, contains most of the samples tested, including a mix of Rawsons, Leigh Spinners and American (vertical orientation) artificial sports turfs, and a mix of 1150 and 1300 artificial sports turfs. ANOVA analysis of the average fracture points showed statistical significance (p value = 1.16824E-36). Subsequent t-Tests gave the data shown in Table 6.

Comparison	T Stat	T critical two tail
High medium	11.23801139	2.034515297
Medium Low	10.5631466	2.039513446
High Low	24.38019095	2.030107928

Table 6 - Results for t-tests of fracture points.

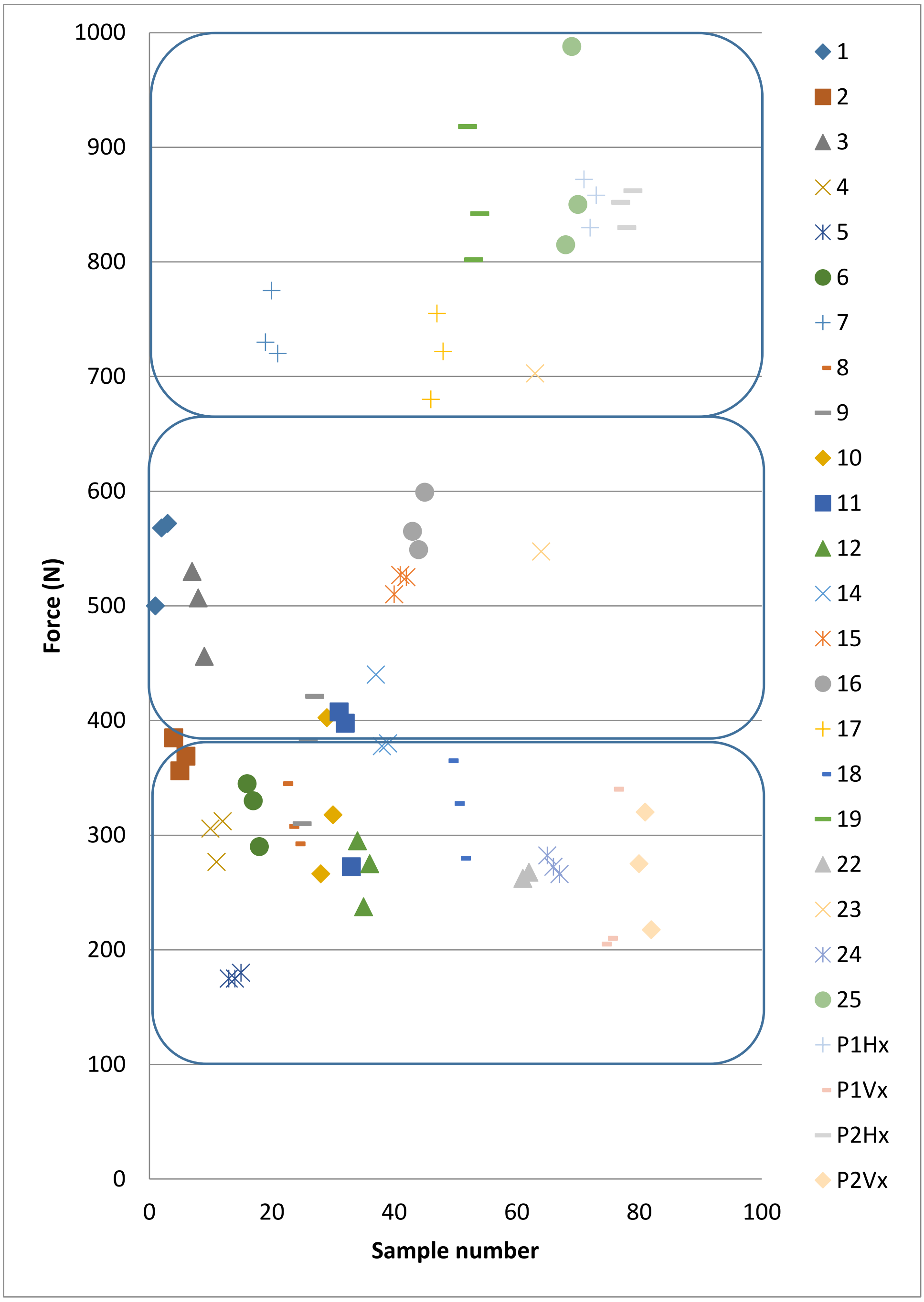

Figure 92 - Fracture points of the artificial sports turfs

Manufacturer	Average Pile Yarn Weight	Orientation	Sample no.	Fig.	Mean Fracture Point (N)	Mean Stiffness (N/mm)	Mean Extension (mm)	P value
Leigh Spinners	1150	Horizontal	1.x	Figure 77	546.67	15.488	67.79	0.002057
	1150	Vertical	2.x		360.93	11.655	79.28	
	1300	Horizontal	3.x	Figure 79	497.67	24.520	37.17	0.001217
	1300	Vertical	4.x		298.13	18.364	39.17	
	1150	Horizontal	19.x	Figure 78	854.00	35.703	44.11	0.000226
	1150	Vertical	18.x		324.13	17.195	56.89	
	1300	Horizontal	7.x	Figure 80	741.67	32.105	36.35	4.96E-05
	1300	Vertical	8.x		314.93	17.976	48.37	
Rawsons	1150	Horizontal	15.x	Figure 81	520.67	17.137	70.40	0.00452
	1150	Vertical	14.x		399.20	16.892	65.17	
	1150	Horizontal	17.x	Figure 82	719.00	22.049	65.83	0.004862
	1150	Vertical	16.x		571.00	16.193	78.47	
	1300	Horizontal	9.x	Figure 83	371.13	12.874	61.53	0.456105
	1300	Vertical	10.x		328.83	17.511	47.74	
	1300	Horizontal	11.x	Figure 84	359.16	13.394	59.25	0.12635
	1300	Vertical	12.x		269.30	9.454	73.98	
American	---	Horizontal	23.x	Figure 87	625.40	17.207	60.84	0.043522
	---	Vertical	22.x		265.00	21.974	39.90	
Unknown	1300	Horizontal	P1Hx	Figure 89	853.33	46.709	26.25	0.000195
	1300	Vertical	P1Vx		251.67	14.511	35.64	
	1300	Horizontal	P2Hx	Figure 90	848.00	43.417	29.27	4.99E-05
	1300	Vertical	P2Vx		270.90	18.065	35.00	

Unknown	1300	Horizontal	25.x	Figure 88	884.30	49.268	28.33	0.000324
	1300	Vertical	24.x		273.60	16.129	34.33	
NottsFilm stiff	---	Horizontal	5.x	Figure 85	321.60	13.643	51.07	0.000916
	---	Vertical	6.x		176.67	23.372	37.76	
No latex	---	Horizontal	21.x	Figure 86	190.20	2.704	54.64	0.037386
	---	Vertical	20.x		70.17	0.857	110.23	

Table 7 - Data from Tensile Testing

5.6 Product Comparisons

Across the majority of the artificial sports turfs there is a statistically significant difference in the tensile performance for most of the artificial sports turfs when they are cut with different orientations, as evidenced by the P values listed in Table 7. This difference between orientations is discussed in 7.1.

For the majority of the artificial sports turfs, the horizontal orientation achieved higher fracture points, whereas the vertical orientation achieves slightly higher extension values.

5.6.1 1150/1300 and Leigh Spinners/Rawsons

Comparing the 2 weights of fibre (ignoring the differences caused by the differing manufacturers) it can be said, the fracture point for the 1150 artificial sports turfs is typically higher in both orientations than the fracture point of the 1300 artificial sports turfs. Additionally the extensions and stiffness's for the 1150 artificial sports turfs are also comparable or higher than those for the 1300 artificial sports turfs.

Comparing the two manufacturers, the fracture point of the Rawsons artificial sports turfs in the horizontal direction is lower although the vertical test results are very similar. The stiffness's of the Rawsons artificial sports turfs are also lower in comparison to the Leigh Spinners. Conversely the extension of the Rawsons artificial sports turfs perform better than the Leigh Spinners.

5.6.2 Leigh Spinners and Rawsons/Worn in Situ Artificial sports turf

Figure 88 to Figure 91 show the samples cut from opposite ends of the longer piece of worn in situ turf behaved similarly to each other, and to the other piece of worn artificial sports turf.

By comparison between Figure 80 and Figure 88 it is evident the worn in situ artificial sports turf, from an unknown manufacturer, behaves similarly to the Leigh Spinners 1300 grass green. This is evident in both the extension and fracture point, although there is a slight difference.

5.6.3 Leigh Spinners and Rawsons/American.

From Figure 87, it is clear the directionality is distinctly apparent in the American artificial sports turf, with sample 23.1 being nearly 3 times, and sample 23.2 being 2 times, stronger than samples 22.1 and 22.2. It can also be seen that the vertical orientation plateaus before failure, which is drastically different to the previous Leigh Spinners/Rawsons artificial sports turfs. When compared to the artificial sports turfs previously tested, the American artificial sports turfs stiffness's and ultimate tensile strengths are of a similar magnitude.

It was also evident the horizontal samples failed in a similar manner to the previous artificial sports turfs, with a steady increase in load until a sudden failure, although the transition from the elastic region to the plastic region is less clear with the American samples. It can also be seen that sample 23.2, the one cut from the other piece of artificial sports turf, failed at a lower load, which may be due to sample 23.2 weighing 1.6467 grams less. All the samples lost approximately 0.07 grams during the test.

The vertical extension is comparable to the Leigh Spinners artificial sports turf, but lower compared to the Rawsons artificial sports turf. The horizontal extension is lower than the Leigh Spinners, and much worse than the Rawsons artificial sports turfs.

The stiffness of the American artificial sports turf is again comparable to the Leigh Spinners in the vertical orientation, whilst superior to the Rawsons. The stiffness of the American artificial sports turf is again superior to the Rawsons in the horizontal orientation however Leigh Spinners is superior to the others.

Additionally, the American artificial sports turfs appear to twist and become contorted when they fail, which did not occur in such an apparent way in the others, although some necking was observed.

5.6.4 Other – NottsFilm Stiff/No Latex

Figure 85 shows the NottsFilm Stiff product behaves similarly to the other artificial sports turfs, in that one orientation exhibits a higher fracture point but at a shorter extension whereas the other orientation exhibits the reverse, despite the lack of visible directionality. This is evidence that these properties are due to the structure and not the material.

Figure 86 shows the directionality is still present in the samples with no latex backing applied, and that as the fibres break there is a brief period before the other fibres take up the load. It is also clear the horizontal orientation is stronger than the vertical, and as there is no latex present this would suggest that the needling step in the manufacturing process is indeed the cause of the directionality.

5.7 Tensile Testing Summary

The tensile testing showed that the horizontal orientation is stronger than the vertical for all the artificial sports turfs, and the failures occur at loads far higher than could be achieved in normal usage which are of the order of 184.5 N as described in 9, and so fatigue testing was used to assess how repeated loading applied to the artificial sports turf caused a failure.

6 - Wear, Hardness and Fatigue Testing

6.1 Wear Testing

Figure 93 shows the frictional force of a sample of Leigh Spinners 1150 without sand infill worn against a steel ball bearing across a preliminary 2 hour experiment. As time goes by, the frictional force increases as evidenced by the increasing gradient of the trend line, suggesting that as the fibres become worn, they also provide more grip. For this experiment the mean value of friction is 3.75 N.

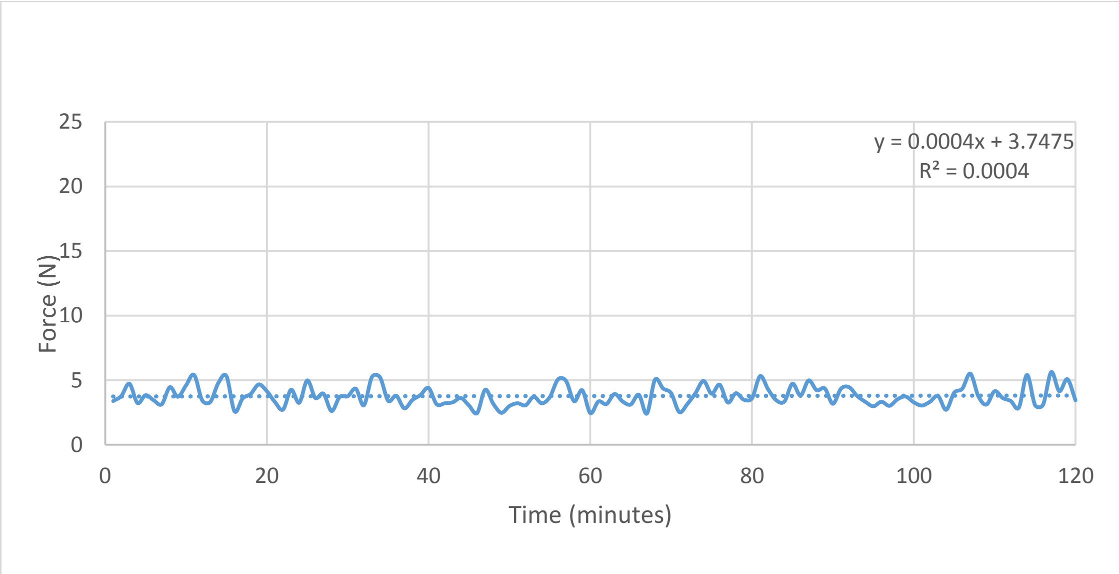

Figure 93 – Wear test result from preliminary experiment

6.1.1 Leigh Spinners 1150 artificial sports turfs

Figure 94 to Figure 97 shows the frictional force of a sample of Leigh Spinners 1150 worn against a polymeric stud across an 1800 second experiment. Figure 95 and Figure 97 have the higher load on the counter face (7.65 N), and Figure 96 and Figure 97 have a filler layer of sand applied.

For Figure 94, the frictional force increases slightly with time. The increase is roughly a quarter of what is seen in Figure 93, implying the rate of change is linear (as the experiment is ¼ of the length). In this experiment the mean value of friction is 4.66 N. However for Figure 95, the frictional force decreases with time, unlike the previous experiments. Here, mean value of friction is 8.80 N.

Figure 96 shows the frictional force remains almost constant. This experiment found the mean value of friction is 4.35 N. This is contrasted by Figure 97 the frictional force decreases slightly with time. In this experiment mean value of friction is 8.22 N.

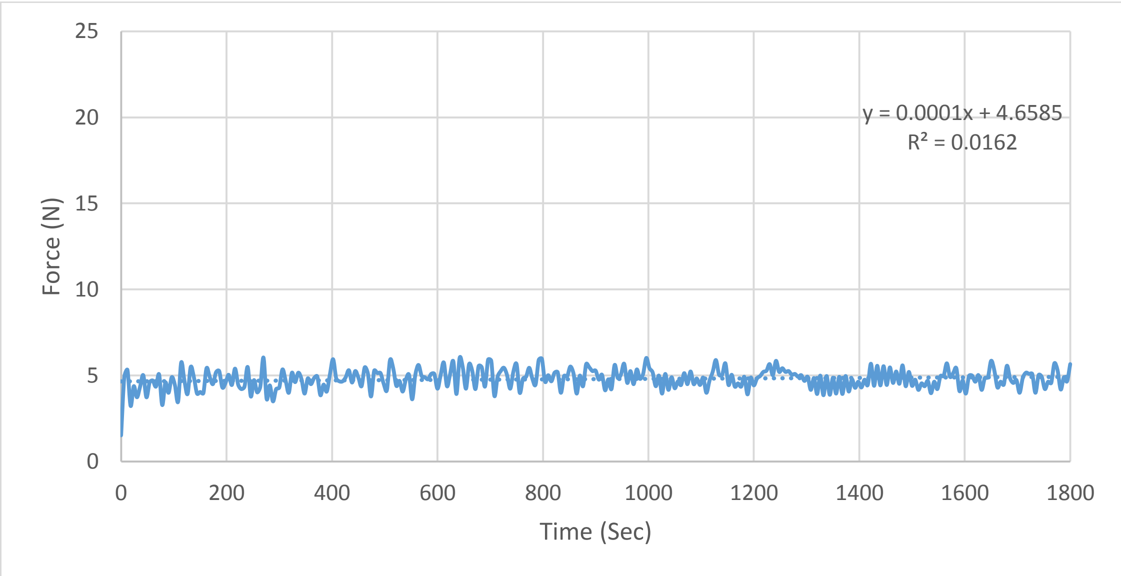

Figure 94 - Wear test result for Leigh Spinners 1150 with 2.55 N load on counter face

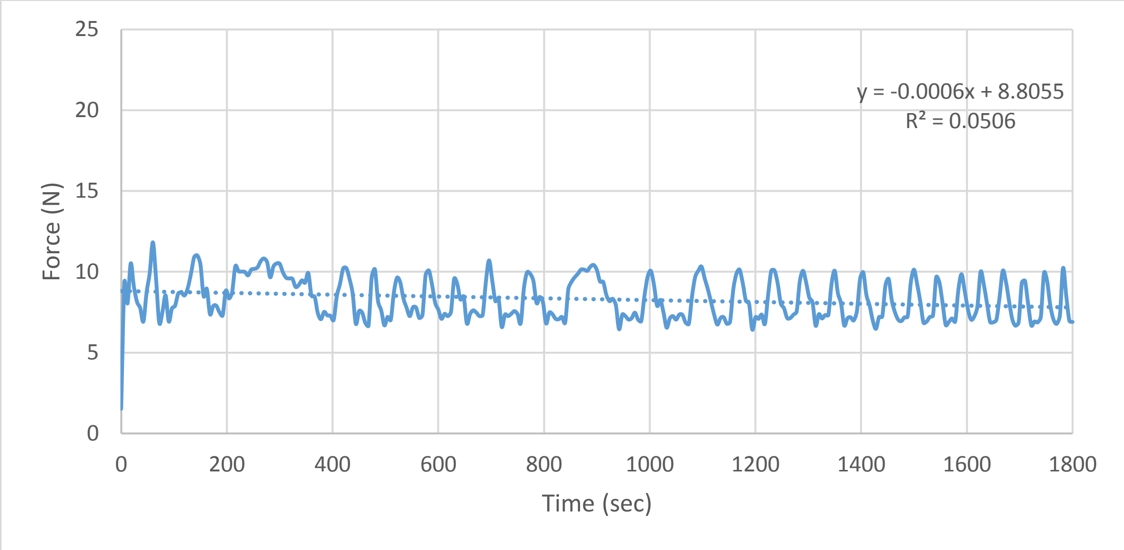

Figure 95 - Wear test result for Leigh Spinners 1150 with 7.65 N load on counter face

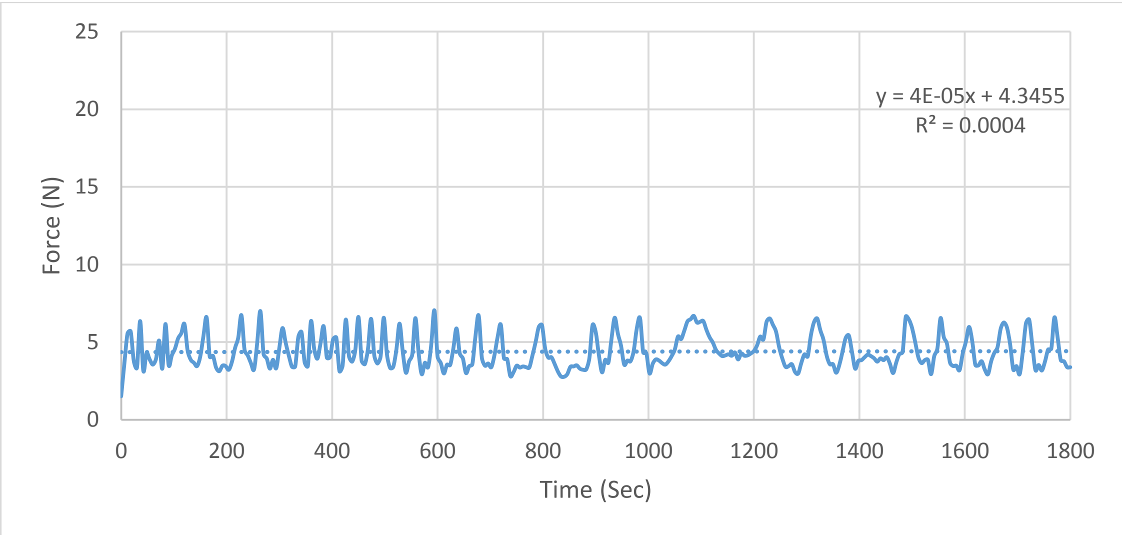

Figure 96 - Wear test result for Leigh Spinners 1150 with 2.55 N load on counter face with sand filler

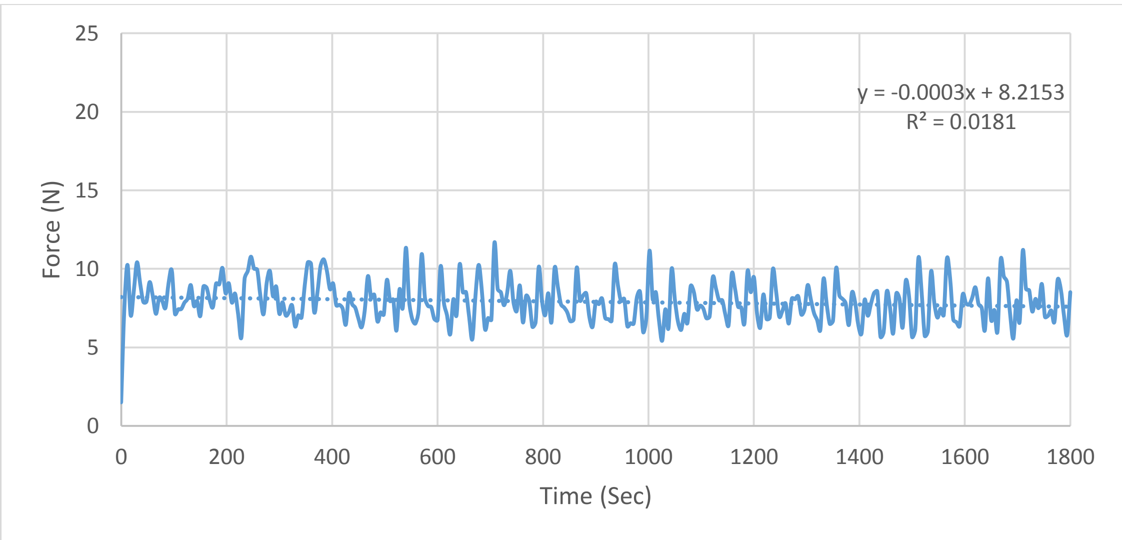

Figure 97 - Wear test result for Leigh Spinners 1150 with 7.65 N load on counter face with sand filler

6.1.2 Leigh Spinners 1300 artificial sports turfs

Figure 98 to Figure 101 show the frictional force of a sample of Leigh Spinners 1300 worn against a polymeric stud across an 1800 second experiment. Figure 99 and Figure 101 have the higher load on the counter face, and Figure 100 and Figure 101 have a filler layer of sand applied.

For Figure 98 the frictional force increases slightly with time. Here, mean value of friction is 4.51 N. Whereas in Figure 99, the frictional force decreases with a very large amount of fluctuation, unlike the previous experiments. Here mean value of friction is highest 9 of all at 11.85 N.

Figure 100 shows the frictional force decreases very slightly with some, but not constant fluctuations. This experiment found mean value of friction as 4.04 N. In Figure 101 the frictional force also decreases slightly, with a large fluctuation (approx. 10 N) in a similar manner seen in Figure 99. Here, mean value of friction is 9.38 N.

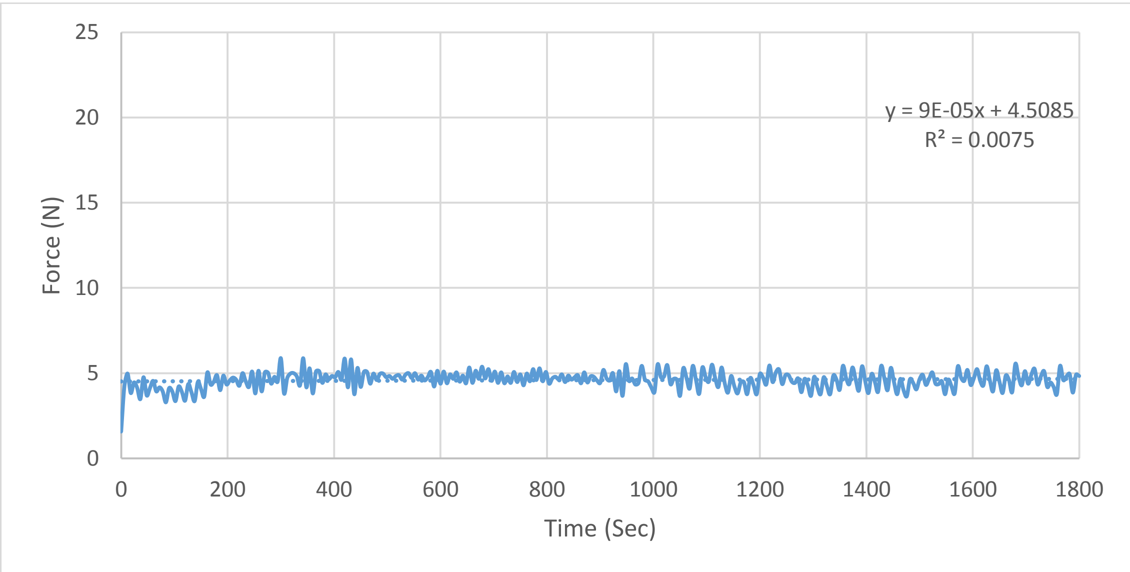

Figure 98 - Wear test result for Leigh Spinners 1300 with 2.55 N load on counter face

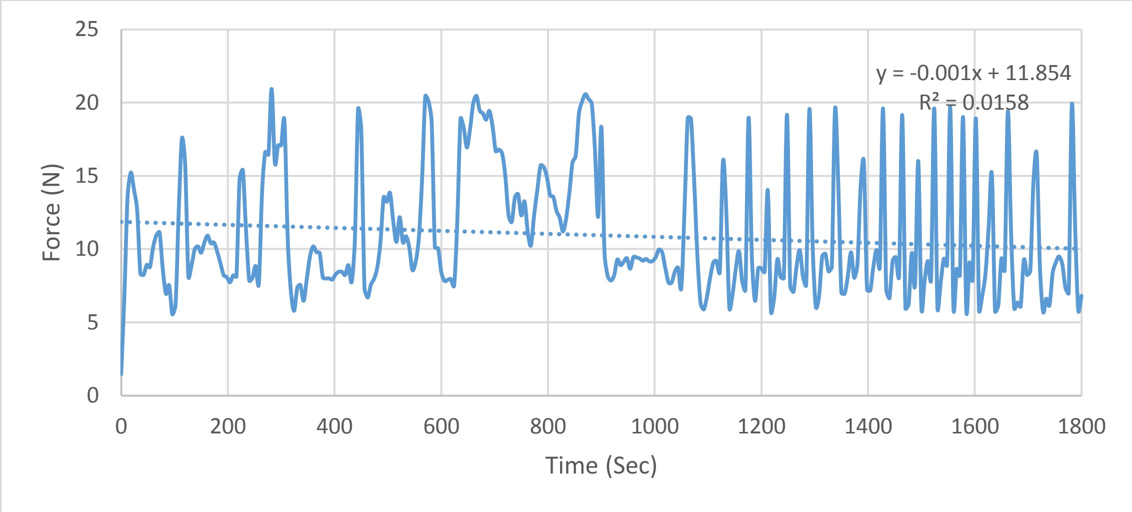

Figure 99 - Wear test result for Leigh Spinners 1300 with 7.65 N load on counter face

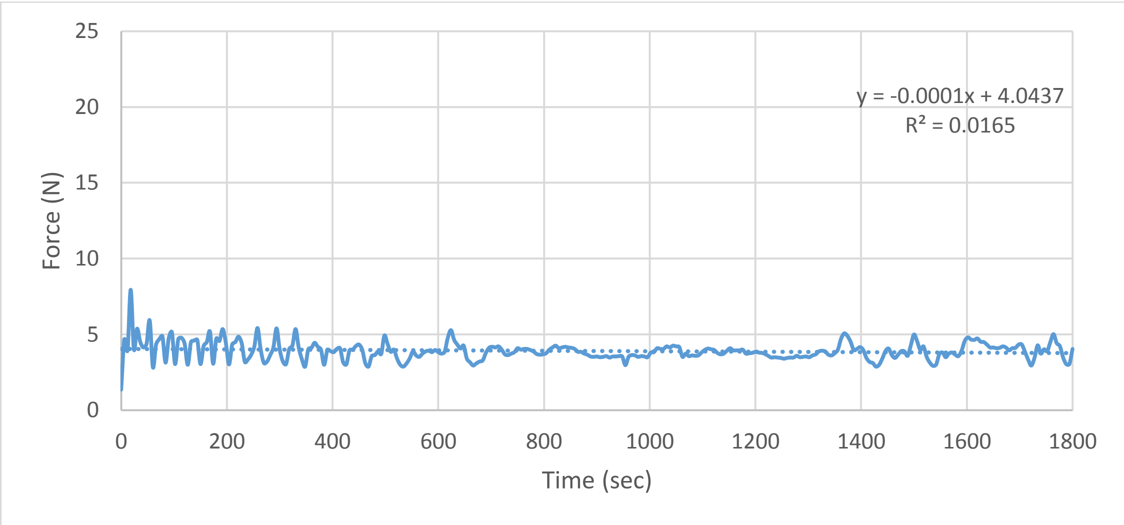

Figure 100 - Wear test result for Leigh Spinners 1300 with 2.55 N load on counter face with sand filler

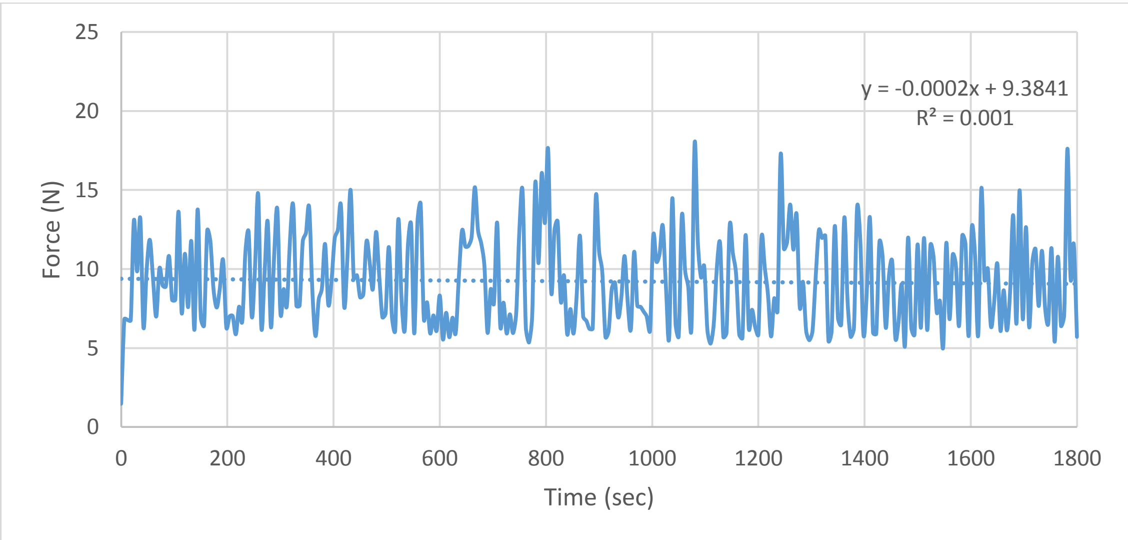

Figure 101 - Wear test result for Leigh Spinners 1300 with 7.65 N load on counter face with sand filler

6.1.3 Rawsons 1150 artificial sports turfs

Figure 102 to Figure 105 show the frictional force of a sample of Rawsons 1150 worn against a polymeric stud across an 1800 second experiment. Figure 103 and Figure 105 has the higher load on the counter face. Figure 104 and Figure 105 have a layer of sand filler applied.

Figure 102 shows the frictional force remains almost constant as in Figure 96, however there is much less noise than in Figure 96. The mean value of friction is also slightly lower at 4.07 N. In Figure 103 the frictional force decreases with time and there is little deviation, similar to what can be seen in Figure 102. Here mean value of friction is 6.93 N.

For Figure 104 the frictional force decreases slightly. There is little difference between this and Figure 102, implying the sand does not affect the grip of the surface. The mean value of friction was found to be 4.00 N in this experiment. In Figure 105, the frictional force increases throughout, unlike the previous experiments, although the deviation from the mean is large, suggesting the sand filler is affected by the increased load. The mean value of friction is 8.31 N.

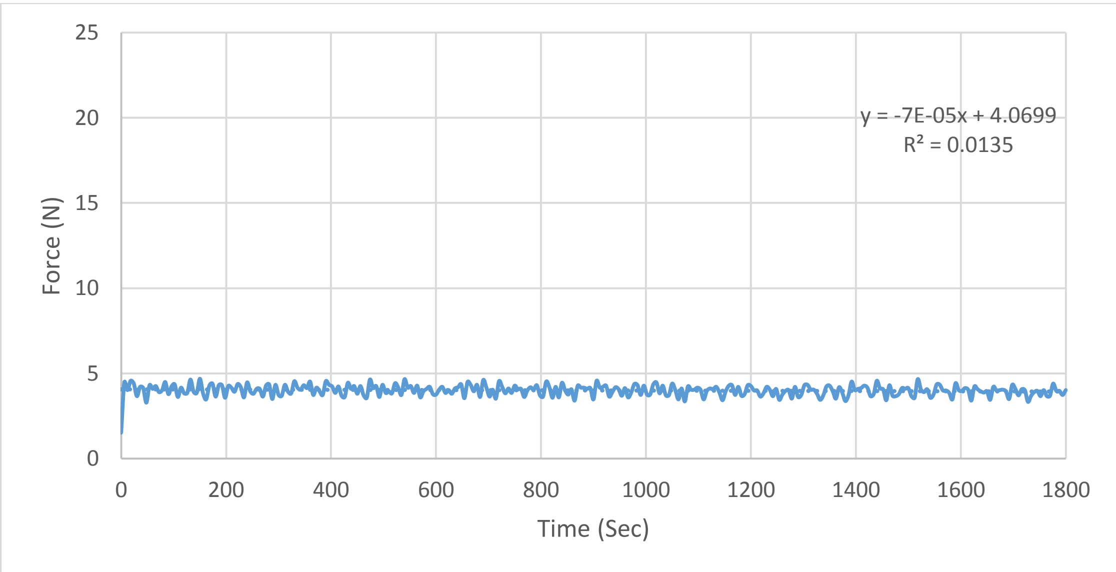

Figure 102 - Wear test result for Rawsons 1150 with 2.55 N load on counter face

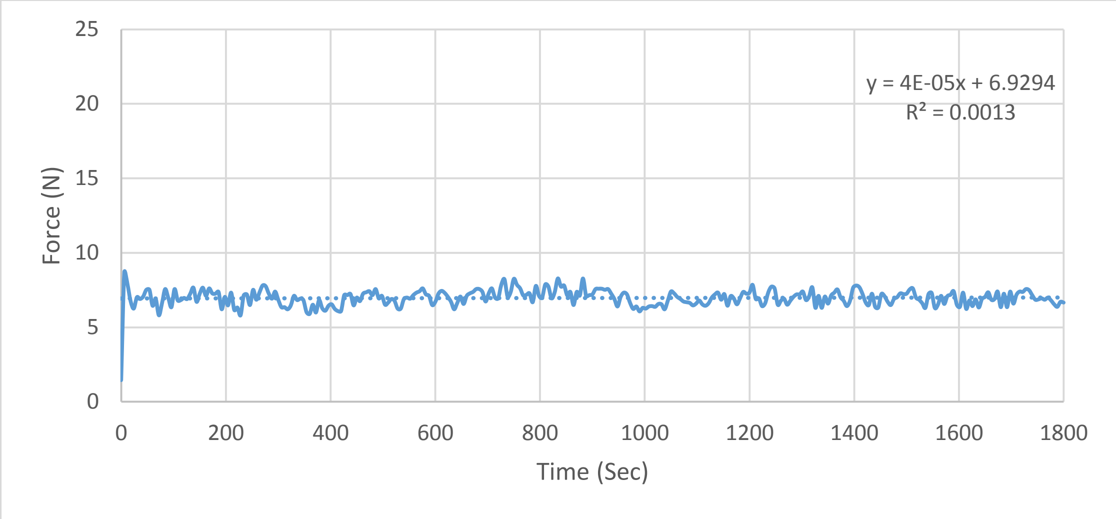

Figure 103 - Wear test result for Rawsons 1150 with 7.65 N load on counter face

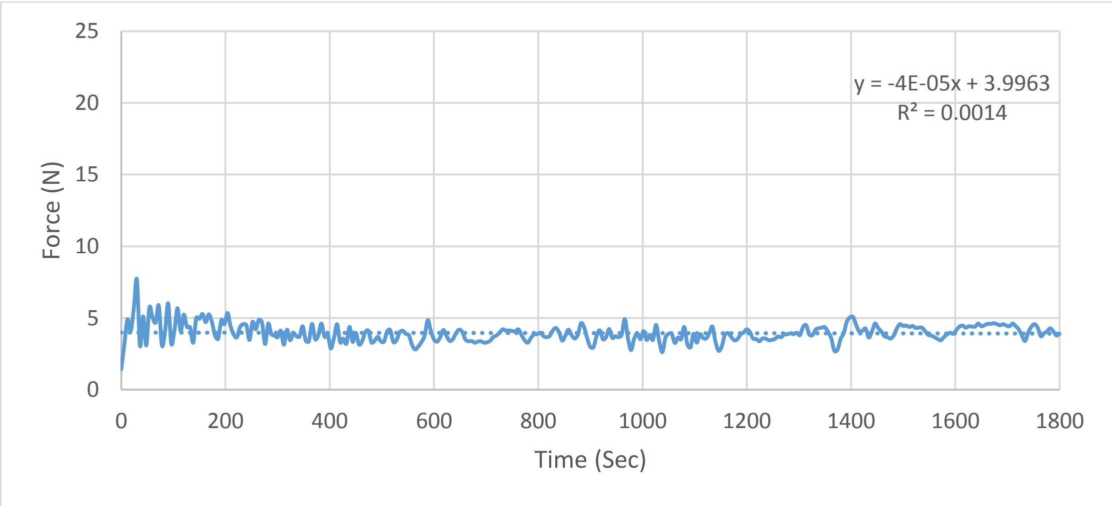

Figure 104 - Wear test result for Rawsons 1150 with 2.55 N load on counter face with sand filler

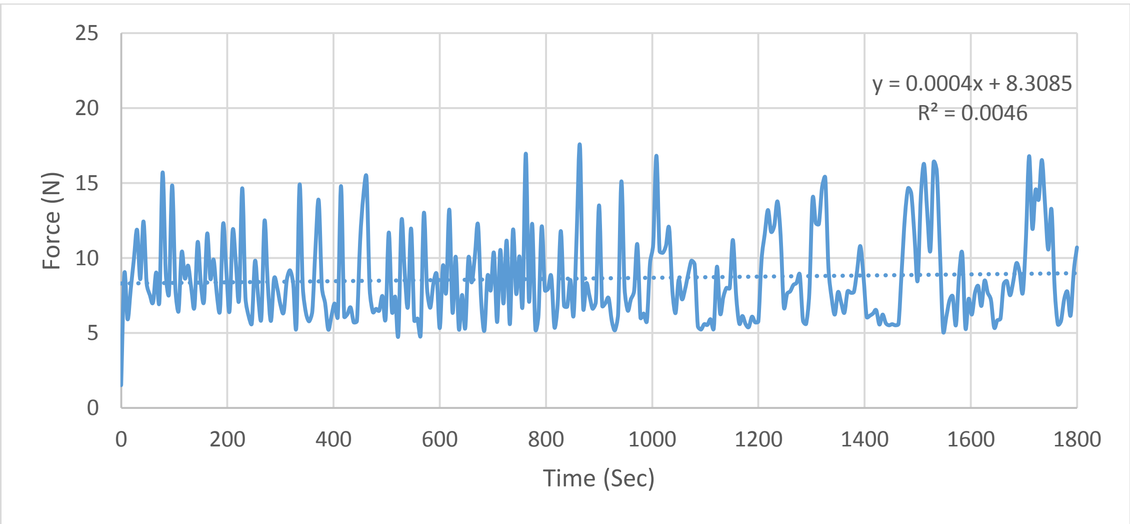

Figure 105 - Wear test result for Rawsons 1150 with 7.65 N load on counter face with sand filler

6.1.4 Rawsons 1300 artificial sports turfs

Figure 106 and Figure 107 show the frictional force of a sample of Rawsons 1300 worn against a polymeric stud across an 1800 second experiment. Figure 107 has sand filler applied.

Across Figure 106, the frictional force remains almost constant. This experiment found mean value of friction is 4.08 N. In Figure 107 the frictional force decreases slightly with small fluctuations. For this experiment mean value of friction is 3.44 N.

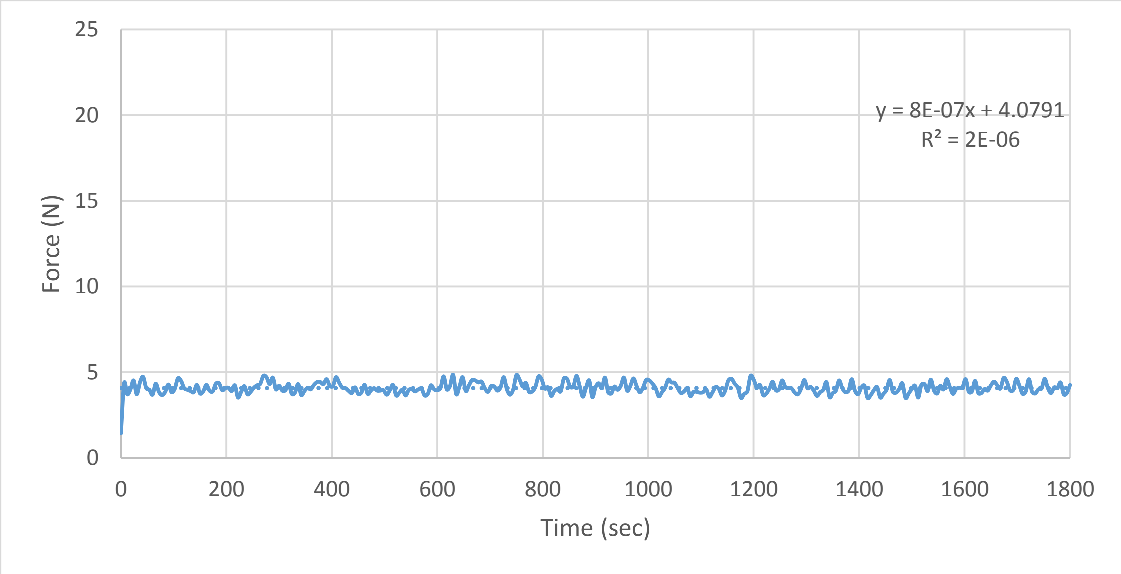

Figure 106 - Wear test result for Rawsons 1300 with 2.55 N load on counter face

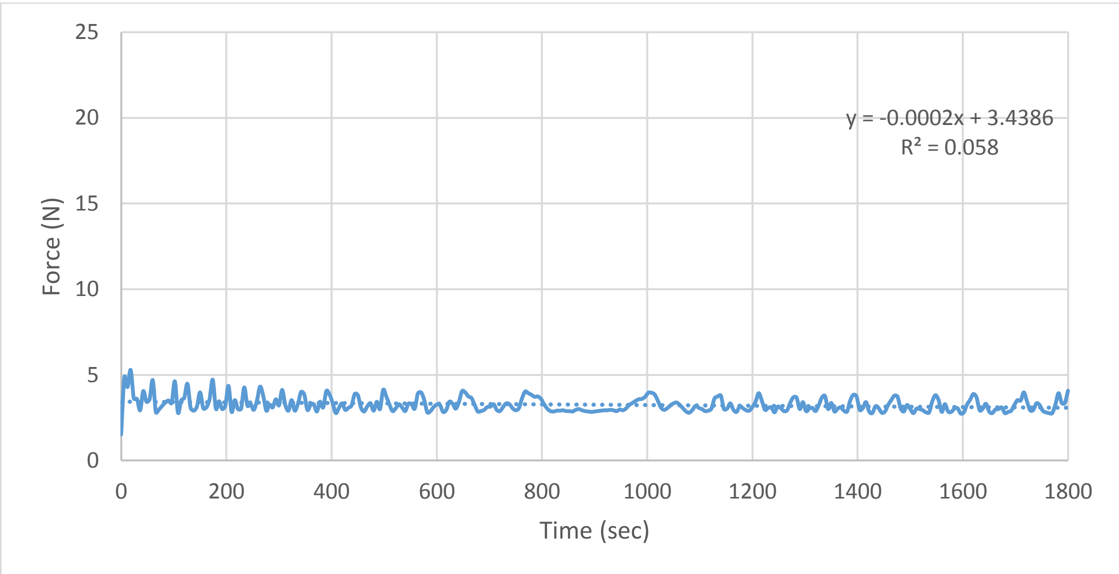

Figure 107 - Wear test result for Rawsons 1300 with 2.55 N load on counter face with sand filler

6.1.5 Mass changes and counter faces

Table 8 shows the mean mass change of the samples after a wear test. It can be seen that whilst the mass of some samples decreased, others increased (negative mass change), suggesting that in some instances mass from the counter face transferred into the sample, whilst other times material was removed from the sample.

Sample	Load on Counter face (N)	Mass Change (grams)
Leigh Spinners 1150	2.55	-0.06406
	7.65	+0.00798
Rawsons 1150	2.55	-0.00238
	7.65	-0.00370
Leigh Spinners 1300	2.55	+0.00092
	7.65	+0.01344
Rawsons 1300	2.55	+0.01276

Table 8 - Mass changes of samples

By comparison of Figure 108 and Figure 109 it can be seen that the sand filler is pushed out of the sample by the counter face and or the constant rotation of the sample. It also appears that some of the sand particles have become embedded in the wear track.

Figure 108 - Optical Image of a sample of Leigh Spinners 1150 before a test.

Figure 109 - Optical Image of a sample of Leigh Spinners 1150 after a test.

From Figure 110, Figure 111, Figure 112 and Figure 113 show how the damage accumulated to the counter face across the testing of an unfilled sample. Note that in these images the sliding direction is from the top left towards the bottom of the counter face (as indicated in Figure 110), due to the rotation of the sample.

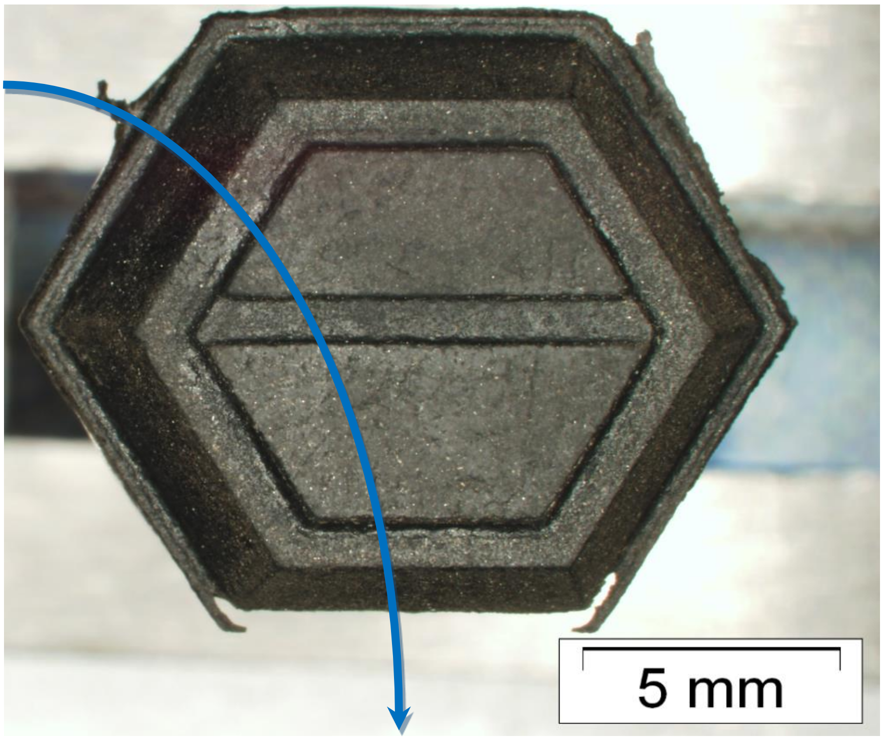

Figure 110 - Undamaged counter face - no sand counter face

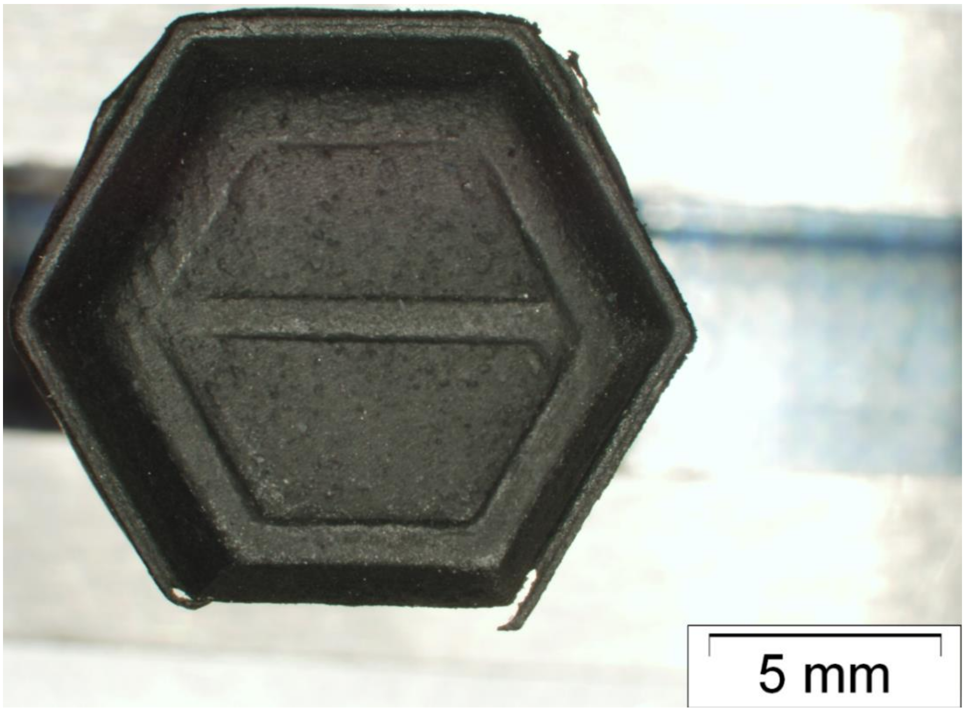

Figure 111 - No sand counter face (after 1 test)

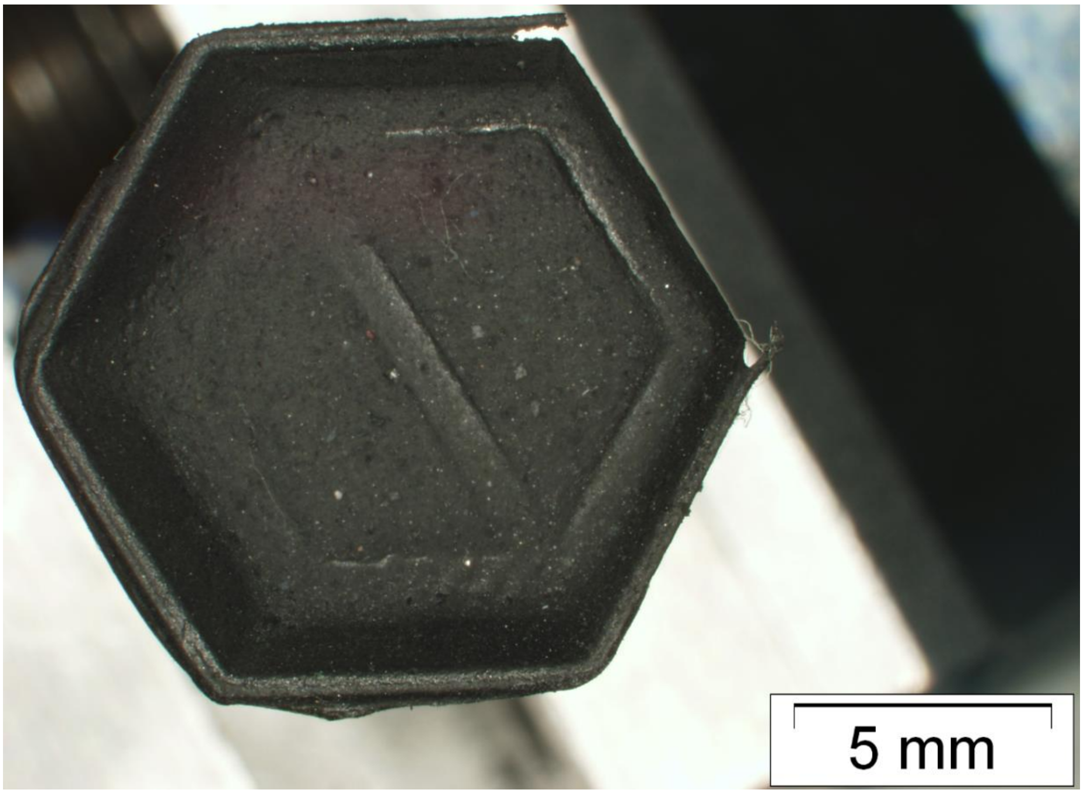

Figure 112 – No sand counter face, 2.55 N load (after 2 tests)

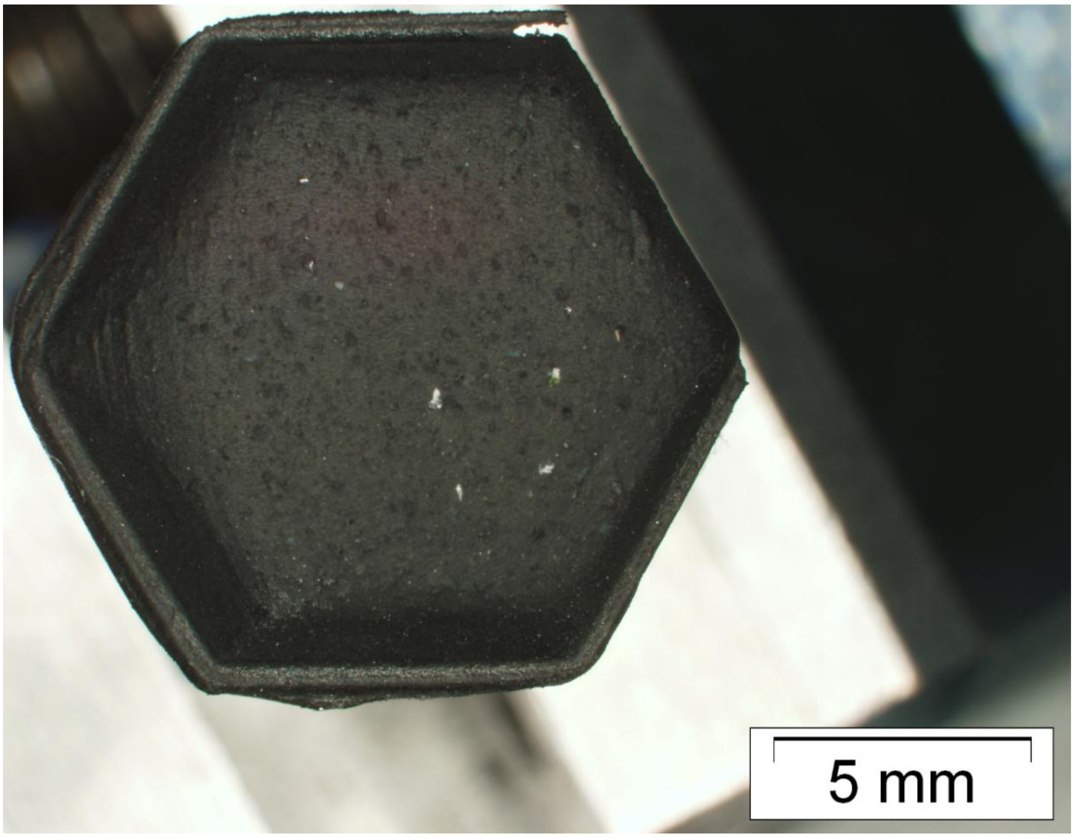

Figure 113 – No sand counter face 2.55 N load (after 4 tests)

Figure 114, Figure 115 and Figure 116 show the counter face before (Figure 114) and after successive wear tests against samples of artificial sports turf with sand filler. It can be observed that more damage is incurred faster due to the presence of the sand filler. Note that in these images the sliding direction is from the top right towards the bottom of the counter face (as indicated in Figure 114), due to the rotation of the sample.

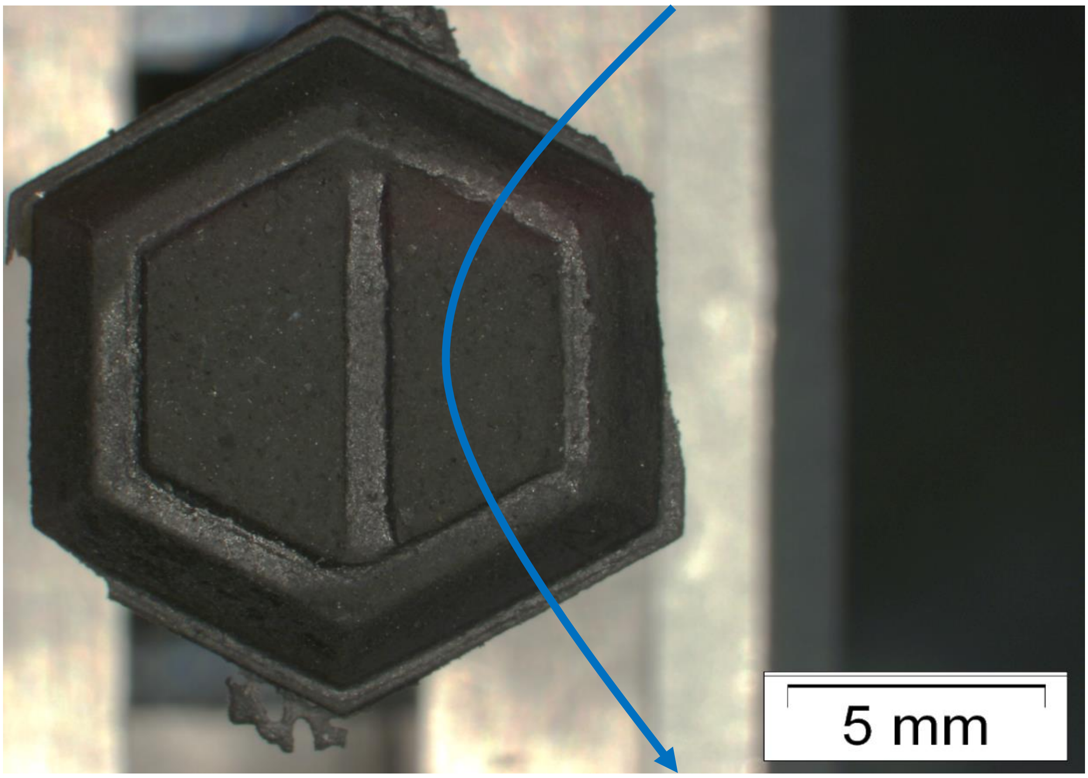

Figure 114 – Sand counter face (before test)

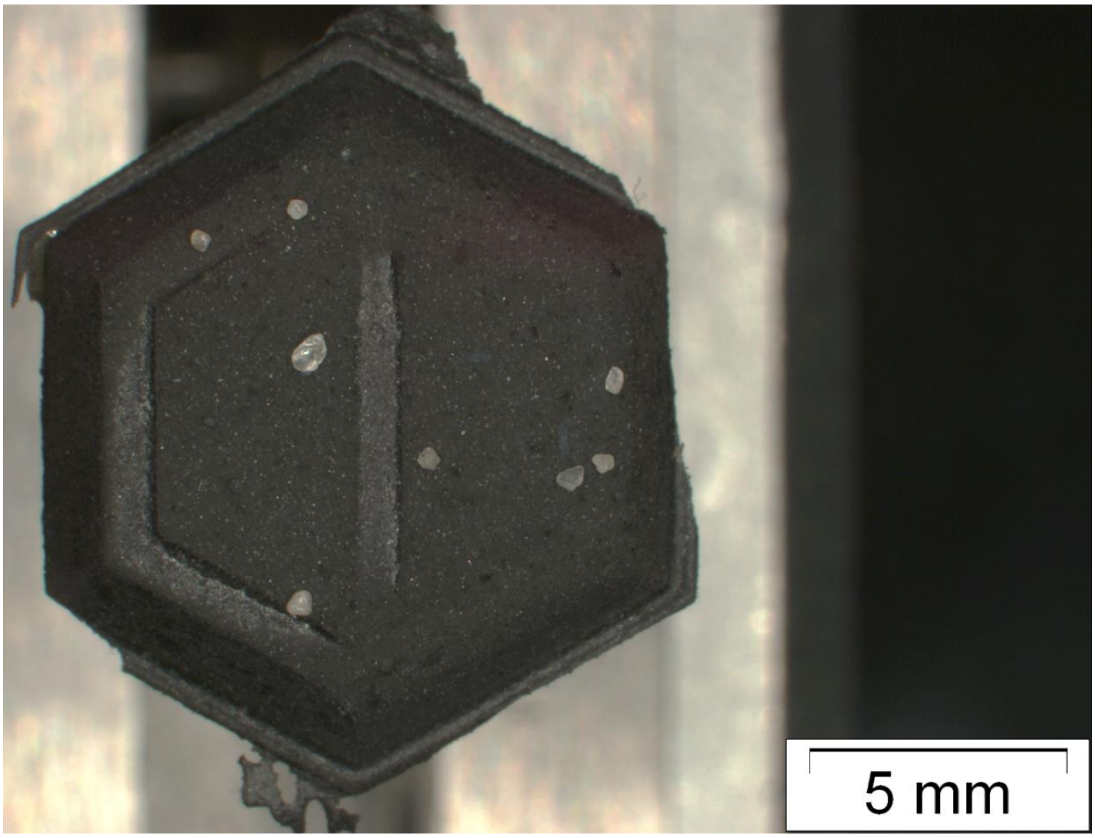

Figure 115 – Sand counter face (after 1 test)

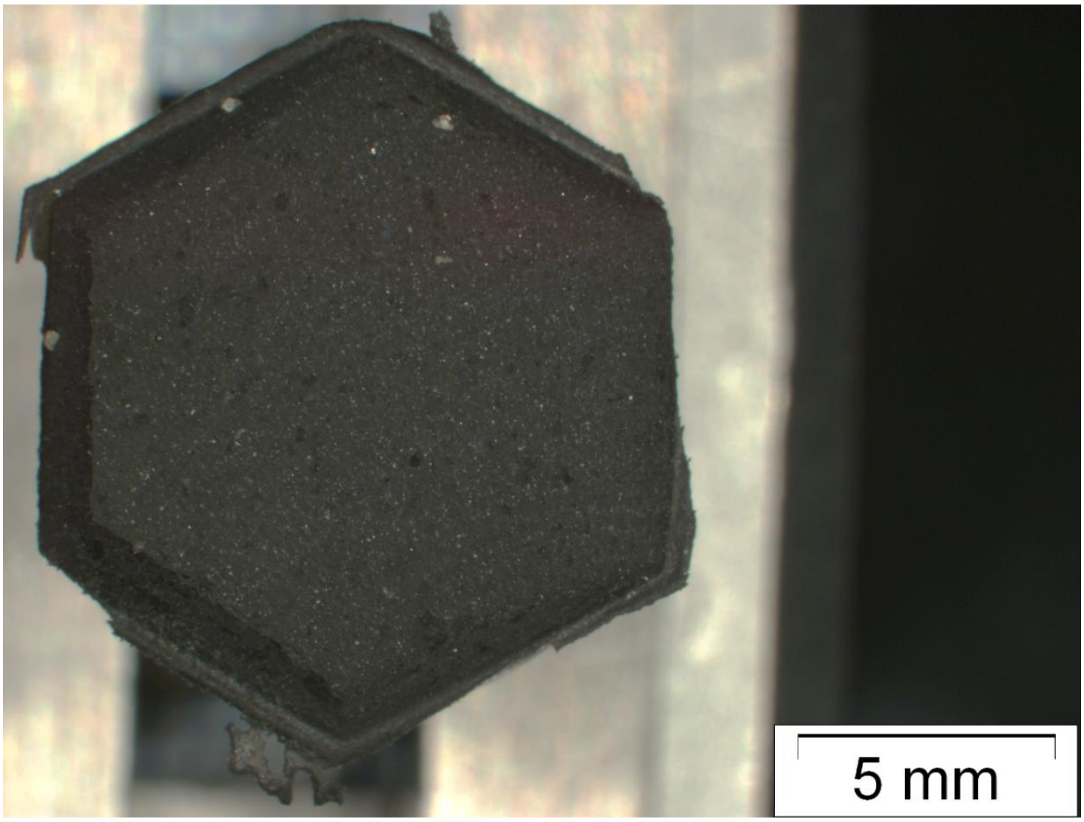

Figure 116 – Sand counter face (after 4 tests)

From Figure 117 and Table 9 it can be seen how the mass of the polymeric counter face (including the attaching pin) decreases with each test. From the gradient of counter faces 3 and 4, it is clear the wear of the counter face increases with the addition of sand.

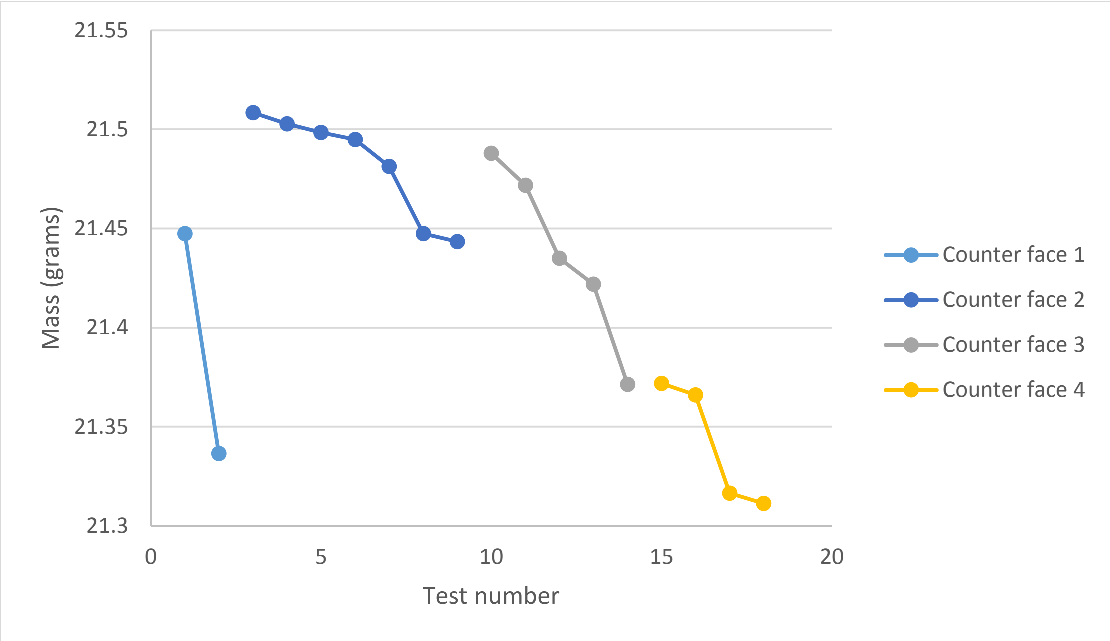

Figure 117 - Mass of counter faces

Test number	Artificial sports turf	Load (N)	With Sand?	Mean Frictional Force (N)	µ	Mass Lost (pin) grams
1	Leigh Spinners 1150	2.55	No	-	-	New counter face
2	Leigh Spinners 1150	2.55	No	4.6585	1.82	0.11098
3	Leigh Spinners 1300	2.55	No	-	-	New counter face
4	Leigh Spinners 1300	2.55	No	4.5085	1.77	0.00558
5	Rawsons 1150	2.55	No	4.0699	1.60	0.00436
6	Rawsons 1300	2.55	No	4.0791	1.60	0.00356
7	Leigh Spinners 1150	7.65	No	8.8055	1.15	0.01360
8	Leigh Spinners 1300	7.65	No	11.854	1.55	0.03384
9	Rawsons 1150	7.65	No	6.9294	0.91	0.00400
10	Leigh Spinners 1150	2.55	Yes	-	-	New counter face
11	Leigh Spinners 1150	2.55	Yes	4.3455	1.70	0.01600
12	Leigh Spinners 1150	7.65	Yes	8.2153	1.07	0.03694
13	Rawsons 1150	2.55	Yes	3.9963	1.57	0.01296
14	Rawsons 1150	7.65	Yes	8.3085	1.09	0.05056
15	Leigh Spinners 1300	2.55	Yes	-	-	New counter face
16	Leigh Spinners 1300	2.55	Yes	4.0437	1.59	0.00586
17	Leigh Spinners 1300	7.65	Yes	9.3841	1.23	0.04964

18	Rawsons 1300	2.55	Yes	3.4386	1.35	0.00520

Table 9 - Wear testing data

6.1.6 Product comparison

In the preliminary 2 hour experiment, the measured force fluctuated randomly, which was also seen in the shorter experiments. This suggests the fluctuations in the shorter tests are valid, although potentially cutting off before severe wear occurs.

6.1.6.1 1150/1300

Under lower loads the 1150 and 1300 artificial sports turfs behaved roughly the same in terms of frictional force (approx. 4 N for each sample), and the coefficient of friction reflects this.

Under the higher load (7.65 Ns on the pin) the artificial sports turfs behave slightly differently. The 1150 artificial sports turfs exhibit both a lower frictional force and a lower coefficient, whereas the 1300 artificial sports turfs produce a higher force and higher coefficient.

Mass change of the sample shows the 1150 artificial sports turf gained mass whilst the 1300 lost mass, which suggests a change in mechanism depending on the density of the fibres. Mass change of the sample seems to be dependent on the manufacturer at higher loads.

With the addition of sand it becomes impossible with the equipment available to measure the mass change of the sample, because weighing the sample and holder combined is not precise enough (the holder is too heavy to place on the precision balance), removing the sample from the holder will cause some sand to be lost each time (and so measuring the mass loss with sand still present in the sample is unreliable) and it is too difficult to remove all of the sand from each sample. It can be seen there is little change in the 1150 samples frictional behaviour, however the coefficient decreases for the 1300 artificial sports turfs under lower load. At higher loads the difference in coefficient seems best explained by manufacturer rather than weight.

6.1.6.2 Leigh Spinners/Rawsons

Under the lower load the Rawsons artificial sports turfs have a lower frictional force than the Leigh Spinners which is also seen under the higher loads, which is reflected in the coefficient of friction.

With the addition of sand filler there is a slight reduction in the frictional force for all the artificial sports turfs, but when the coefficient of friction is considered there is almost no change for the Rawsons 1150 under low load, whereas there is a decrease in the Leigh Spinners artificial sports turfs under low load. There is an even greater decrease for the Rawsons 1300 artificial sports turf under this load.

Under higher loads the Leigh Spinners artificial sports turfs both see a reduction in the coefficient of friction where are the Rawsons artificial sports turf sees an increase in the coefficient.

Mass change of the samples suggests that under higher loads the Leigh Spinners artificial sports turfs lose mass, whereas the Rawsons artificial sports turfs gain mass. At the lower load, as regardless of manufacturer the 1150 artificial sports turfs gained mass whilst the 1300 artificial sports turfs lost mass.

From these results it is difficult to determine precisely which artificial sports turf has the best wear rate. Whilst all of the Leigh Spinners artificial sports turfs lost mass, some of the Rawsons artificial sports turfs gained mass from the counter face, which suggests the manufacturing methods Rawsons use gives the best wear rate. However, the sample that did lose mass lost more than the Leigh Spinners counterpart.

Additionally, the Rawsons artificial sports turfs typically exhibited fewer fluctuations throughout the experiments.

6.2 Hardness Testing of Filler Materials

The data acquired from the micro-hardness tests on the sand and egg shell particles is given in Table 10, which shows the mean hardness of the sand to be 1357.9 Hv (676.2), whilst the resin has hardness of 24.9 Hv (8.4). The mean hardness of the egg shell particles is 49.2 Hv (9.2). This is well above the hardness of the resin, which is 17.4 Hv (0.2).

Sand Hardness (HV)	Sand Resin (Hv)	Egg shell Hardness (Hv)	Egg shell resin (Hv)
1564	35.5	62.4	17.1
1253	24.3	60	17.4
2983	15	37.1	17.6
908		53.3	

1144		52.2	
1448		37.3	
927		46	
636		55.3	
		38.8	

Table 10 - Hardness testing data

6.3 Fatigue Testing – Small Samples

The data from the preliminary experiments are shown in Table 11. The drastic variation in this data suggested a change in method was required to obtain reliable data.

Test	Cycles to failure
1	10815
2	2
3	257
4	17038
5	4431
6	25313
7	1
8	2

Table 11 - Data from preliminary fatigue experiments

Figure 118 and Figure 119 are extension time curves for a Leigh Spinners 1150 grass green sample and a manually cut Rawsons 1150 grass green sample respectively. There is a clear running in period up to approximately 2 mm extension followed by gradual extension to failure at 5 mm extension in both figures; however there are jumps in the extension due to the resetting of the machine in Figure 119. For the Leigh Spinners 1150 grass green sample, N_f = 17038 and for the manually cut Rawsons 1150 grass green sample, N_f = 28843.

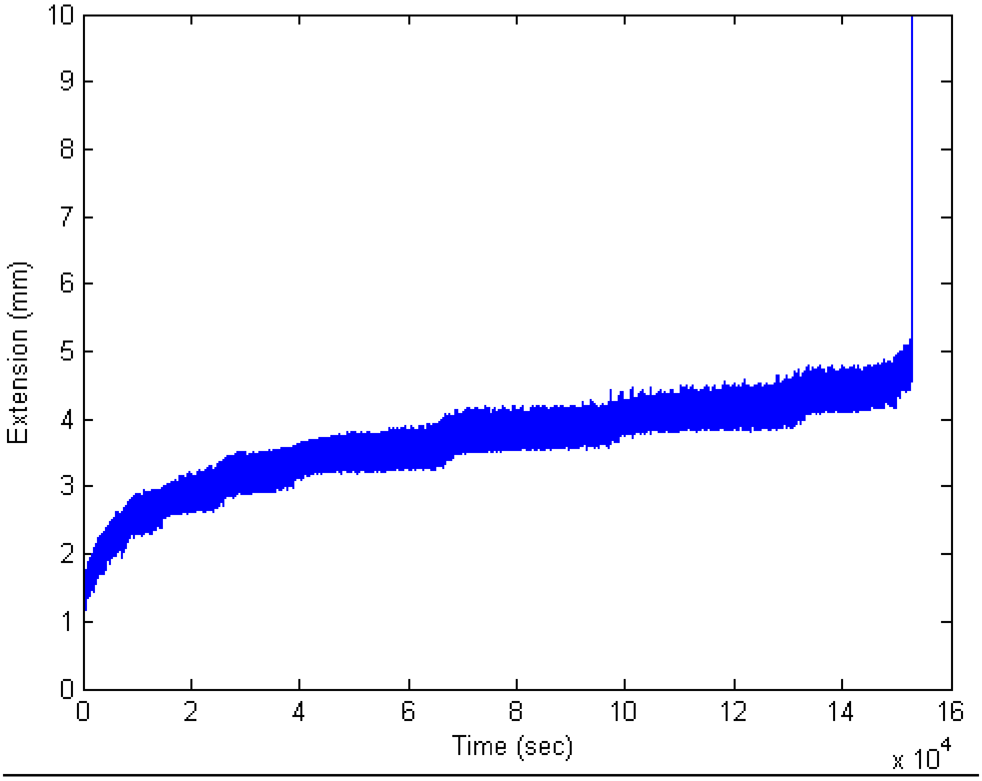

Figure 118 - Typical fatigue performance of the better samples of the Leigh Spinners 1150 artificial sports turf in preliminary fatigue tests.

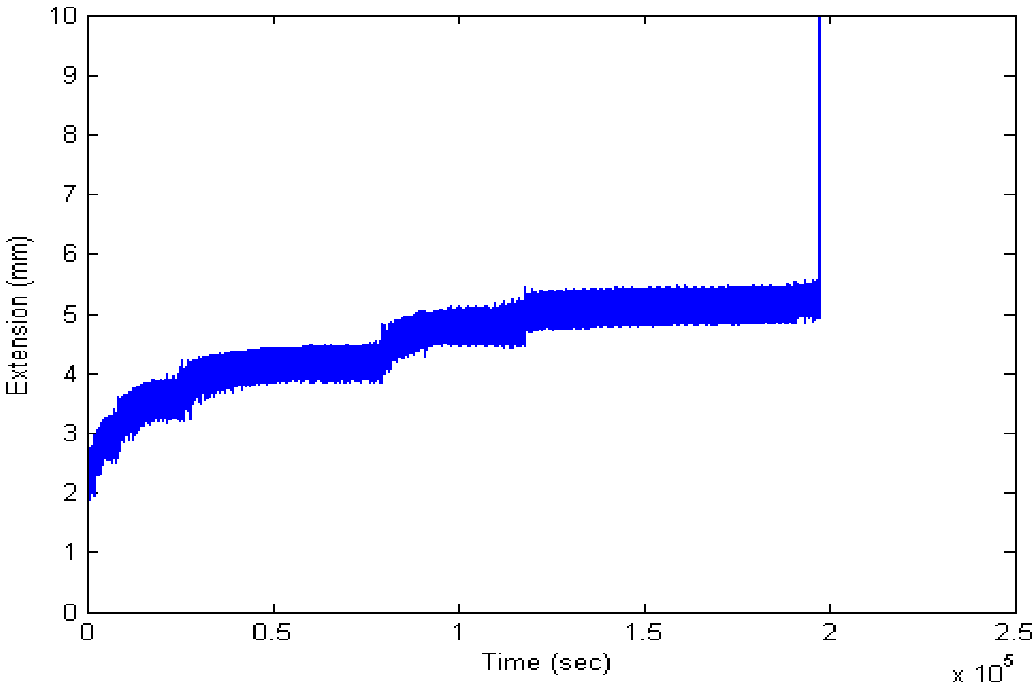

Figure 119 - Manually cut small sample

Figure 120 shows an extension time curve for the Rawsons 1150 green sample 8. It is clear the sample failed at just 3 cycles, suggesting some defect was present in the sample.

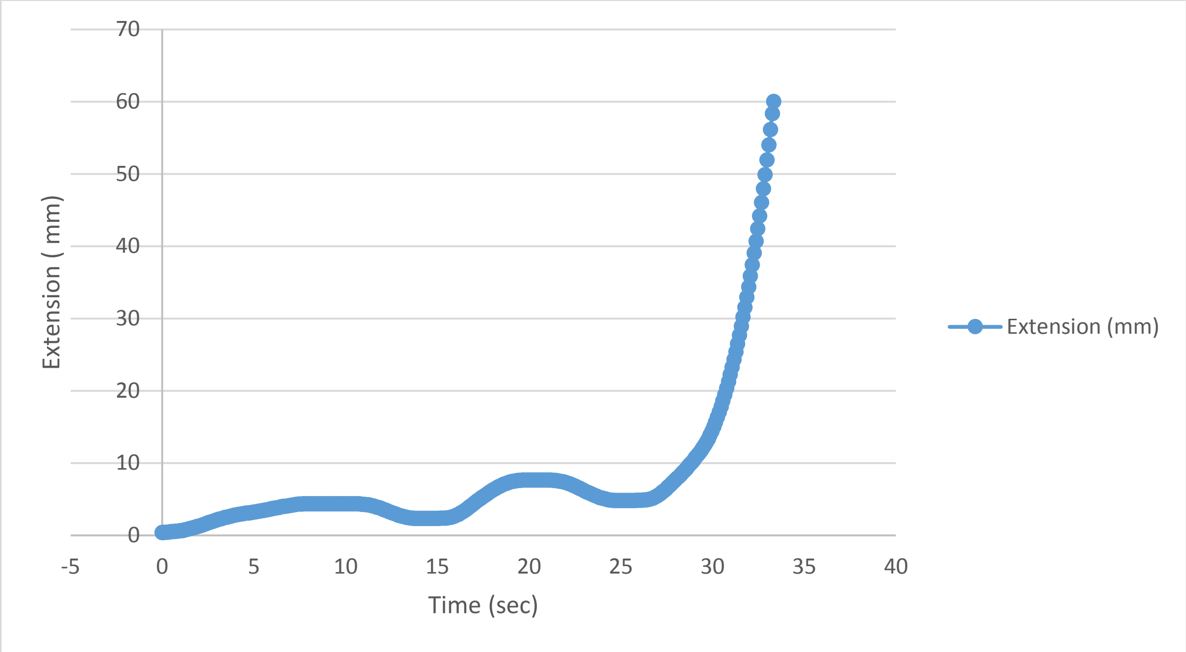

Figure 120 - Typical fatigue performance of a poor sample (Rawsons 1150 green sample 8)

6.4 Fatigue Testing – Large Samples Preliminary

Figure 121 shows an extension time curve for the Leigh Spinners 1150 grass green full size sample 1. There is a short running in period up to 1 mm extension followed by gradual extension to approximately 2.75x10^5 seconds, at which point the change in experimental procedure (described in 3.16) causes a shift in the extension until failure at approx. 1.8 mm extension after 28435 cycles.

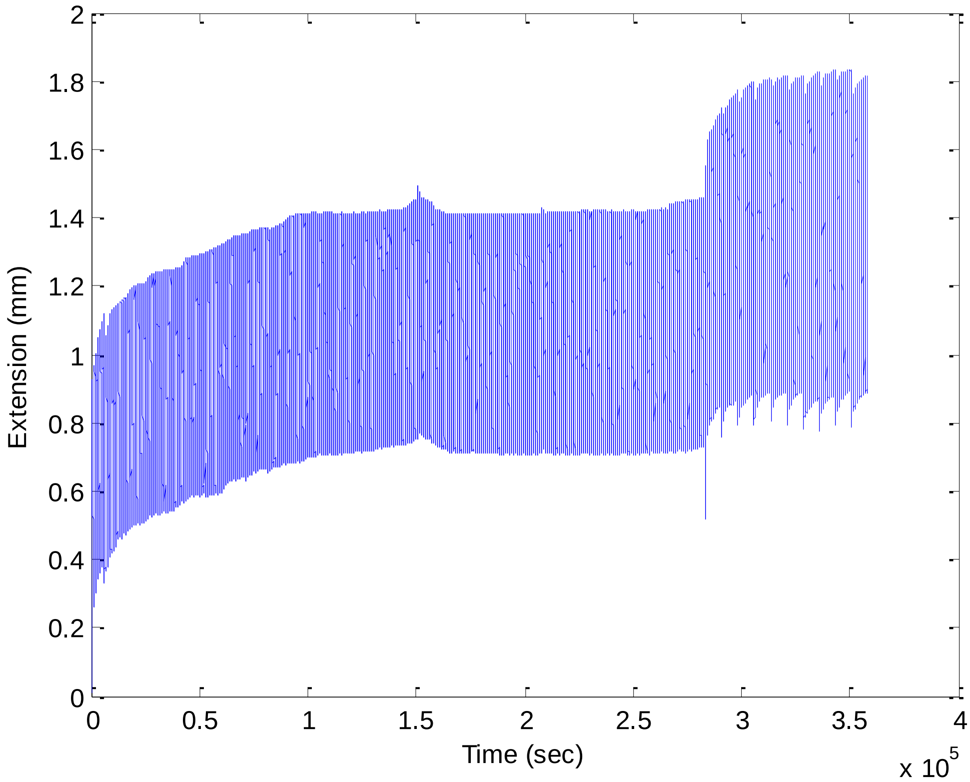

Figure 121 - Fatigue performance of the 1st full size sample.

6.5 Fatigue Testing – Large Samples

After the preliminary experiments were completed and the larger samples were tested, more reliable data was beginning to be generated, however time constraints meant only two samples were tested to failure, with a third timing out. The data from these experiments are shown in Table 12.

Manufacturer	Artificial sports turf	Orientation	Number of Cycles	Completed?
Leigh Spinners	1150 Green	Vertical	725662	Yes
American	American	Vertical	496590	Yes
American	American	Horizontal	+1118654	No

Table 12 - Fatigue data

6.6 Product Comparison

6.6.1 Leigh Spinners/Rawsons

Whilst it is difficult to make any sound conclusions from a data set with such a wide spread, it can be seen that both the Leigh Spinners and Rawsons artificial sports turfs exhibited an inconsistent number of cycles to failure.

6.6.2 Leigh Spinners/American.

Whilst it is difficult to make sound conclusions from such a small data set, it can be said the Leigh Spinners 1150 green did outperform the American artificial sports turf in the tests conducted.

6.7 Wear, Hardness and Fatigue Testing Summary

Wear testing investigated how sliding wear damaged samples of the artificial sports pitches and the counter faces, and how the friction between the two surfaces changes between different artificial sports turfs and with the addition of a filler material. Hardness testing found the hardness of the filler materials. Fatigue testing found the fatigue life of the artificial sports turfs and showed that defects in the samples affected the fatigue life.

After the wear, hardness and fatigue testing was finished the experimental work of the project was completed.

7 - Discussion

7.1 Tensile Testing

From the tensile testing it is believed the artificial sports turfs tested behave like a composite material with randomly orientated short fibres, in that the SBR backing material is the matrix and the PP fibres are the fibres of a reinforced material. That is to say, the backing carries the applied load and does not effectively transfer the load to the fibres.

It is therefore expected that the types of failures experienced by this type of composite would be a crack forming in the backing due to localised stress concentrations, which then “grows” through the sample.

This is evidenced by the differing performances of the orientations. The vertical orientation fails sooner as the regions where the backing is present break, but the horizontal orientation is stronger because the fibres take the load.

This is further evidenced by the differing regions of the force-extension graphs, which are governed by the differing nature of the component taking the load. Whilst the styrene butadiene elastomer is carrying the applied load the response is purely elastic however when this fails and the fibres take the load the samples transition to a plastic deformation failure mode until the fibres reach their UTS and fail.

Figure 86 shows the effect of orientation, in that all the fibre entanglement or density is strongly directional. The differences between the Leigh Spinners and the Rawsons manufactured artificial sports turfs suggests that this effect is dependent on manufacturing process, as the smaller difference in the fracture points between the performance of the 2 orientations tested in the Rawsons artificial sports turfs implies these products are more unidirectional.

It is discussed in the literature that unorientated fibres will fail at similar strengths but greater extensions, because they have to reconfigure to take the load. This could explain why the Rawsons artificial sports turfs failed at greater extensions, suggesting that Rawsons artificial sports turfs have more unorientated fibres.

This greater fibre mixing is believed to promote better capillary flow of the liquid SBR latex in to the backing during manufacture, which may contribute to the improved directionality the Rawsons artificial sports turfs exhibit. As it is known by Notts Sport Ltd. that approximately 20% of the applied SBR is retained by the fibre web.

The tensile testing of the worn in situ sample suggests that the latex becomes stiffer and more brittle (in the horizontal orientation) with age, which is evidenced in the stiffness increasing in the horizontal orientation, although in the vertical orientation the stiffness remained roughly the same, assuming that the worn in situ samples are comparable to the Leigh Spinners 1300 grass green. Additionally, during the test of the worn in situ artificial sports turfs the failure sounded much more like a sudden snap, rather than a slower ripping sound for the others, suggestive of a more brittle failure. The shape of the force-extension curve is also brittle in comparison to the other samples, as discussed in 2.3.2.

The American samples behave in a much more thermoplastic manner, whereas the Leigh Spinners and Rawsons artificial sports turfs behave much more like an elastomer. This is because the backing in the American sample is a thermoplastic (powdered polypropylene) and so the tensile response has less elastic and more plastic deformation in comparison to the others, which have an elastomer backing. This is further evidence that the artificial sports turfs act as composites, and that failure originates in the backing.

7.2 Fatigue/X-ray CT

The fatigue testing combined with the X-ray CT investigations showed that there were small defects in the small samples which became averaged out in the larger samples. These voids/pores were expected from the literature, as mentioned in 2.2, although the voids found in this research were much larger than those described in the literature. Additionally, the X-ray CT imaging (Figure 74 and Figure 75) shows the damage from these fatigue failures accumulates along the sample, however the tensile failures do not, which is behaviour typical of a composite, as discussed in 2.3.2.2.

As the stress intensity increased with the change to full size samples, so did the number of cycles to failure. This is not expected from Paris' law therefore it is concluded that the weaknesses observed in the backing, described in 2.3.3 and 4, became averaged out i.e. the scale of the void/pore becomes smaller in comparison to the size of the sample.

It is suspected that the Rawsons artificial sports turfs would exhibit a smaller difference in number of cycles to failure between both orientations than the Leigh Spinners artificial sports turfs as was seen in the tensile testing. This is due to the suspected more evenness of the horizontal/vertical orientations in the Rawsons artificial sports turfs.

The American artificial sports turf was out performed by the Leigh Spinners artificial sports turf during fatigue testing. This is believed to be due to the greater elastic response of the Leigh Spinners artificial sports turfs in comparison to the thermoplastic American artificial sports turf.

Given that the artificial sports turfs failed, it is possible to say that the loading was above the fatigue limit, (assuming the artificial sports turfs have a fatigue limit – not enough testing was completed to confirm if it is present), which suggests fatigue failures could occur in service.

7.3 Wear/Hardness Testing

The wear testing showed the artificial sports turfs very much behave like polymers, with a film transfer occurring in the preliminary experiments and counter face wear occurring in the main experiments, as discussed in 2.3.4.1. Longer duration experiments than those conducted may show a transition in wear mechanism as the fibres become removed and the wear becomes dominated counter face against matrix.

By comparison of Figure 94 through to Figure 97 and Table 9, it is evident that increasing the load on the counter face has the effect of increasing the frictional force, which is to be expected, and repeated for the others. It is also inferred that the addition of sand greatly increases the variation of the frictional force, suggesting that as the sand is not removed in a smooth manner. The addition of the sand appears to reduce the frictional force for the 1300 artificial sports turfs. It is suspected but unconfirmed that the sand particles are sliding underneath the pin to give this reduced value of μ, and contributing to the wear of the artificial sports turf.

Comparing Figure 108 to Figure 109 shows that some of the sand filler has become embedded in the backing. Therefore it is difficult to measure the mass loss of the sample to give an indication of the wear rate, as despite the mass loss the samples due to the wear, the mass of the sand causes them to all weigh substantially more after the test than before, as removing all of the applied sand is difficult. This also makes investigation of the wear mechanisms difficult, as it would require potentially placing loose sand particles into the ESEM. Attempts were made to measure the length of the fibres before and after the tests to measure wear as a function of fibre length, however cutting the fibres close to the backing proved difficult. What can be inferred from the mass changes of the samples without sand is that the way in which they are manufactured can affect the tribological performance, as the Rawsons gain mass, whilst Leigh Spinners lost mass under the lower load. It is known from Hearles' literature that the damage to the fibres should result in debris from the fibres falling in to the sample, suggesting the samples should retain mass. The mass did decrease for some samples, suggesting the rotating of the sample is removing mass. An increase in mass would be caused by the counter face wearing in to the sample.

Figure 114, Figure 115 and Figure 116, show the counter face before (Figure 114) and after successive wear tests against samples of artificial sports turf with sand filler. It can be observed that more damage is incurred faster due to the presence of the sand filler. This is confirmed by Figure 117 and Table 9, where the gradient of counter faces 3 and 4 show that the wear of the counter face increases with the addition of sand, which is to be expected from the addition of a hard asperity into the wear mechanism. Figure 115 also shows some sand particles have become embedded in the polymeric counter face, which was suspected to occur as stated in 2.3.4.1. From the ESEM investigations, it is believed adhesive and abrasive wear mechanisms dominate the wear process (which may be promoted by the presence of the sand filler), as discussed in 7.5.4.

Given the Rawsons artificial sports turfs typically exhibited less fluctuation throughout the testing than the Leigh Spinners artificial sports turfs, it is believed the horizontal and vertical orientations of the Rawsons artificial sports turfs is more equal in comparison to the Leigh Spinners artificial sports turfs. As an unequal distribution would cause the pin to "see" a more uneven path, rather than a flatter path, and thus cause increased fluctuations in the test.

From all of the images of the counter face it can be observed that no film transfer occurred, suggesting a likeness (polymeric material against polymeric material) of the counter face material and the fibres, however some sand filler particles can be seen to have transferred to the counter face during the later wear tests, as discussed in 2.3.4.1.

The hardness testing of the eggshell particles was performed easily however testing the hardness of the sand particles proved more troublesome. As a result it is difficult to draw conclusions from the results obtained and so a comparison to other sand is required. It is therefore assumed sand is SiO_2, which has a hardness of 800 Hv (27).

It is believed the grinding/polishing of the resin was removing some of the sand particles from the surface of the resin, resulting in some tests being measurements of the hardness of a pit in the resin. If this is the case, it will only serve to lower the apparent hardness of the sand. The load may also have been too low, resulting in indents that were too small to measure and then calculate the hardness. Additionally, there may have been composite response of the sand and resin, further skewing the data. As it was believed the issues would skew the measured hardness down, it is thought there was a flaw in the hardness testing of the sand particles.

Hardness testing of the sand and egg shell particles suggests that whilst the egg shell particles appear to be sharper than the sand particles the difference in hardness between the two means it is expected that the wear life of the artificial sports turfs would increase if eggshell was used, as the sand particles are substantially harder. However, the sand particles appear to reduce the coefficient of friction which may help extend the wear life, and further testing is required to investigate whether the eggshell particles have the same effect. This reduction in friction is suggestive of a sliding action under the pin, promoting the abrasive wear mechanism, as discussed in further detail in 7.5.4.

7.4 Optical Imagery

The optical imagery showed the structure seen in all of the samples to a varying degree is suspected to be caused by the needling looms, as evidenced by the structure being visibly present in the samples that had no latex backing applied, and samples that had backing applied in different ways.

7.5 ESEM Imagery

7.5.1 Unworn

From the ESEM images of the samples that had not undergone any testing it can be seen that the fibres are typically round and smooth (as shown in some of the images by Hearle), although there is some manufacturing damage on all the artificial sports turfs, which can be seen in some images.

7.5.2 Worn in situ

The ESEM images of the worn in situ samples show a drastic difference to the unworn samples. There is clear flattening and material removal in the form of scratches. These scratches could be indicative of either adhesive or abrasive wear, or both are occurring, but it is not possible to tell purely from the scratches. There would appear to be damage identified by Hearle as types A B C and G, Axial splitting, ranging from one or two splits to extensive fibrillation, which may be spread over a range of lengths.

This flattening was seen in the literature by Onder and Berkalp, but no evidence of melting was found in the artificial sports turfs. Narrowing and longitudinal splitting reported by Hearle is also present. No tensile damage can be seen on the fibres, but surface abrasion can be seen.

7.5.3 Wear testing worn fibre

Figure 57 is an ESEM image of a fibre damaged from the wear testing. Damage type D was seen, suggesting the pin on wheel does not reproduce the wear seen in situ, which hwas types A B C and G. The fibres have become bent, which may lead to axial/biaxial splitting, but this is not present in the image presented. Surface abrasion is again present.

7.5.4 Worn Fibre Length

From Figure 58 we see surface abrasion along the entire length. The wear is least at the end of the fibre closest to the backing and worsening along the length. The narrowing observed in Figure 54 can still be seen in this figure. This suggests the shape and position of the fibres within the artificial sports turf has an effect on how the fibres experience the wear. It is known from Dayiary et al that the deflection of the fibres changes with age, which is suspected could contribute to flattening by allowing increased surface abrasion along the length of the fibre.

The surface abrasion observed on the fibres in the backing is less than the wear on the fibres in the pile, and roughly equal along the length of the fibre, which would suggest that the backing fibres do not experience much movement, which is believed to contribute to the wear on the pile fibres. Kink bands appear to be present, which are formed by compressive loading, likely to be caused ahead/behind a foot during the breaking and acceleration phases of a step.

The flattening and fraying along a significant length of the fibres observed on these samples shows the damage is incurred as a result of multiple interactions between the fibres and other constituent parts of the artificial sports turfs and footwear. Material can be seen to have been removed in either an adhesive or abrasive mechanism, as severe surface damage (which is indicative of adhesive wear) as well as fine cuts and deep gouges (indicative of abrasive wear) are present on the fibres in the images. The hard sand particles in the samples may have contributed to an abrasive wear mechanism, as discussed in 2.3.4. There is damage identified by Hearle as types A or B present.

7.5.5 Resin ESEM

The investigations of the samples that had been mounted in resin did not find regions of unsintered powder in the American samples, which was believed to occur. Areas where the latex had not properly adhered to the fibres were found, which suggests that the way the backing is applied to the artificial sports turf needs to be improved. It is believed this would improve the elastic response of the backing in the material.

7.5.6 Sand and Egg Particles

From the ESEM images of these particles it is inferred that a change from sand may lead to altered wear behaviour, due to the change in shape of the particles. The significant difference in the hardness of the Eggshell and sand particles, may prevent a reduction in wear life and possibly increase the wear life. As discussed previously, the sand particles are a hard asperity which may serve to promote abrasive wear. The differing shapes of the sand particles is expected to affect the wear characteristics throughout the pitch, with the much smoother particles causing less wear. Sand particles with sharp edges could negatively affect the wear rate and thus reduce the lifetime, given the hardness of the particles.

7.6 X-ray CT

Both the X-ray CT and micro X-ray CT had difficulties distinguishing between the latex and the fibres, but could see the difference between the product and voids in the product, which were known to exist in the similar products from the literature. The defects found are much larger than the voids described by Zhou and Warner, on the scale of a few millimetre, rather than sub millimetre. An issue with the investigations in this project is that the grey value setting determines whether a particular voxel/pixel appears in the image. This is set manually so there is some uncertainty to the scans, which may explain why the observed voids are larger than those described in the literature. Some further work could be to remove this uncertainty, by determining the grey values of the PP fibres and SBR separately.

However the X-ray CT investigations determined the distribution of the latex backing is non uniform, and this leads to small defects in the artificial sports turf, which explains why the preliminary fatigue tests exhibited such wild inconsistencies, as the defects approach the size of the samples. It is believed the directionality of the fibres affect the distribution of the latex, as it is believed the SBR latex will follow the fibres as a result of capillary action during manufacture.

The X-ray CT investigations also showed the structure of the backing is damaged in different ways by different failures.

With regards to the investigations into the effect of observed voids in the structure of the samples and tensile strength, it was expected that the samples with more latex, and therefore heavier samples, would be stronger, depending on the directionality. Therefore it was expected samples 6, 7, 5 and 8 to be the strongest, with 4, 11, 10 and 3 to be the weakest in order.

When tested, the horizontal samples were stronger than the vertical, which is to be expected due to the directionality. It is also inferred from Figure 68 that the overall behaviour of the samples is in line with the others, with the distinct difference between the vertical and horizontal orientations, as discussed in 5.

Figure 69 gives the relationship between the mass of a sample and its fracture point. It can be seen that there is some correlation, for the vertical orientation with increasing mass increasing the fracture point, but no correlation for the horizontal. The discrepancies could be due to inaccuracies during cutting, and as such further testing is needed to say this for certain.

The random distribution of the voids suggests the reason for the voids is not a systematic issue with the manufacturing process, but rather an issue with how the backing is applied to the artificial sports turf and how the backing permeates the fibres on application. This will of course be affected by the needling process, but this process is not causing voids to form in specific positions.

7.7 MRI

The MRI scans were an unsuccessful attempt to image the structure of the artificial sports turfs, because the samples did not generate enough signal when it was on its own, and when the sample was immersed in water, in an attempt to take a negative there was no improvement.

In comparison to the optical, ESEM and MRI images taken, it can be observed that the MRI offers no better imaging of the backing or fibres.

8 - Conclusions, Further Work.

8.1 Conclusions

To recap as stated in 1, the aims of the project were to: 1) Develop techniques for analysing the tribological performance of materials used in artificial sports pitches. 2) Develop techniques for tribological study of artificial sports pitches. 3) Develop techniques for identifying wear mechanisms in different polymers. 4) Research the different factors contributing to damage of artificial sports pitches.

Optical imagery is not a good choice for examining wear. Although it is possible to get a view of a wider area, it is difficult to get a good image of the surface damage on fibre. In particular, it is difficult to get good lighting on a surface that is deeper into the pile.

ESEM imaging is a good technique for observing the wear and surface damage on individual fibres. Although it is better for imaging deeper into the fibres than compared to optical, it is still difficult to image deep into the fibres. From the ESEM imagery it is possible to say the wear mechanisms are predominantly adhesive and abrasive, due to fibre – fibre, fibre – boot and fibre – sand contacts. Surface abrasion along with damage types A B C and G were observed.

X-ray CT is a reasonable method for imaging the distribution of the latex backing within the artificial sports turfs. Whilst is it possible to see the areas in which there is not much material, it is not possible to distinguish between the latex backing and the polymer fibres. This means it is possible to see how the backing is affected by a tribological test, but not how the latex/fibre adhesion is affected.

MRI imaging is not a good technique for analysing the distribution of the latex in the backing, and thus not good for analysis of how the backing is affected by tribological tests. In addition to this, the resolution is too low to see any surface defects as it is not designed for this purpose, and thus is not suitable for analysing wear mechanisms.

From the wear testing it can be seen the friction and therefore grip increases with wear, however the wear testing did not reproduce the same surface abrasion seen on worn in situ samples.

The hardness testing of the sand and egg shell particles showed that whilst the egg shell particles appear much sharper, due to the drastic difference in the hardness in comparison to the sand particles, using egg shell as the filler would improve the wear life of the artificial sports turfs.

From the tensile results it can been seen that the best material in terms of fracture point is the Leigh Spinners 1150 grass green artificial sports turf because it has the highest fracture point as can be seen in Figure 78. The second best material is the Leigh Spinners 1300 grass green, which implies this manufacturer is better. This conclusion is furthered when it can be seen that none of the Rawsons artificial sports turfs exhibit any better attributes, with the exception of the extension at failure, although they are more uniform which may be better if a particular sample of artificial sports turf experiences repeated loading from multiple directions.

It is also concluded from the tensile testing the artificial sports turfs behave like a composite material with randomly orientated short fibres, as from the tensile testing it appears the backing carries the applied load without effectively transferring the load to the fibres. It can also be seen in the tensile results that the artificial sports turfs appear to get stiffer with age.

From the preliminary fatigue testing combined with the X-ray CT results it can be concluded that the backing latex is not applied uniformly, and thus research into smoothing out the distribution is required.

Conclusions from the main fatigue testing are difficult to make due to the number of tests completed, and the long nature of the experiments. It does appear that the directionality does have an affect the fatigue performance of the samples, and the increase in size of the samples averages out some of the defects seen in the backing. It does appear that the load used exceeded the fatigue limit of the materials, implying fatigue failures could occur in situ.

Based on the results from the tensile and wear testing, it is hypothesized that the Rawsons artificial sports turfs have more even fibre distribution in the horizontal/vertical directions in comparison to the Leigh Spinners artificial sports turfs, as a result of differing manufacturing processes. This is hypothesized because the Rawsons artificial sports turfs all exhibit a smaller difference in fracture points between the vertical and horizontal orientations in the tensile testing, a known property of woven composites. This is further supported by the observation in the wear testing results that the Rawsons artificial sports turfs produced less variation during the tests, implying there are less peaks/troughs for the counter face to ride over/drop into due to a more equal distribution of fibres in the 2 directions.

8.2 Further Work

It is believed the correct direction is to complete a full program of fatigue testing following the method described in section 3.16, to get statistically significant results and to give a complete picture of the strength and durability of the backing in all the artificial sports turfs provided. If the results from the completed fatigue testing reflect the results from the tensile testing, then the tensile testing would not need to be continued. However if there is a disparity, further testing to make the results statistically significant must be conducted. In either case, it would be useful for Notts Sport Ltd to have S-N curves developed for the current artificial sports turfs, to allow for comparison with new artificial sports turfs.

Once this is complete the next step would be to construct a mechanism for replicating the repeated loading of an athlete's foot impacting the artificial sports turfs for comparison against the fatigue testing.

As mentioned before, further research into evening out the distribution of the latex backing is required. Factors to consider are how the latex flows into the fibres, as it is likely to follow the fibres. Additionally, the distribution may also have an effect on the porosity of the artificial sports turf, which could negatively affect the drainage of a pitch. Additionally, more samples need to be scanned for pores/voids and then tensile tested to achieve statistically significant results, preferably relating the size and distribution of the voids to the mechanical properties of the samples. It would be preferable to remove the uncertainty in grey value setting, by finding the grey values of the PP fibres and SBR separately.

Additionally, more wear testing is required, to compare the effects the sand and eggshell have on the lifetime of the artificial sports turfs. A method of weighing the samples after the filler has been applied is required. In addition, comparison to more real world samples is required. Ideally, it would be preferential to assess the wear and the wear mechanisms, and other mechanical properties, on samples of differing age to develop an understanding of how these properties change as the wear accumulates in the artificial sports turf. It may be useful to determine precisely which wear mechanisms dominate at which point in the turfs lifetime with such a testing regime. The method needs revising to ensure that the tests do produce the same surface abrasion seen on the worn in situ samples.

Further to this, developing a wear test that measures the shortening of fibres with time may give a more suitable measure of the age of an artificial sports turf, as this would be measureable “in the field”.

It may also be useful to compare the effects of varying the amount of sand and eggshell used to fill the artificial sports turf has on the lifetime of the artificial sports turfs, although Notts Sport Ltd. have requested that investigation into eggshell should not be pursued, owing to issues with the production of the eggshell particles.

Investigation into the proposed hypothesis is required. It is believed observing the distribution of fibres in cross sections of the artificial sports turfs horizontal/vertical orientations would either prove or disprove this hypothesis.

Finally, the effect of weathering on the properties of the artificial sports turfs also needs to be investigated.

9 Appendix 1 – Foot loading force calculation for fatigue testing

6.15 N and 40 N were chosen as the upper limits for the parameters of the test based on the calculation that if an athlete's foot is 0.125 m wide and the athlete weighs 89 kg and is running at a speed of 3.75 m/s then the vertical ground reaction force is 1922 N.

$$F_z = 2.2Mg = 1922\ N$$

The longitudinal force through his foot is an order of magnitude lower than this therefore;

$$F_{ml} = \frac{F_z}{10} = \frac{1922}{10} \approx 192\ N$$

This force is distributed evenly across the foot and therefore the ground, which must oppose the force entirely to prevent the foot from slipping. Thus, dividing the width of the foot by the width of the gauge length (0.004 m and 0.125 m respectively) gives the factor by which the force must be reduced by to give a realistic experiment.

$$\frac{192}{(\frac{0.125}{0.004})} = 6.15\ N$$

$$\frac{192}{(\frac{0.125}{0.025})} = 38.4\ N\ \approx 40\ N$$

The upper limit of 80 N corresponds to some literature which suggests that the force in the direction of propagation is equal to half the body weight of the athlete when running at 3.75 m/s (7).

$$F_{ml} = 0.5Mg = 436.54\ N$$

$$\frac{400}{(\frac{0.125}{0.025})} = 80\ N$$

10 Appendix 2 – Wear testing variables calculation

The force was chosen to be 16 N as this corresponds to the load under a stud (assuming an even distribution across all of the studs) of an athlete of mass 80 kg running at a speed of 3.75 m/s wearing shoes with 24 studs we find:

$$F = \frac{0.5Mg}{2 * 12} = \frac{392.4}{24} = 16.35\ N\ \approx 16\ N$$

The speed was determined from contact time.

11 Appendix 3 – Calibration data for LVDT

The calibration experiments produced Figure 122, which allows for the conversion of voltage measured by the LVDT (x) to force (y) by using the equations of the lines of best fit. The input was run through all 3 and the mean of these values was used.

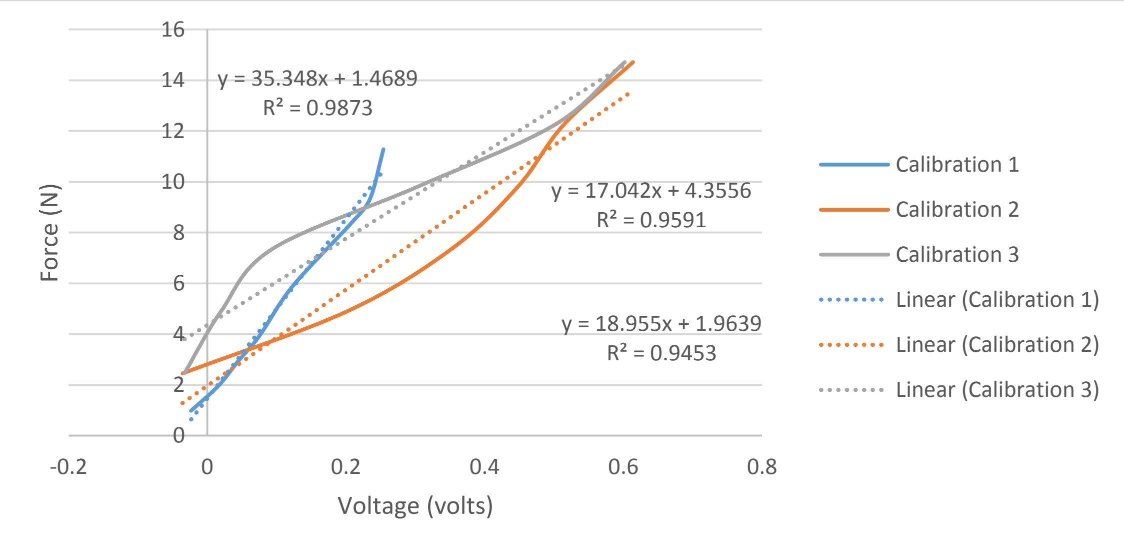

Figure 122 - Calibration data for Pin on wheel wear testing

12 Appendix 4 – Fatigue Raw Data

See attached cd/usb stick for raw data from fatigue experiments.

13 Bibliography/References

1. Notts Sport Ltd. Our Company [cited 2015 17/09/15]. Description of Notts Sport Ltd.]. Available from: http://www.nottssport.co.uk/artificial-grass-surfaces/company-introduction.html.
2. Notts Sport Ltd. Personal Communication. In: Timothy Devenport, editor. Description of products provided ed2014.
3. Ltd LS. Factory tour/guide. 2014.
4. Callister WD, Jr., Rethwisch DG. Materials science and engineering. Hoboken, N.J: Wiley; 2011.
5. John V. Introduction to Engineering Materials: Palgrave Macmillan; 2003.
6. Reed WF, Alb AM. Rubbers and Elastomers. Hoboken, NJ: John Wiley & Sons. p. 409-25.
7. Running: Olympic Handbook of Sports Medicine. GB: Wiley-Blackwell; 2000.
8. Trautmann C, Rosenbaum D, Martinelli N. Foot loading characteristics during three fencing-specific movements. Journal of sports sciences. 2011;29(15):1585-92.
9. Dixon SJ, Collop AC, Batt ME. Surface effects on ground reaction forces and lower extremity kinematics in running. Medicine and science in sports and exercise. 2000;32(11):1919-26.
10. Worthington P, King M, Ranson C. The influence of cricket fast bowlers' front leg technique on peak ground reaction forces. Journal of sports sciences. 2013;31(4):434.
11. Hong Y, Wang L, Li JX, Zhou JH. Comparison of plantar loads during treadmill and overground running. Journal of science and medicine in sport / Sports Medicine Australia. 2012;15(6):554.
12. FIFA I. FIFA Quality Concept for Football Turf Handbook of Test Methods. January; 2012.
13. Textiles Ia. Glossary of Carpet Terms 2013 [updated 3/10/2013; cited 2016 13/01/2016]. Glossary of carpet terms]. Available from: http://www.interiorstextiles.com/glossary-of-carpet-terms/.
14. Onder E, Berkalp OB. Effects of Different Structural Parameters on Carpet Physical Properties. Textile Research Journal. 2001;71(6):549-55.
15. Zhou W, Warner SB. Pore Sizes in Carpet. Textile Research Journal. 1999;69(6):423-30.
16. Dayiary M, Najar SS, Shamsi M. A new theoretical approach to cut-pile carpet compression based on elastic-stored bending energy. Journal of The Textile Institute. 2009;100(8):688.
17. Wu J, Pan N, Williams KR. Mechanical, Biomechanical and Psychophysical Study of Carpet Performance. Textile Research Journal. 2007;77(3):172-8.
18. Hearle JWS. SEM Study of Wear on Wool Stair-carpet. Journal of The Textile Institute. 2000;91(4):616.
19. Hearle JWS, Sengonul A, Tandon SK. Type and Location of Fatigue Breaks in Wool Carpets. Part I: Qualitative Examination. Journal of The Textile Institute. 2001;92(1):75.
20. Cassidy B, Hearle J, Sengonul A. Type and Location of Fatigue Breaks in Wool Carpets. Part II: Quantitative Examination. Journal of the Textile Institute. 2001;92(1):88-102.
21. Elices M, Llorca J. Fiber fracture: Gulf Professional Publishing; 2002.
22. Hearle J. Forms of fibre fracture. Fiber fracture Elsevier Science, Amsterdam. 2002:57-71.
23. Hearle JWS. Fracture of common textile fibres. Elices M, Llorca J, editors. Amsterdam: Elsevier Science Bv; 2002. 329-53 p.
24. Liu H, Tandon SK, Wood EJ. Probability fracture mechanics of wear in wool carpet: Part I: Wear model of cut pile carpet. Textile Research Journal. 2002;72(11):954.

25. Zanetti EM, Bignardi C, Franceschini G, Audenino AL. Amateur football pitches: mechanical properties of the natural ground and of different artificial turf infills and their biomechanical implications. Journal of sports sciences. 2013;31(7):767.
26. Vasilev VV, Morozov EV, Books24x I. Advanced mechanics of composite materials and structural elements, third edition. Kidlington, Oxford; Waltham, MA: Elsevier; 2013.
27. Callister WD, Jr., Rethwisch DG. Materials science and engineering. Hoboken, NJ: Wiley; 2015.
28. Hull D, Clyne TW. An introduction to composite materials. Cambridge: Cambridge University Press; 1996.
29. Suresh S. Fatigue of materials. Cambridge: Cambridge University Press; 1998.
30. Neale MJ, Gee MG. Guide to wear problems and testing for industry. Bury St Edmunds; London: Professional Engineering Pub; 2000.
31. Engineers IoM. Tribological Design Guide Part 5 2015 [cited 2015 23.09.2015]. Available from: http://www.imeche.org/knowledge/industries/tribology/trib-design-guides.
32. Kopeliovich D. Mechanisms of Wear Substech2015 [updated 12/03/15; cited 2015 27/05/15]. Descriptions and depictions of wear mechanisms]. Available from: http://www.substech.com/dokuwiki/doku.php?id=mechanisms_of_wear.
33. Hiraoka N, Yamane E. A Study on the Mechanism of Generating Wear Track Grooves. Tribology Letters. 2011;41(3):479-84.
34. Sinha SK, Briscoe BJ. Polymer Tribology: Imperial College Press; 2009.
35. Marcus K, Ball A, Allen C. On the nature of the transfer film at the interface of a water lubricated sliding polymer-metal couple. Journal of Physics D: Applied Physics. 1992;25:A57.
36. Rohatgi PK, Blau PJ, Yust CS, Group ASMIWRM, United States. Department of Energy.Office of Advanced Transportation Materials.Tribology P. Tribology of composite materials: proceedings of a conference, Oak Ridge, Tennessee, 1-3 May 1990. Materials Park, Ohio: ASM International; 1990.
37. Stachowiak GW, Batchelor AW, Books24x I. Engineering tribology, fourth edition. Waltham, MA; Kidlington, Oxford, UK: Butterworth-Heinemann; 2014.
38. Friedrich K, Reinicke P. Friction and wear of polymer-based composites. Mechanics of Composite Materials. 1998;34(6):503-14.
39. Bradbury S, Bracegirdle B, Royal Microscopical S. Introduction to light microscopy. Oxford: Bios Scientific Publishers; 1998.
40. Stokes DJ. Principles of SEM. Chichester, UK: John Wiley & Sons, Ltd. p. 17-62.
41. Stokes D, Royal Microscopical S. Principles and practice of variable pressure/environmental scanning electron microscopy (VP-ESEM). Chichester, U.K: Wiley; 2008.
42. Lisle D. Imaging for students. London: Hodder Arnold; 2012.
43. Non-traditional sterilization techniques for biomaterials and medical devices. 2012. p. 97-116.
44. Sterilisation techniques for polymers. 2012. p. 151-211.
45. Standards B. Surfaces for sports areas - Determination of tensile properties of synthetic sports surfaces. BS EN 12230:2003: British Standards; 2003. p. 12.
46. Gottschall JS, Kram R. Ground reaction forces during downhill and uphill running. Journal of Biomechanics. 2005;38(3):445-52.